

AD-A110 432

MASSACHUSETTS INST OF TECH CAMBRIDGE GAS TURBINE AND--ETC F/G 20/4
CURRENT PROBLEMS IN TURBOMACHINERY FLUID DYNAMICS.(U)
NOV 81 E M GREITZER, W T THOMPkins F49620-78-C-0084

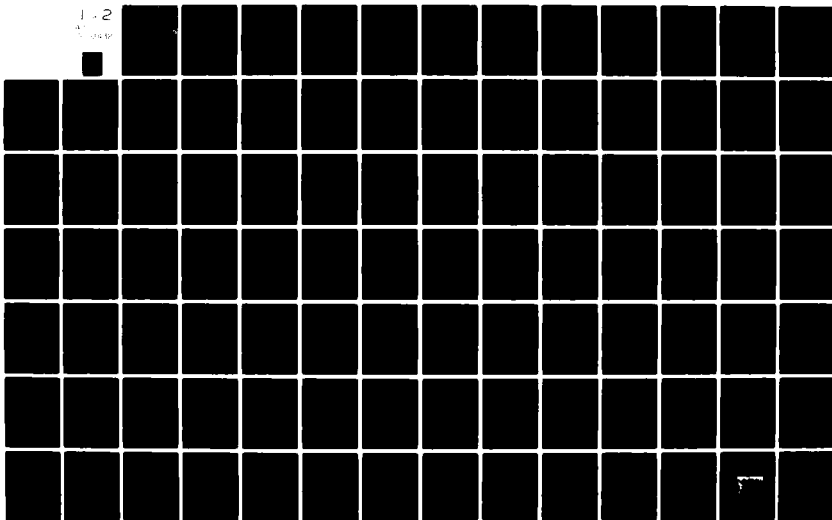
UNCLASSIFIED

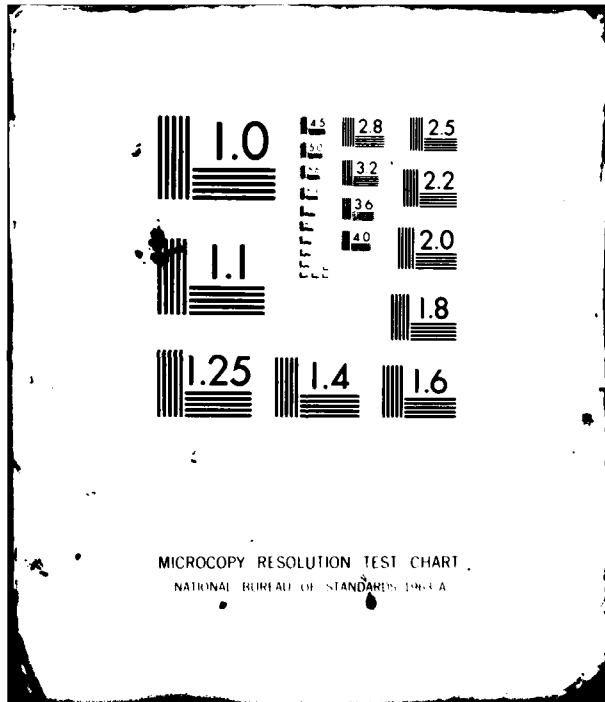
AFOSR-TR-82-0027

NL

1-2

1-2





AFOSR-TR- 82 -0027

LEVEL

GAS TURBINE & PLASMA DYNAMICS LABORATORY
DEPARTMENT OF AERONAUTICS & ASTRONAUTICS
MASSACHUSETTS INSTITUTE OF TECHNOLOGY
CAMBRIDGE, MASSACHUSETTS 02139

11

FINAL REPORT

on

CONTRACT NO. F49620-78-C-0084

126

entitled

CURRENT PROBLEMS IN TURBOMACHINERY FLUID DYNAMICS

for the period

June 1, 1979 to September 30, 1981

submitted to

AIR FORCE OFFICE OF SCIENTIFIC RESEARCH

Attention of: Dr. James D. Wilson, Program Manager,
Directorate of Aerospace Sciences, AFOSR (AFSC)
Bolling Air Force Base, DC 20332

Principal Investigators: Edward M. Greitzer
William T. Thompkins, Jr.
James E. McCune

Co-Investigators: Alan H. Epstein
Choon S. Tan

Collaborating Investigators: Eugene E. Covert
Sir William R. Hawthorne
Frank H. Durgin

November 30, 1981

DTIC
SELECTED
FEB 3 1982
H

AD A110432

DTIC FILE COPY

410354 82 03 02 037

Approved for public release;
distribution unlimited.

REPORT, DOCUMENTATION PAGE		READ INSTRUCTIONS BEFORE COMPLETING FORM	
1. AFOSR-TR- 82 - 0027		2. GOVT ACCESSION NO. AD-A110 432	3. RECIPIENT'S CATALOG NUMBER
4. TITLE (and Subtitle) CURRENT PROBLEMS IN TURBOMACHINERY FLUID DYNAMICS		5. TYPE OF REPORT & PERIOD COVERED Final Report 10/1/79-9/30/81	
7. AUTHOR(s) E.M. Greitzer, W.T. Thompkins, Jr., J.E. McCune, A.H. Epstein, C.S. Tan, W.R. Hawthorne		6. PERFORMING ORG. REPORT NUMBER	
9. PERFORMING ORGANIZATION NAME AND ADDRESS GAS TURBINE & PLASMA DYNAMICS LABORATORY DEPARTMENT OF AERONAUTICS & ASTRONAUTICS MASSACHUSETTS INSTITUTE OF TECHNOLOGY, CAMBRIDGE, MA		8. CONTRACT OR GRANT NUMBER(s) F49620-78-C-0084	
11. CONTROLLING OFFICE NAME AND ADDRESS AIR FORCE OFFICE OF SCIENTIFIC RESEARCH DIRECTORATE OF AEROSPACE SCIENCES AFOSR (AFSC) BOLLING AFB, DC 20332		10. PROGRAM ELEMENT, PROJECT, TASK AREA & WORK UNIT NUMBERS 61102F 2307/A4	
14. MONITORING AGENCY NAME & ADDRESS (if different from Controlling Office)		12. REPORT DATE November 30, 1981	
		13. NUMBER OF PAGES 132	
		15. SECURITY CLASS. (of this report) Unclassified	
		15a. DECLASSIFICATION/DOWNGRADING SCHEDULE	

Approved for Public Release; Distribution Unlimited

17. DISTRIBUTION STATEMENT (of the abstract entered in Block 20, if different from Report)

18. SUPPLEMENTARY NOTES

19. KEY WORDS (Continue on reverse side if necessary and identify by block number)

casing treatment	three-dimensional flow
axial flow turbomachinery	flow measurements in transonic fans
axial flow compressors	transonic flow
computational fluid dynamics	vortex flows
compressor stall	inlet distortion

20. ABSTRACT (Continue on reverse side if necessary and identify by block number)

A multi-investigator effort on problems of current interest in turbomachinery fluid dynamics is being carried out in the Gas Turbine & Plasma Dynamics Lab. of MIT. Within the overall program, four different tasks having to do with a wide range of design and off-design flow fields have been identified. These are: 1) Investigation of fan and compressor design point fluid dynamics (including formulation of design procedures using current three-dimensional transonic codes and development of techniques for instantaneous temperature measurements in transonic fans); 2) Studies of compressor stability enhancement (including basic investi-

DD FORM 1 JAN 73 1473

UNCLASSIFIED
SECURITY CLASSIFICATION OF THIS PAGE (When Data Entered)

82 03 02 03

20. Abstract (continued)

gations of the fluid dynamics of compressor casing/hub treatment); 3) Fluid mechanics of gas turbine engine operation in inlet flow distortion (including inlet vortex distortion and combined circumferential/radial distortions); and 4) Investigations of three-dimensional flows in highly loaded turbomachines (including actuator duct theory and blade-to-blade flow analysis) and linearized analysis of swirling three-dimensional flows in turbomachines. This report summarizes the work carried out to date as well as indicates the direction of future efforts on these tasks.

UNCLASSIFIED

SECURITY CLASSIFICATION OF THIS PAGE (When Data Entered)

TABLE OF CONTENTS

<u>SECTION</u>	<u>PAGE NO.</u>
1. INTRODUCTION AND RESEARCH OBJECTIVES	1
2. STATUS OF THE RESEARCH PROGRAM	
Summary	3
Task I: Investigation of Fan and Compressor Design Point Fluid Dynamics.	
A: Inverse (Design) Calculation Procedure	5
B: Development of Techniques for Time Resolved Temperature Measurement in Transonic Fans and Further Measurements of AFAPL High Through-Flow Compressor Stage.	37
Task II: Investigation of Basic Mechanisms for Compressor Stability Enhancement Using Casing/Hub Treatment.	48
Task III: Investigation of the Response of Gas Turbine Engines to Inlet Distortion.	
A: Basic Studies of the Inlet Vortex Flow Field	73
B: Combined Radial/Circumferential Inlet Total Pressure Distortion	98
Task IV: Investigation of Three-Dimensional Flow in Highly Loaded Turbomachines.	116
3. PUBLICATIONS	124
4. PROGRAM PERSONNEL	127
5. INTERACTIONS	128
6. DISCOVERIES, INVENTIONS, AND SCIENTIFIC APPLICATIONS	131
7. CONCLUDING REMARKS	132

AIR FORCE OFFICE OF SCIENTIFIC RESEARCH (AFSC)
NOTICE OF TRANSMITTAL TO DTIC
This technical report has been reviewed and is approved for public release IAW AFR 190-12. Distribution is unlimited.
MATTHEW J. KEMPER
Chief, Technical Information Division

Section For	
DTIC	
Classified	
Exemption	
Classification/	
Availability	
Restrictions	
Special	

A

1. INTRODUCTION AND RESEARCH OBJECTIVES

This report describes work carried out at the Gas Turbine and Plasma Dynamics Laboratory at MIT, as part of a multi-investigator effort on current problems in turbomachinery fluid dynamics. Support for this program is provided by the Air Force Office of Scientific Research under Contract Number F49620-78-C-0084, Dr. J. D. Wilson, Program Manager.

The program, which was initiated on 1 June 1979, has as its continuing objective the improved understanding of the complex three-dimensional and unsteady flows inherent in turbomachinery applications. Within this general objective, four different tasks having to do with a wide range of design and off-design flow fields have been identified. These are:

1. Investigation of fan and compressor design point fluid dynamics (including the formulation of design procedures using current three-dimensional transonic codes, and development of techniques for instantaneous, time resolved, total temperature measurements in transonic fans).
2. Studies of compressor stability enhancement (including basic investigations of the fluid dynamics of compressor casing/hub treatment).
3. Fluid mechanics of gas turbine engine operation in inlet flow distortion (including inlet vortex distortions as well as combined radial/circumferential total pressure distortion).
4. Investigations of three-dimensional flows in highly loaded turbomachines (including actuator duct theory and blade-to-blade flow analysis) and linearized analysis of swirling three-dimensional flows in turbomachines. The overall thrust is a numerical-experimental/analytical attack on those areas which are seen as being of high technological import as well as fundamental interest.

This final report summarizes progress on the four tasks during the period 1 June 1979 to 30 September 1981. A summary of significant accomplishments is first given. The work accomplished in each specific task is then described

in more detail. Although an attempt has been made to make this report self-contained, it should be emphasized that much of the work has appeared in papers and/or reports, and reference to these will be made wherever possible.

Accession For	
NTIS GRA&I	<input checked="" type="checkbox"/>
DTIC TAB	<input type="checkbox"/>
Unannounced	<input type="checkbox"/>
Justification	
By _____	
Distribution/ _____	
Availability Codes	
Dist	Avail and/or Special
A	



2. SUMMARY OF THE SIGNIFICANT ACCOMPLISHMENTS OF THE RESEARCH PROGRAM

Task I: Investigation of Fan and Compressor Design Point Fluid Dynamics

A) **Inverse Design Calculation Procedure:** A previously described inviscid design technique has been substantially improved to allow the generation of either shock-free, weak shock, or low total pressure loss supersonic rotor cascade designs. The scheme investigated uses an input target pressure distribution and attempts to determine a profile shape through a sequence of direct calculations on known trial geometries. Improvements have been introduced in inflow-outflow boundary conditions, imposition of geometric constraints and in shock pressure rise specifications. Calculational examples are presented for pre-compression type rotor designs.

B) **Advanced Measurements:** Work has continued on the development of a high frequency (20 ~ 30 kHz) temperature transducer, using a dual wire aspirating probe, for use in unsteady transonic flows in compressor environments. The first version of the probe proved to have inadequate frequency response due to a thick thermal boundary layer in the region of the wire plane. The probe has been redesigned to minimize the boundary layer growth construction. This new probe is presently under construction.

Time resolved measurement on the AFAPL high through flow (HTF) stage continued with a new technology combination angle and pressure probe. The new probe is a significant improvement in that it has no discernible thermal drift.

Task II: Investigation of Basic Mechanisms for Compressor Stability Enhancement Using Casing Treatment

An experimental study has been conducted to examine the effects, on stator stall margin and performance, of a slotted hub treatment rotating beneath the stator of an axial flow compressor. The compressor was run with this hub treatment and the results compared to those taken with a smooth rotating hub. It was determined that, for the configuration tested, the hub treatment was ineffective in the improvement of stall margin but resulted in a measurably higher static pressure rise across the stator and a significant decrease in flow deviation and blockage in the stator midspan region. Although it is the hub section of the stator that sets the stall limit in this configuration, measurements of the stator exit flow field indicated that the type of stall that is occurring is a blade stall rather than a pure wall stall. Absence of a wall stall is thus seen as a key possibility for the lack of stall margin improvement. This will be investigated further using a different configuration, since we are now able (using an exit fan) to exercise considerably more freedom in the design of the stage to achieve a wall stall.

Task III: Investigation of the Response of Gas Turbine Engines to Inlet Distortion

A) **Inlet Vortex Flow Distortion:** An experimental and theoretical study of the inlet vortex (or ground vortex) phenomenon has been carried out. The experiments were conducted in a water tunnel using hydrogen bubble flow visualization techniques. The theoretical study was based on a secondary flow approach in which vortex filaments in a (weak) shear flow are viewed as convected (and deformed) by a three-dimensional irrotational primary flow;

the latter being calculated numerically using a three-dimensional panel method. Two basic mechanisms of inlet vortex generation were identified. The first of these, which has been alluded to qualitatively by other investigators, is the amplification of ambient (i.e., far upstream) vorticity as the vortex lines are stretched and drawn into the inlet. Quantitative calculations were carried out to illustrate the central features connected with this amplification. In contrast to what has been supposed, however, there is another mechanism of inlet vortex formation which does not appear to have been recognized previously and which does not require the presence of ambient vorticity. It was shown that an inlet vortex can therefore arise in an (upstream) irrotational flow, for an inlet in crosswind. In this situation, the vortex is accompanied by a variation in circulation along the axial length of the inlet. The ratio of inlet velocity to upstream velocity is an important parameter for both mechanisms.

B) Combined Circumferential/Radial Flow Distortion and Distortion in Low Hub/Tip Radius Ratio Turbomachines in Compressible Flow

The behavior of a highly loaded annular blade row in a combined circumferential/radial distortion has been analyzed. In the analysis the flow is assumed to be steady and incompressible, and the distortions taken to be of magnitude such that a linearized description of the problem can be adopted. Calculations have been carried out based on this three-dimensional theory and comparison made with a two-dimensional strip theory approach. It is found that significant differences exist between the two procedures since only the former properly includes centrifugal effects as well as the two distinct types of vorticity (trailing vorticity and vorticity associated with total pressure variations) that generally exist in these types of flows. The analysis has also been extended to the compressible flow regime, for a free vortex type swirling flow. Calculations have been carried out of the three-dimensional flows associated with a total pressure (or total temperature) circumferential distortion in a low hub/tip ratio blade row. It is found that the ambient Mach number can have a significant effect on the magnitude and evolution of the axisymmetric flow disturbances downstream of the blade row. In addition to this above-mentioned analysis, a simple theory has been developed to give general guidelines on the magnitude of these effects to be expected in practical situations.

Task IV: Investigations of Three-Dimensional Flows in Highly Loaded Turbomachines

A method of designing highly loaded blades to give a specified distribution of swirl has been developed. The method is based on a newly-developed three-dimensional analysis. In the present application the flow is assumed to be incompressible and inviscid and the blades are of negligible thickness; however, the blades can be stacked at any chordwise location so that the effects of stacking can be elucidated. The results presented assume a free vortex swirl distribution and they show the effects of deflection, blade number, solidity, aspect and hub/tip ratios on the final blade shape. Thickness effects are to be included in examples to follow. The analysis shows that the mean throughflow cannot be fully determined until the blade shape and spacing are known. The results can also be used the check computer programs for estimating the flow given the blade shape.

TASK I: INVERSE DESIGN CALCULATION FOR TRANSONIC COMPRESSORSIntroduction

Design of transonic airfoil shapes, either isolated airfoils or airfoils in cascade, which possess specific aerodynamic characteristics, is now an extremely active research area. Many current analyses concentrate on producing shock-free airfoil designs for subsonic freestream conditions [see 1.1 and 1.2 for example]. Other workers recognize that shock-free designs may not necessarily represent optimum airfoil shapes and have concentrated on full potential flow solutions, with isentropic shock waves [see 1.3, 1.4, and 1.5. A concise discussion of the role of constraints in such schemes is available in 1.6. These results may now be applied to turbomachinery stator row and turbine design and should be quite successful.

For the rotor design problem, it is expected that optimum designs will involve both normal and oblique shock waves at high Mach number, 1.5 to 2.0, and a potential flow analysis appears inadequate. Design schemes for supersonic, rotor cascades are considered in this report and in an earlier paper 1.7 using Euler equation flow simulations. This earlier paper demonstrated that an inverse or design calculation scheme was possible for general inviscid flow, and this paper explores the use of such inverse schemes to design supersonic inflow cascades. The scheme investigated uses an input target blade pressure distribution and attempts to determine a profile shape through a sequence of direct calculations on known trial geometries. Due to the fact that quite a number of geometric constraints, as well as the pressure distribution, must be satisfied, the final calculated blade pressure may match the target pressure only in a least squares sense. The geometric construction technique proceeds by first assuming a trial geometry and coordinate system. Flow equations are then numerically integrated using

MacCormack's time-marching method for a small number of time steps. The difference between the current blade pressure and the target wall pressure is then used to predict a geometry change which will move the computed wall pressure toward the target and the process is repeated to convergence. During the blade geometry calculations, constraints on the blade geometry such as leading and trailing edge closure or minimum thickness are obeyed.

Flow Equations

The flow calculation presented in this paper use the strong conservation law form of the Euler equations expressed in a form suitable for use with time dependent, body-fitted coordinate systems [see 1.7 or 1.8]. For two-dimensional flow, these equations written in vector form for Cartesian coordinates are:

$$\partial_t \bar{q} + \partial_x \bar{F} + \partial_y \bar{G} = 0 \quad (1.1)$$

where

$$\bar{q} = \begin{pmatrix} \rho \\ \rho u \\ \rho v \end{pmatrix} \quad F = \begin{pmatrix} \rho u \\ \rho u^2 + P \\ \rho uv \end{pmatrix} \quad G = \begin{pmatrix} \rho v \\ \rho uv \\ \rho v^2 + P \end{pmatrix}$$

These equations express conservation of mass and momentum. In inverse code applications where only steady state solutions are required, the energy equation may be replaced with the assumption of iso-energetic flow, or the assumption that the stagnation enthalpy (h_o) is constant everywhere. This assumption provides a simple algebraic relation between the pressure, density and velocity components.

$$P = \rho \frac{(\gamma - 1)}{\gamma} \left(h_o - \frac{(u^2 + v^2)}{2} \right) \quad (1.2)$$

Following Viviand (1.8), a coordinate mapping may be defined as

$$\xi = \xi(x, y, t) \quad \eta = \eta(x, y, t) \quad t = t \quad (1.3)$$

where ξ and η are general mapping functions that may depend on time. Subject to such a mapping, the flow equations may be written as

$$\partial_t \hat{q} + \partial_\xi \hat{F} + \partial_\eta \hat{G} = 0 \quad (1.4)$$

The flow equations in finite difference forms are numerically integrated using MacCormack, explicit, time marching scheme (1.9) which may be written in symbolic form as:

$$\hat{q}_{j,k}^{n+2} = (\mathcal{L}_\xi \mathcal{L}_\eta \mathcal{L}_\eta \mathcal{L}_\xi) \hat{q}_{j,k}^n \quad (1.10)$$

Here \mathcal{L}_ξ and \mathcal{L}_η are each multiple step operators which include finite difference operations in only one space direction. For example \mathcal{L}_η is defined as:

$$\hat{q}_{j,k}^n = \mathcal{L}_\eta \hat{q}_{j,k}^n = (\mathcal{L}_{3\eta} \mathcal{L}_{2\eta} \mathcal{L}_{1\eta}) \hat{q}_{j,k}^n \quad (1.11)$$

where

$$\begin{aligned} \hat{q}_{j,k}^* &= \mathcal{L}_{1\eta} \hat{q}_{j,k}^n = \hat{q}_{j,k}^n - \frac{\Delta t}{\Delta \eta} \left(\hat{G}_{j+1,k}^n - \hat{G}_{j,k}^n \right) \\ \hat{q}_{j,k}^{**} &= \mathcal{L}_{2\eta} \hat{q}_{j,k}^* = \frac{1}{2} \left[\hat{q}_{j,k}^n + \hat{q}_{j,k}^* - \frac{\Delta t}{\Delta \eta} \left(\hat{G}_{j,k}^* - \hat{G}_{j-1,k}^* \right) \right] \\ \hat{q}_{j,k}^n &= \mathcal{L}_{3\eta} \hat{q}_{j,k}^{**} = \left\{ \hat{q}_{j,k}^{**} + \left(K_{j+\frac{1}{2},k} \right) \left(\hat{q}_{j+1,k}^{**} - \hat{q}_{j,k}^{**} \right) + \left(K_{j-\frac{1}{2},k} \right) \right. \\ &\quad \left. \left(\hat{q}_{j-1,k}^{**} - \hat{q}_{j,k}^{**} \right) \right\} \end{aligned}$$

\mathcal{L}_ξ is defined in a similar fashion. Convergence is checked after each sequence of operators in equation (10).

The damping operators $\mathcal{L}_{3\xi}$ and $\mathcal{L}_{3\eta}$ are required for stability of the scheme and involve coefficients, K , which depend on the flow solution. Two forms for this coefficient were used in computational examples. These forms were:

$$(K_{j,k}) = \alpha \left| u_{j+1} - u_j \right| \quad (1.12)$$

or

$$(K_{j,k}) = \alpha \frac{(P_{j+1} - 2P_j + P_{j-1})}{|P_{h+1} + 2P_j + P_{j-1}|} \quad (1.13)$$

where α is a constant which was chosen to be 0.25.

Geometry Construction

The wall movement

algorithm is expressed in terms of a design wall momentum flux and a transient wall momentum flux. Since the solid wall boundary condition is that the contravariant velocity \bar{V} is zero, the design wall momentum flux can be expressed in terms of the known wall pressure and the coordinate mapping coefficients which are to be determined.

$$\hat{G}_w^d = \left(\begin{array}{c} \eta_x p^d \\ \eta_y p^d \end{array} \right)_{i,0} \quad (1.14)$$

Since a trial geometry will not produce the design pressure distribution, a virtual wall momentum flux vector is formed from the predicted wall pressure and a virtual contravariant wall velocity.

$$\hat{G}_w^v = \left(\begin{array}{c} \rho u^v \bar{V}^v + \eta_x p \\ \rho v^v \bar{V}^v + \eta_y p \end{array} \right)_{i,0}^n \quad (1.15)$$

where

$$\bar{V}^v = \eta_x u^v + \eta_y v^v$$

\bar{V}^v represents a fictitious wall velocity needed to provide a balance between the current wall pressure and the design wall pressure. Equations (1.14) and (1.15) can be solved for u^v and v^v as:

$$v^v = \pm \sqrt{\frac{\eta_y^2}{\eta_x^2 + \eta_y^2} \frac{|p^d - p^n|}{\rho}} \quad (1.16)$$

$$u^v = v^v \frac{\eta_x}{\eta_y} \quad (1.17)$$

Since the wall boundary condition is always $\bar{v}_{i,0}^n = 0$, a correction wall velocity is calculated from:

$$\bar{v}_{i,0}^n = 0 = \left(\eta_t + \eta_x u^v + \eta_y v^v \right)_{i,0}^n \quad (1.18)$$

or

$$\left(\eta_t \right)_{i,0}^u = - \left(\bar{v}^v \right)_{i,0}^n \quad (1.19)$$

The correction wall velocity in the y direction is proportional to η_t , and the signs of u^v and v^v are chosen so that an excess predicted pressure is balanced by a positive wall velocity. For supersonic flow velocity, a similar correction scheme can be derived if the wall is assumed to be a piston whose velocity is chosen such that the excess pressure it creates will balance the wall pressure error.

An analysis of the wall movement scheme stability shows that the predicted wall velocity must be under-relaxed in order to provide overall stability of the algorithm. Consider for example the situation shown in figure (1.1.a) where the correct wall geometry has been obtained for all but one point, i. The calculated wall slope at point i and its neighbors using central differencing is also shown in figure (1.1.a). After the next time step, if the flow is supersonic, the new wall pressure will be higher than specified at point i-1 and lower than specified at point i+1. New wall

positions will be assigned as in figure (1.1.c). After the next time step, the calculated wall pressure will become lower than specified, causing the point i to move toward its correct position.

As may be seen, the assumed error at point i induces a position error at points $i-1$ and $i+1$. For the solution process to converge these induced errors must be smaller than the original position error. Referring to figure (1.1.a) and assuming small deflections, the induced error will be:

$$\Delta h_i = \Delta t k \sqrt{\frac{\Delta P}{\rho}} < \Delta h \quad (1.20)$$

where k is an under-relaxation factor.

Numerical experiments showed that, counter to intuition, the relaxation factor itself should be chosen to be proportional to $\frac{1}{c} \sqrt{\Delta P / \rho}$ for fastest convergence. Choice of this relaxation parameter eliminated small geometry oscillations which retarded global convergence. We may now write equation (1.20) as:

$$\Delta t k \frac{1}{c} \frac{\Delta P}{\rho} < \Delta h \quad (1.21)$$

For small deflections, linearized supersonic flow analysis gives

$$\frac{\Delta P}{P} = \frac{\gamma M^2}{\sqrt{M^2-1}} \theta = \frac{\gamma M^2}{\sqrt{M^2-1}} \frac{\Delta h}{2 \Delta x} \quad (1.22)$$

Equation (1.21) becomes:

$$\Delta t k \frac{1}{c} \left(\frac{P}{\rho} \right) \frac{\gamma M^2}{\sqrt{M^2-1}} \frac{\Delta h}{2 \Delta x} < \Delta h \quad (1.23)$$

or

$$k \frac{\Delta t}{\Delta x} c \frac{1}{2} \frac{M^2}{\sqrt{M^2-1}} < 1 \quad (1.24)$$

If we set the CFL number, $\frac{(\Delta t)}{\Delta x}(u+c)$, equal to one, we may rewrite this as:

$$K < 2 \frac{\sqrt{M^2 - 1}}{M^2(M+1)} \quad (1.25)$$

This analysis shows that the wall update scheme should be strongly under-relaxed in order to provide global stability when the flow is everywhere supersonic. K approaches zero slowly as M goes to one, $K = 0.2$ for $M = 1.02$, but this did not prove to be a problem in general calculation. A similar discrete node stability analysis for subsonic flow shows that the wall update scheme is also stable for subsonic flow. In general it was found numerically that the best value of K was about 0.2, and that the wall geometry should be corrected every 4 integration time steps. In earlier work (1.7) it was reported that an underrelaxation parameter of 0.01 was required.

An initial geometry error will propagate in all directions symmetrically and induce an error with a wavelength to $4\Delta x$ (see figure 1.1.d). These errors of wavelength $4\Delta x$ were eliminated by introducing a wall position smoothing:

$$y_i = y_i + k_s \left(|y_{i+1} - y_i| (y_{i+1} - y_i) + |y_{i-1} - y_i| (y_{i-1} - y_i) \right) \quad (1.26)$$

A value of k_s equal to 0.2 was found to be sufficient to eliminate these errors. However, the correct geometry for arbitrary input pressure may not be as smooth as demanded by equation (1.26) and a real position error may be introduced. A careful balance must be maintained between smoothing out the $4\Delta x$ wavelength errors and producing a geometry which does not fit the specified pressure geometry but is as smooth as requested.

Since a blade position error is eliminated by moving neighboring wall points, the present inverse scheme is not effective at node points next to geometrically constrained points such as leading or trailing edge and maximum

or minimum thickness constraint violation. The wall movement at these points will be constrained by the blade smoothing algorithm so that smooth blade shapes will be produced, but the specified wall pressure will not necessarily be achieved at these points.

Inflow-Outflow Boundary Formulation

As might be expected, we found that the overwhelming factor determining the number of iterations required for convergence of direct or inverse solutions was the physical size of the computational domain. When relatively simple, one-dimensional, inflow-outflow treatments were used, it was required to place the computational boundaries two to three chord lengths upstream of the cascade and one chord downstream in order to insure accuracy in the computed solution. Even when these boundaries were placed three chord lengths away, a spurious reflected wave was introduced at the upstream boundary by the approximate boundary condition. When using the two-dimensional, "non-reflecting," boundary treatment described below, the computational boundary could usually be moved in to approximately 0.2 chords upstream of the cascade with an order of magnitude reduction in computer time usage.

When subsonic, inflow boundaries are encountered in Euler flow simulations, some flow quantities must be specified as boundary conditions and some must be computed as part of the flow solution. For consistency as well as accuracy, the inflow boundary formulation was manipulated so that the entering fluid stagnation pressure and temperature remained constant at all times. The fluid velocity and its derivatives were determined as part of the boundary formulation.

If the inflow boundary quantities are assumed to be periodic, the \mathcal{L}_η operator, equation (1.11) may always be executed without further boundary conditions. Execution of the \mathcal{L}_ξ operator, however, requires an inflow boundary formulation. The scheme chosen was a locally, one-dimensional method of characteristics in the x direction. The fluid equations for an x split operator are:

$$\partial_t(\rho) + \partial_x(\rho u) = 0 \quad (1.27)$$

$$\partial_t(\rho u) + \partial_x(\rho u^2 + p) = 0 \quad (1.28)$$

$$\partial_t(\rho v) + \partial_x(\rho uv) = 0 \quad (1.29)$$

If we assume that the boundary is sufficiently far upstream that any waves may be considered as isentropic "shocks" or compressions, equation (1.29) may be replaced by the statement that the entropy or stagnation pressure is constant in the upstream region. Equations (1.27) and (1.28) may then be rewritten in a characteristic form:

$$u + \frac{2}{\gamma-1} c = J^+ = \text{constant along} \quad (1.30)$$

$$\frac{dx}{dt} = u + c$$

$$u - \frac{2}{\gamma-1} c = J^- = \text{constant along} \quad (1.31)$$

$$\frac{dx}{dt} = u - c$$

For the cascade simulations, the value carried by J^+ characteristic is specified, and the value carried by the J^- characteristic is calculated from the interior point solutions. The J^- characteristic value was calculated by interpolation back to the point that a J^- characteristic intersecting the upstream boundary would originate, see figure (1.2).

If the J^+ characteristic value and an interpolation procedure for the J^- characteristic value is specified, equations (1.30) and (1.31) are two simultaneous equations for the axial velocity and the fluid speed of sound. The tangential velocity is found from the assumption of known stagnation pressure and temperature as:

$$v^2 = c^2 \left(\frac{2}{\gamma-1} \right) \left| \left(\frac{c_{stag}}{c^2} \right)^2 - 1 \right| - u^2 \quad (1.32)$$

where c_{stag} is the speed of sound at stagnation conditions.

It is important to note that specification of the J^+ characteristic value does not directly specify either the mass flow rate through the cascade or the average inlet flow angle. These quantities are determined through interaction of the inflow boundary, the blade entrance region geometry and the exit static pressure of the cascade. The J^+ characteristic value may be regarded as a free parameter which may be chosen to generate an infinite variety of solutions with different mass flow rates and/or different inlet flow angles.

Numerical experiments showed that the fluid static pressure in the downstream region became uniform within $3/4$ to 1 chord length behind the blade exit plane. A similar characteristic formulation was applied at the exit boundary but with the static pressure specified rather than the J^+ characteristic value. A J^+ downstream running characteristic value was calculated by interpolation of the interior point solution and the tangential velocity calculated from a conservation of stagnation pressure condition.

The efficiency of these inflow-outflow formulations is illustrated in figures (1.3) and (1.4). In figure (1.3), a computation with the inflow boundary placed several chords upstream is shown in terms of a Mach number contour plot. The upstream running bow waves are clearly shown. Accuracy of the upstream solution may be checked by looking at the undisturbed waves generated on the suction surface entrance region. On such an upstream running wave path, the flow angle always should be equal

to the suction surface flow angle, see figure(1.5). For this solution, the upstream flow angle is 67.88 degrees and the corresponding suction surface angle is 67.98 degrees. In figure (1.4) a computation with the inflow computational domain truncated 0.2 chords upstream is shown. The change in the airfoil lift from the original domain is 0.02%, and the upstream running wave strength and flow angles are nearly identical. The number of iterations to convergence was reduced from 2000 to 400 and the computation time from 70 minutes to 6.5 minutes by using the truncated domain and the maximum value of the steady state residual,

$$SSR^n = \partial_{\xi} \hat{F}^n + \partial_{\eta} \hat{G}^n + \partial_{\xi} \hat{q}^n + \partial_{\eta} \hat{q}^n \quad (1.33)$$

at any node point is approximately 1×10^{-5} .

Trailing Edge Flow Model

These calculational examples show a distinct wake region in which a considerable but erroneous stagnation pressure loss is generated. This wake region is generated by the difference in passage shock strength on the pressure and suction surfaces. The shock stagnation pressure ratio on the pressure surface is 0.93, while the suction surface ratio is 0.68. An ideal, sharp trailing edge flow pattern should have a slip surface across which the velocity varies but the static pressure is constant. This situation requires that the trailing edge Mach number be about 0.70 on the pressure surface side and about 0.2 on the suction surface side in order that the static pressures at the blade trailing edge match. An exact Euler flow simulation would propagate such a slip surface unchanged, but this inviscid wake tends to be quite unstable. Due to the higher stagnation pressure loss on the suction surface and the fact that the static pressures

are expected to be equal, the velocity profile must have a minimum on the suction surface and an inflection point in the wake. It is well known (1.10) that flows with such velocity profiles are unstable.

In our numerical calculations, we generally found that the ideal flow situation did not appear, but rather, a closed, recirculating flow bubble tended to appear near the suction surface. This bubble has a strong influence on the flow solution downstream of the blade row but only a minor influence on the flow solution upstream of the passage shock which is the primary objective of the inverse or design process.

The computed solution shown in figure (1.3) was calculated using a viscosity coefficient, $K_{j,k}$, which itself is dependent on velocity differences, see equation (1.12), and the damping terms in the wake region are comparable in magnitude to those inside the passage shock. The erroneous wake stagnation pressure loss is greatly reduced when a viscosity coefficient calculated from static pressure differences, see equation (1.13) is used, and all remaining computational examples were computed using these artificial viscosity coefficients. It was not possible to reduce the magnitude of these damping terms to zero as this usually led to a numerical instability in the wake region. Explicit numerical schemes such as MacCormack's method have neutral stability points, in a linear sense, at stagnation points as well as sonic points.

Even though the trailing edge region flow details did not significantly influence the flow solution in front of the passage shock, the flow solution downstream of the passage shock near the suction surface and blade lift were sensitive to the artificial viscosity formulation. The major criticism of the present results is not the appearance of the recirculating region,

which appears to be an inevitable result of the inviscid flow assumption, but rather the dependence of the blade lift on the form of the artificial viscosity terms. Further work, including comparisons with fully viscous flow calculations, is underway to understand the full implication of the inviscid flow model.

Computational Examples and Discussion

In order to demonstrate the efficiency of the inverse technique, a sample design problem was attempted. An initial geometry, multiple circular arc with maximum thickness of 5.4% was selected, and an initial solution for an inlet Mach number of 1.52 was computed. The cascade achieved a static pressure ratio of 2.25 with a stagnation pressure loss coefficient, $\Delta P_t/P_T$, of 0.1555. The stagnation pressure loss coefficient for a normal shock at the far upstream Mach number would be 0.077. Mach number contours and blade static pressure distribution are shown in figures (1.6a) and (1.6b). This cascade design is similar to many supersonic cascade blade sections in that the stagnation pressure loss is much larger than would occur if the blade pressure rise were achieved with a normal shock at the far upstream Mach number.

This high stagnation pressure loss originates in the monotonic suction surface expansion, from Mach number 1.52 to 2.08, which is characteristic of circular arc blading. Attempts to limit this expansion require a thicker blade section, and it is difficult to design a thicker section which will pass the same mass flow rate. Thus the constraints on the design problem attempted were to pass the same mass flow rate, to have the same static pressure ratio, and to have the same gap to chord ratio. These constraints are representative of those encountered in a development or preliminary design situation.

The target pressure distribution selected is shown in figure (1.7). On the suction surface, the passage shock was moved forward and weakened. On the pressure surface, the bow shock was strengthened, and the second shock eliminated. The exact position of neither shock was specified. In order to maintain the same mass flow rate, the suction surface entrance region geometry was retained. Figure (1.7) also shows the degree to which the

target blade pressure distribution was obtained, and figure (1.8) shows the Mach number contours and blade shapes obtained. The inlet flow quantities and exit static pressure were retained. The Mach number in front of the passage shock has been reduced all across the passage with the stagnation pressure loss coefficient reduced to 0.085. This value is 55% of the original value and only 10% larger than that required by a normal shock at the upstream Mach number of 1.52. As might be expected, the maximum blade thickness increased to 10.0% from 5.4%.

Figures (1.7) and (1.8) are excellent examples of the influence on the overall flow solution of the trailing edge flow pattern. The slip line originates on the suction surface rather than at the trailing edge, and the passage shock near the suction surface is a strong oblique one rather than a normal

The stagnation pressure loss at the design point is influenced by the detailed trailing edge flow pattern since the shock angle is influenced by the shape of the recirculating region. The effect of the wake region is greatly reduced if the outflow static pressure is raised. The original outflow static pressure boundary condition was retained for comparison purposes, but the design point of a reduced stagnation pressure loss blade should be at a higher exit pressure.

The previous example illustrates that an existing blade shape design can be improved but does not illustrate the extent to which passage Mach number distributions may be controlled. If the requirement that the original blade gap to chord ratio be retained is eliminated, a blade design of substantially improved performance may be generated. A new target pressure is shown in figure (1.9). On the suction surface the pressure distribution is built up from the requirements that a weak oblique bow shock exists, that the original blade entrance region be retained (in order to

retain the original inflow conditions), that the flow pre-compress to a Mach number of 1.3 and that the exit pressure be achieved through a strong oblique shock. The original pressure surface geometry was retained, and the gap to chord chosen such that the original inflow conditions could be retained. The design exit to inlet static pressure ratio was increased to 2.50 from 2.25.

The resulting blade shapes and Mach number contour lines are shown in figure (1.10). The stagnation pressure loss, $\Delta P_t/P_t$, has been reduced to 0.10, and the maximum Mach number reduced to 1.62. This blade design shows clearly that the inverse technique has evolved to the point that it can be used to create blade shapes with controlled Mach number distributions.

While it is not surprising that low stagnation pressure loss blades can be designed for single operating points, it appears that the present design might have good off-design performance. The original blade design had an inlet to exit static pressure rise of 2.25, but the present design can be pushed to 3.21 before the bow shock becomes normal at the passage entrance. The flow through the original blade breaks down completely at a pressure ratio of 2.4. The predicted stagnation pressure loss coefficient is plotted in figure (1.11) for several row static pressure ratios. The minimum loss of 0.10 occurs at a pressure ratio of 2.5 and good performance is maintained for the range from 2.4 to 2.6. For reference, the performance of the original blade row is also illustrated in figure (1.11).

These computational results for a range of off-design conditions while encouraging and interesting must be considered as only preliminary since the effects of viscosity are neglected in the present analysis. Efforts are presently underway to duplicate these calculations with a fully viscous analysis and to include viscous effects in the inverse analysis. These calculations will also attempt to determine the value of the gap to chord ratio which leads to the best off-design performance.

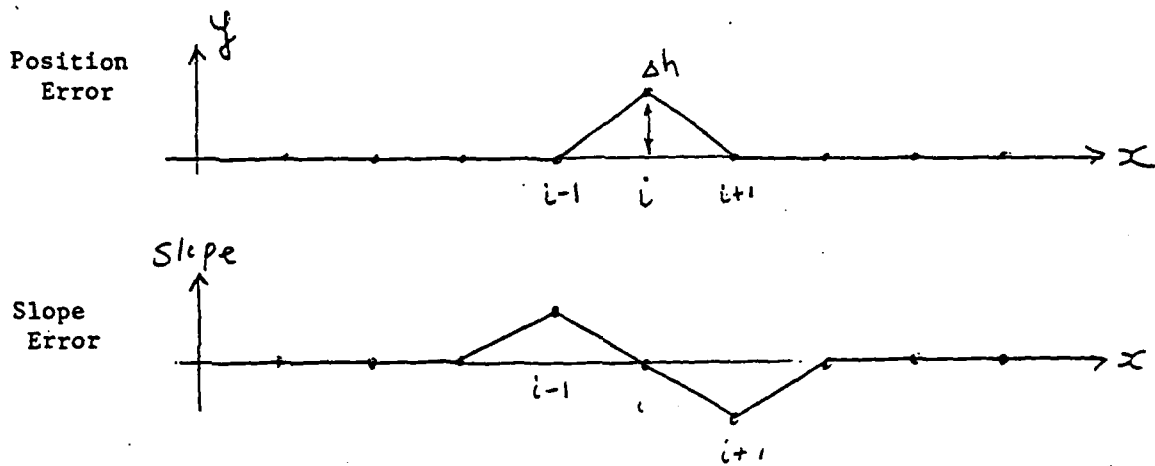


Figure 1.1a -- Idealized Initial Geometry Error

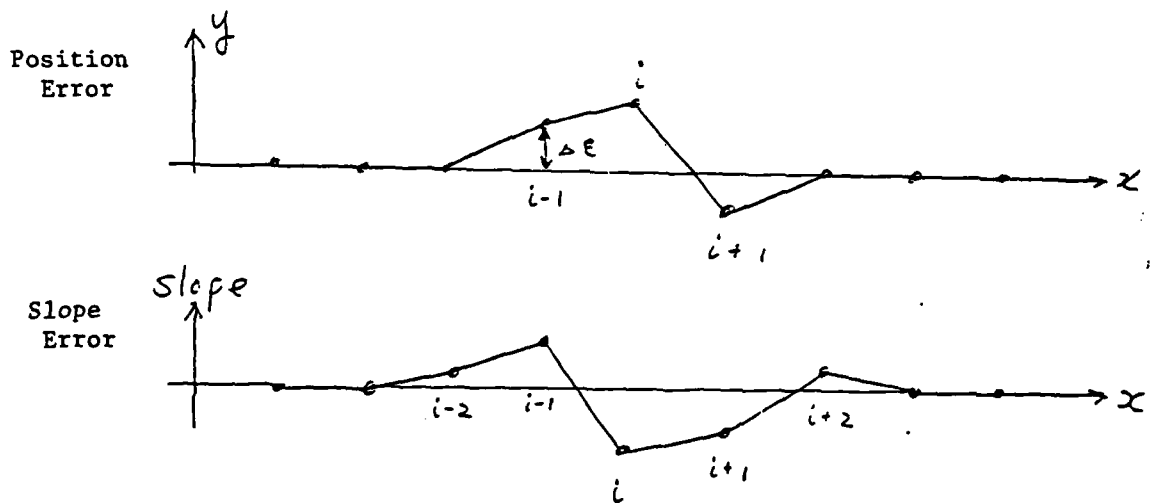


Figure 1.1b -- Idealized Intermediate Geometry Error

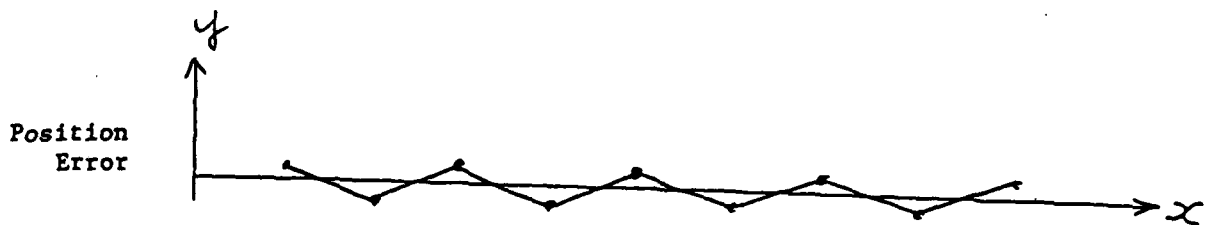


Figure 1.1c -- Idealized Final Geometry Error

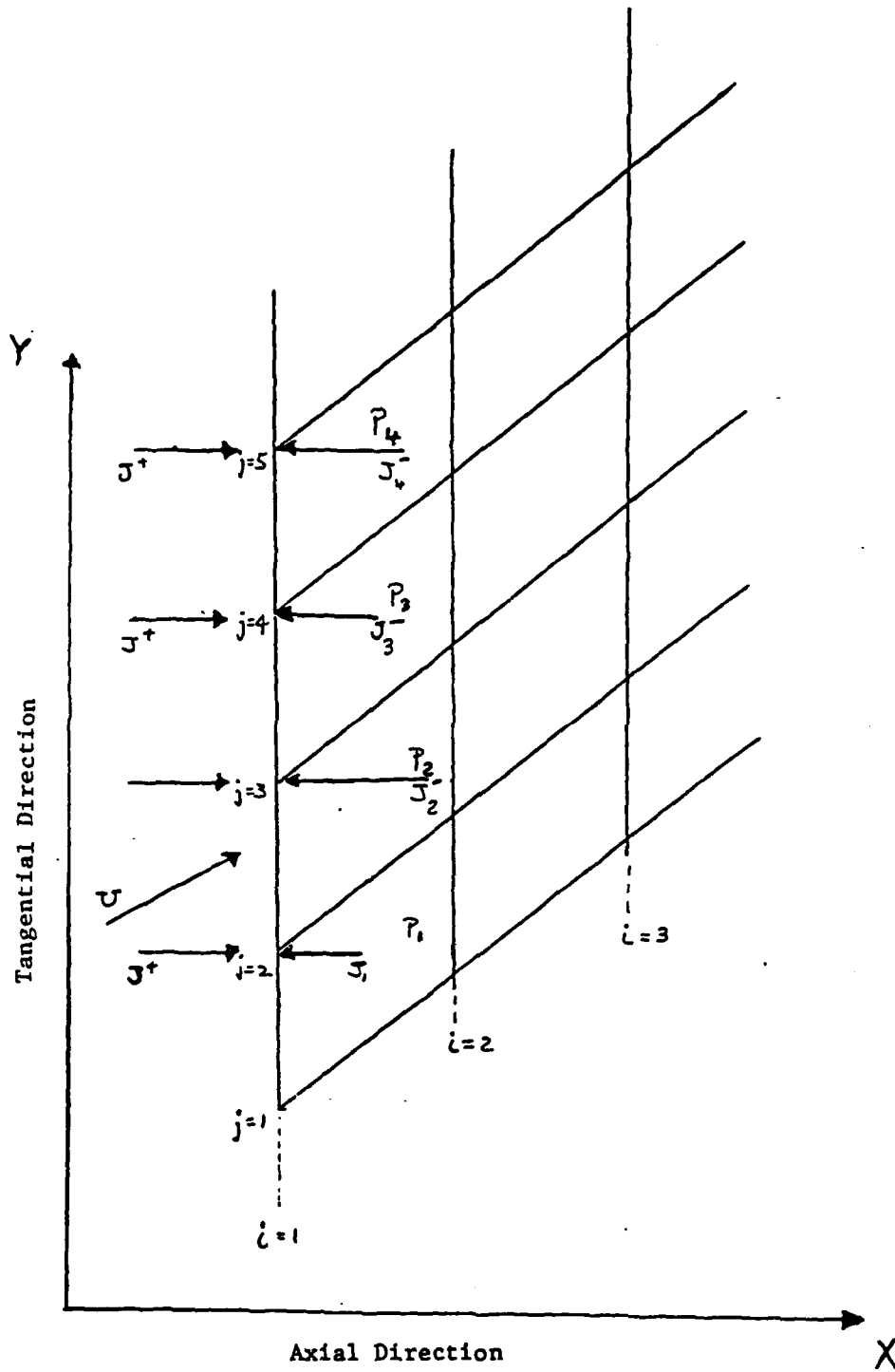


Figure 1.2 -- Assumed Incoming and Outgoing Characteristic Wave Pattern at Inflow Boundary

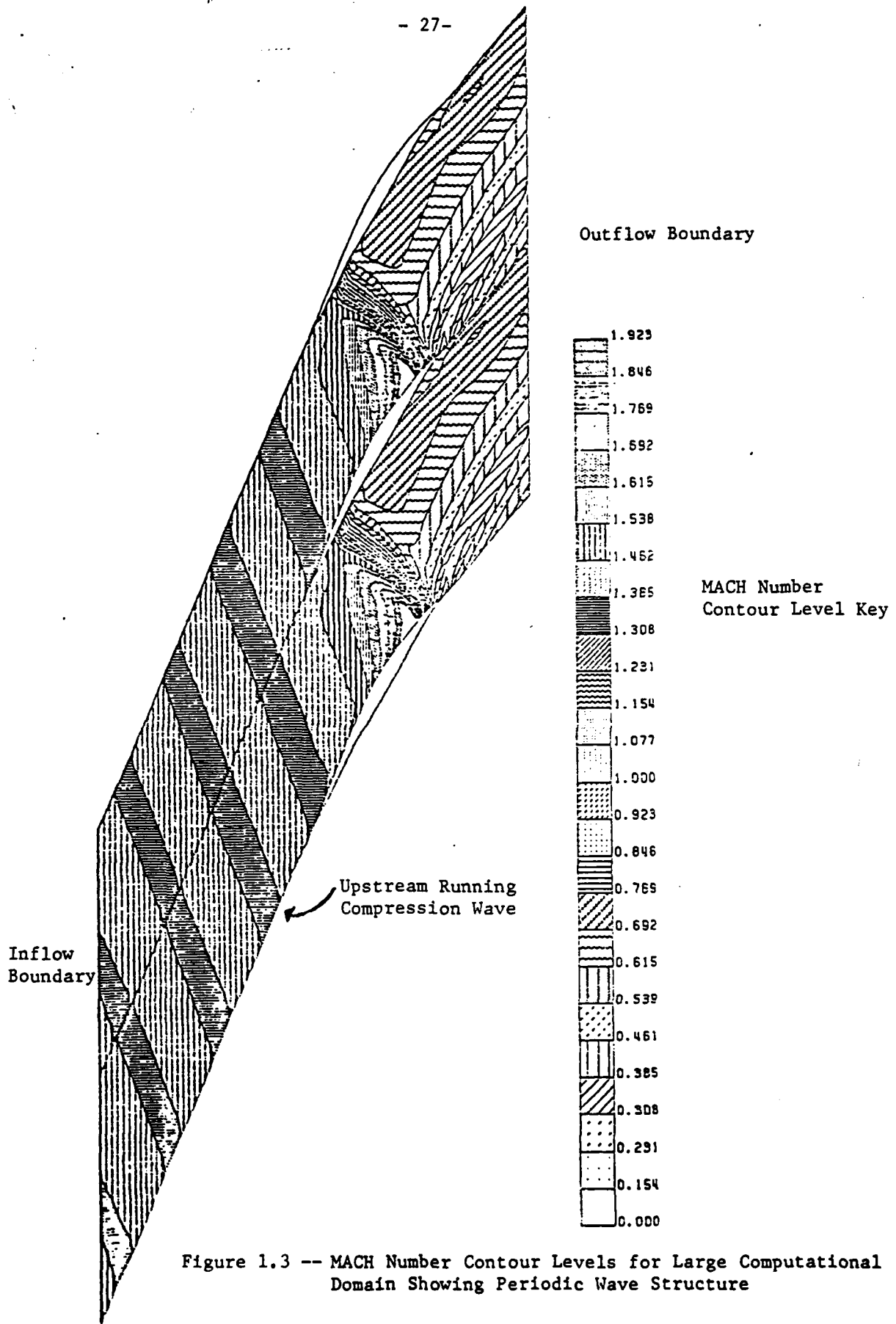


Figure 1.3 -- MACH Number Contour Levels for Large Computational Domain Showing Periodic Wave Structure

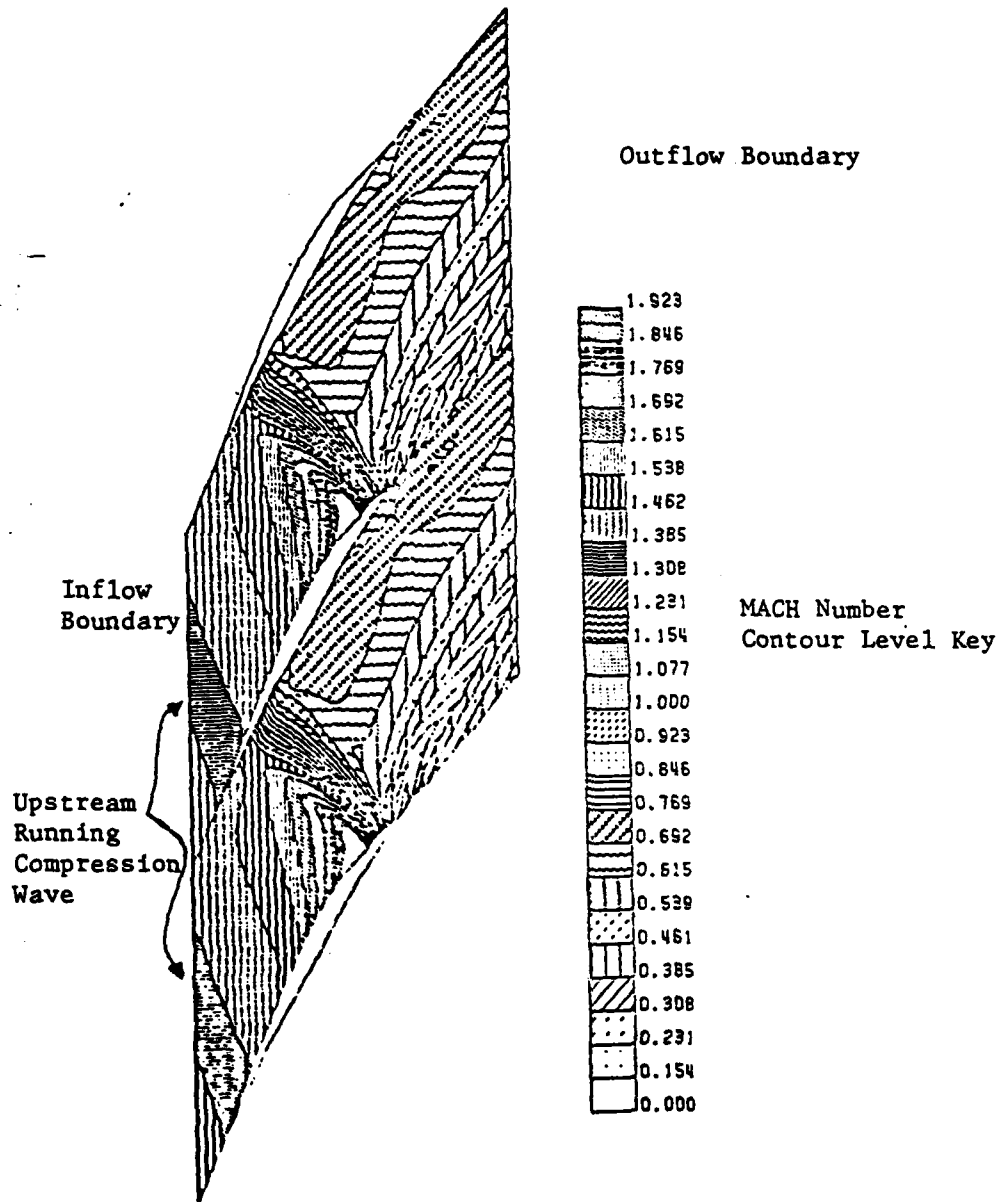


Figure 1.4 -- MACH Number Contour Levels for Truncated Computational Domain

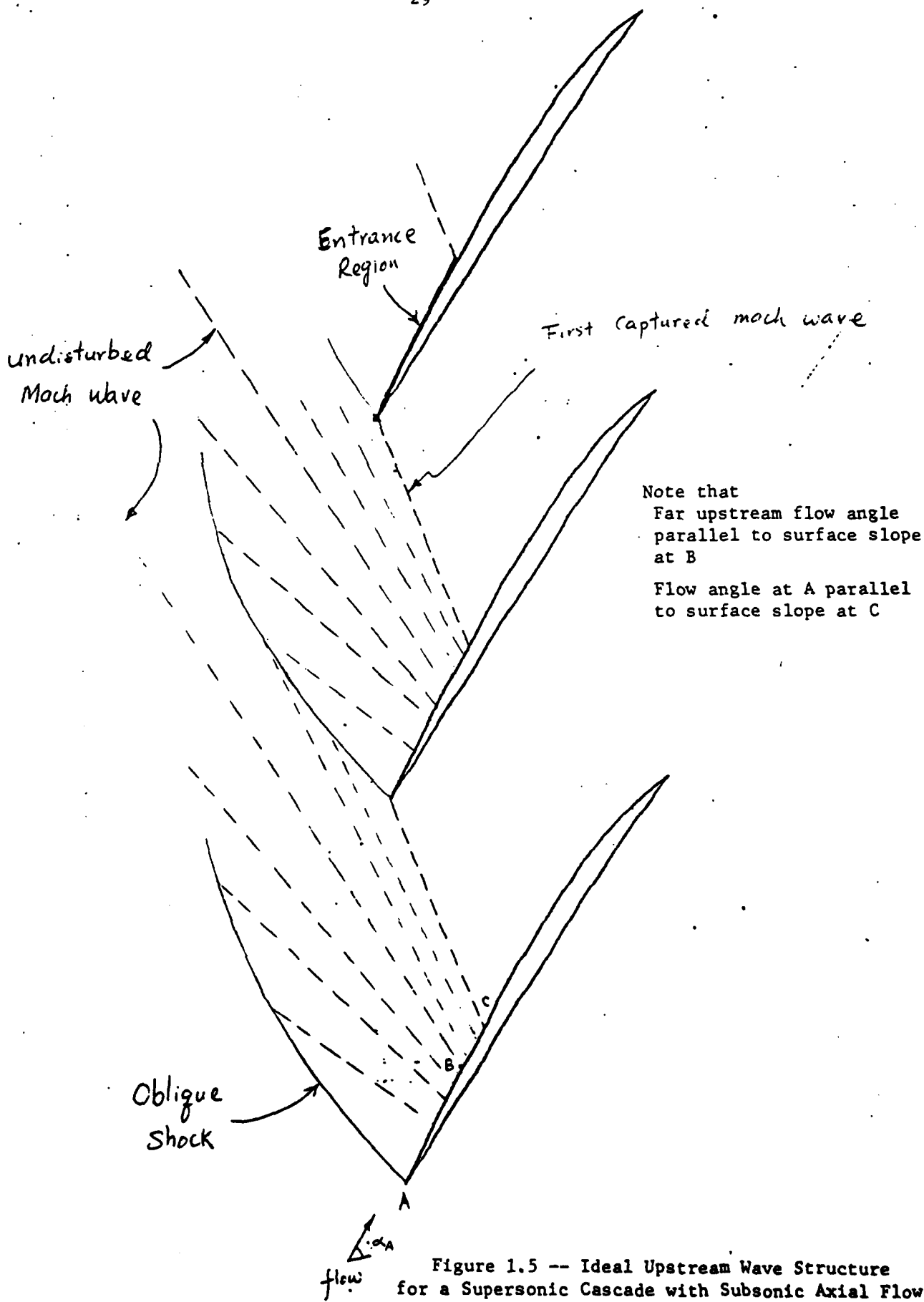


Figure 1.5 -- Ideal Upstream Wave Structure for a Supersonic Cascade with Subsonic Axial Flow

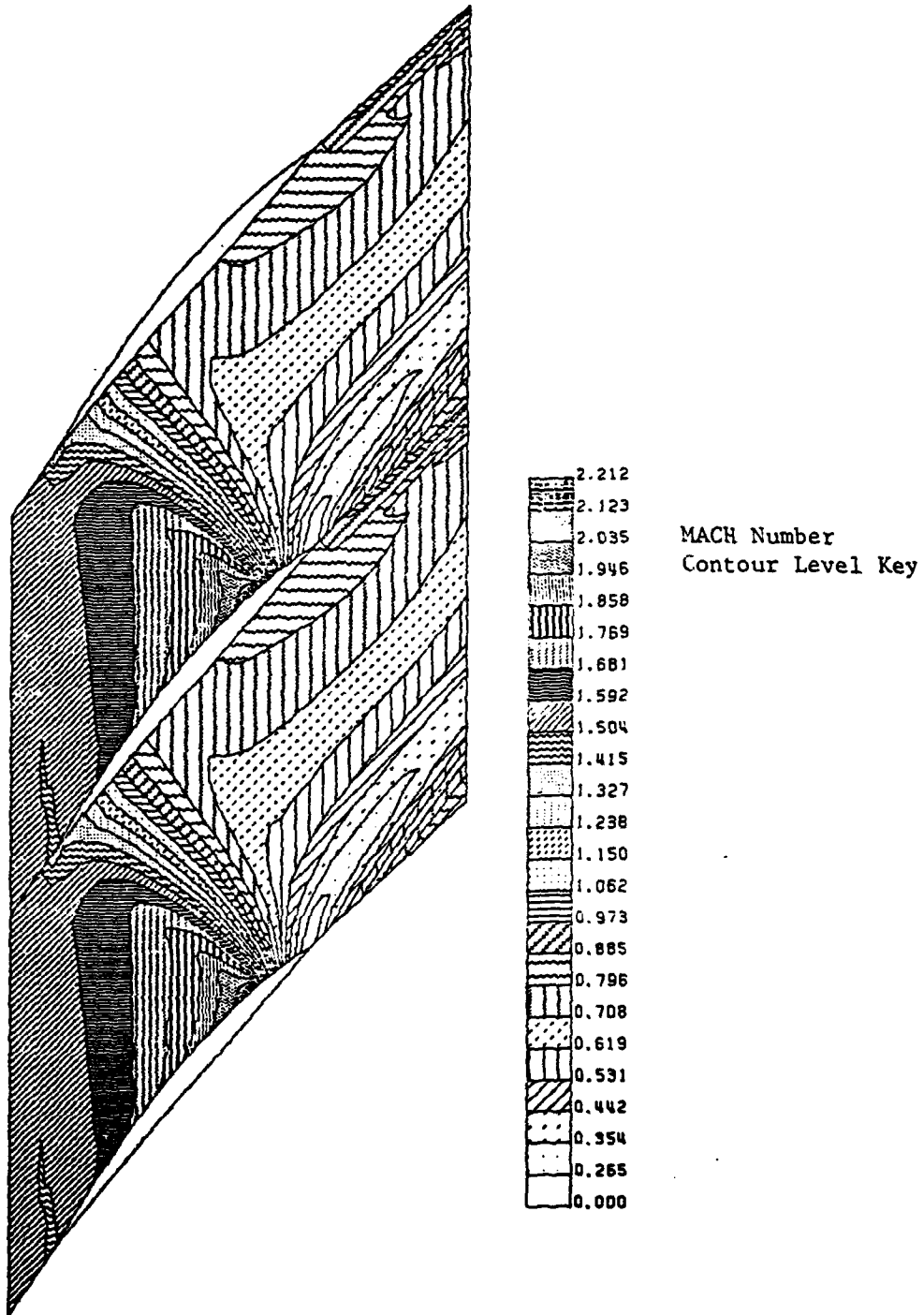


Figure 1.6a -- MACH Number Contour Levels for Original Multiple Circular Arc Cascade

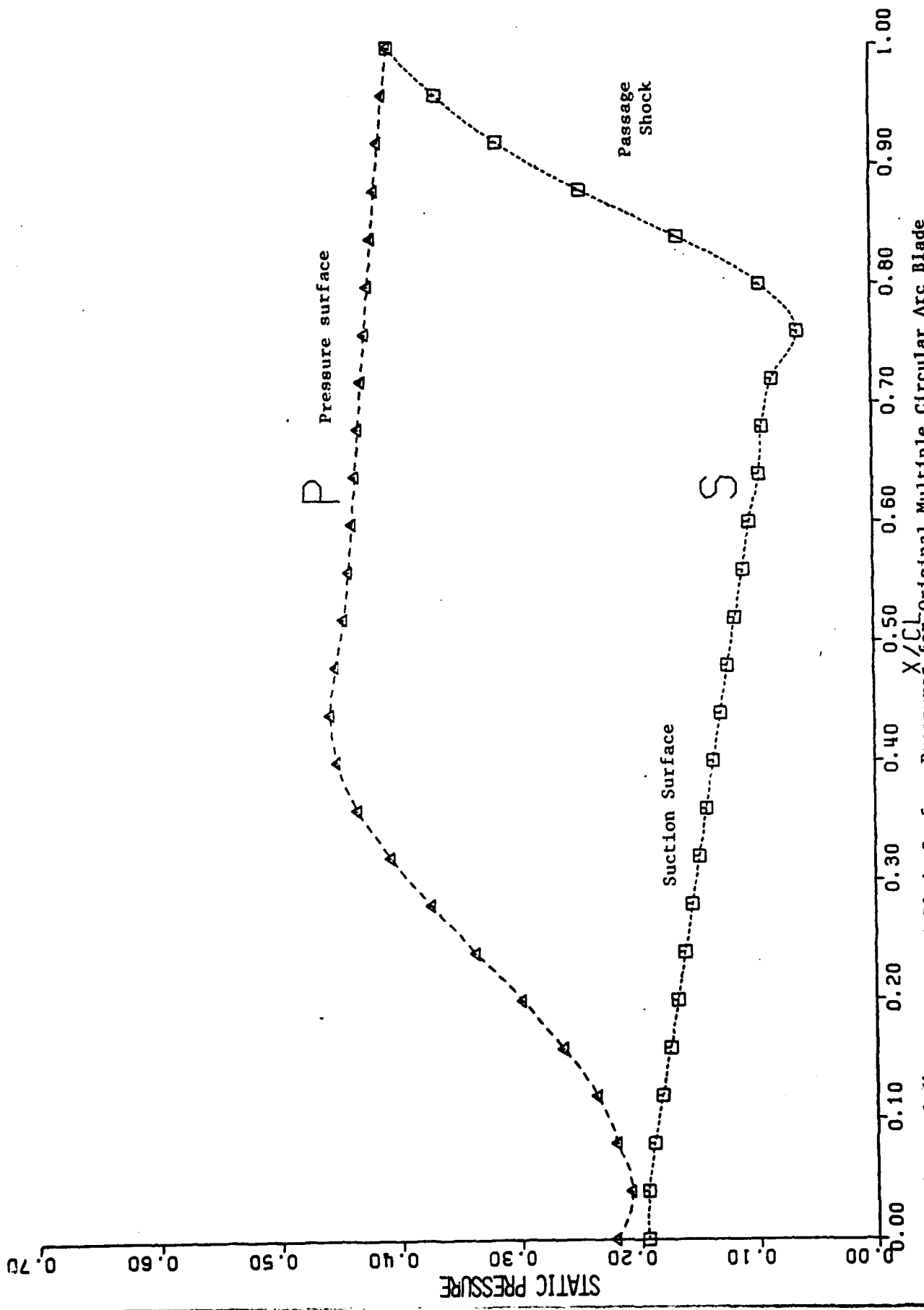


Figure 1.6b --- Computed Blade Surface Pressures for Original Multiple Circular Arc Blade

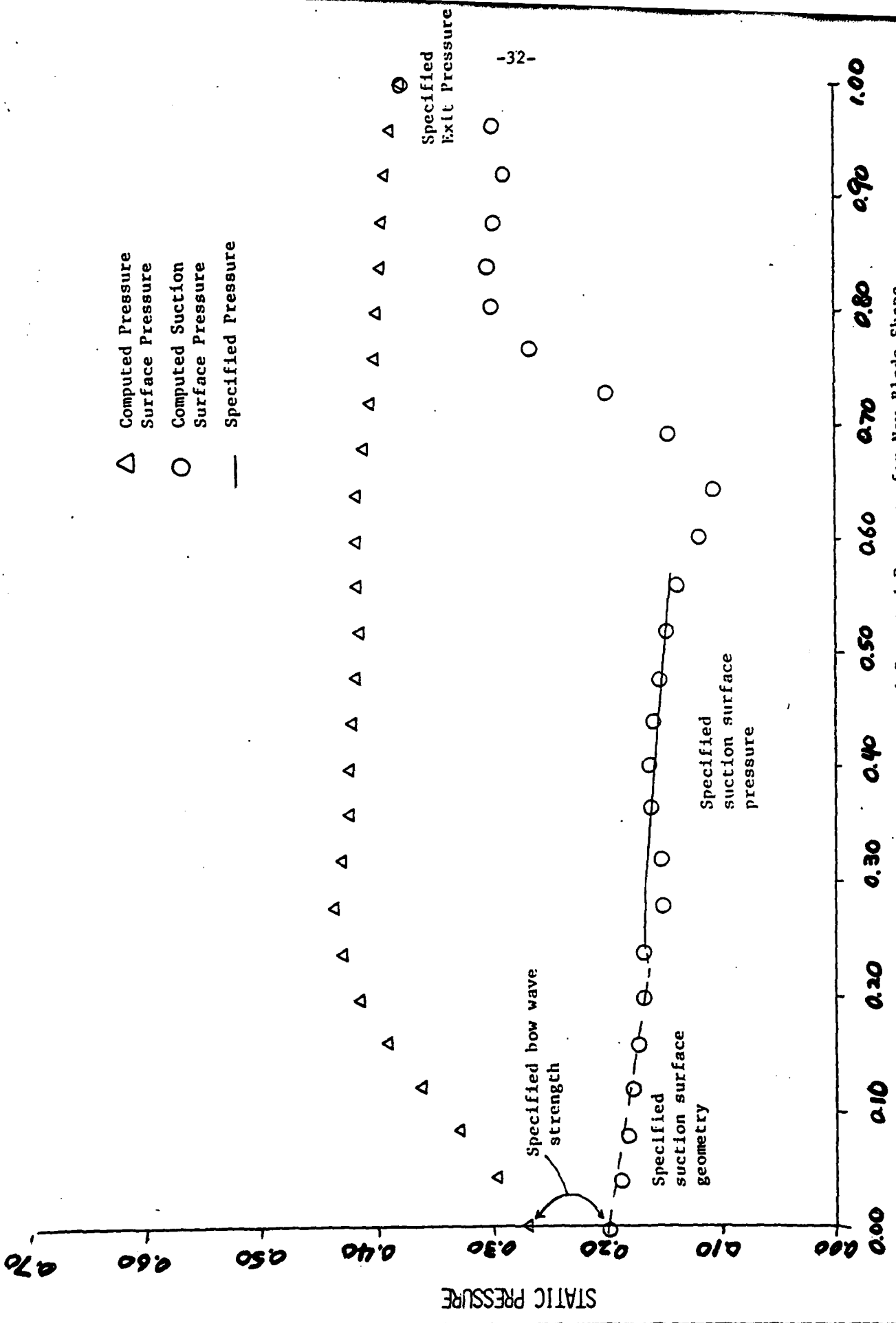


Figure 1.7 -- Blade Pressure Distribution Target and Computed Pressure for New Blade Shape

X/cL

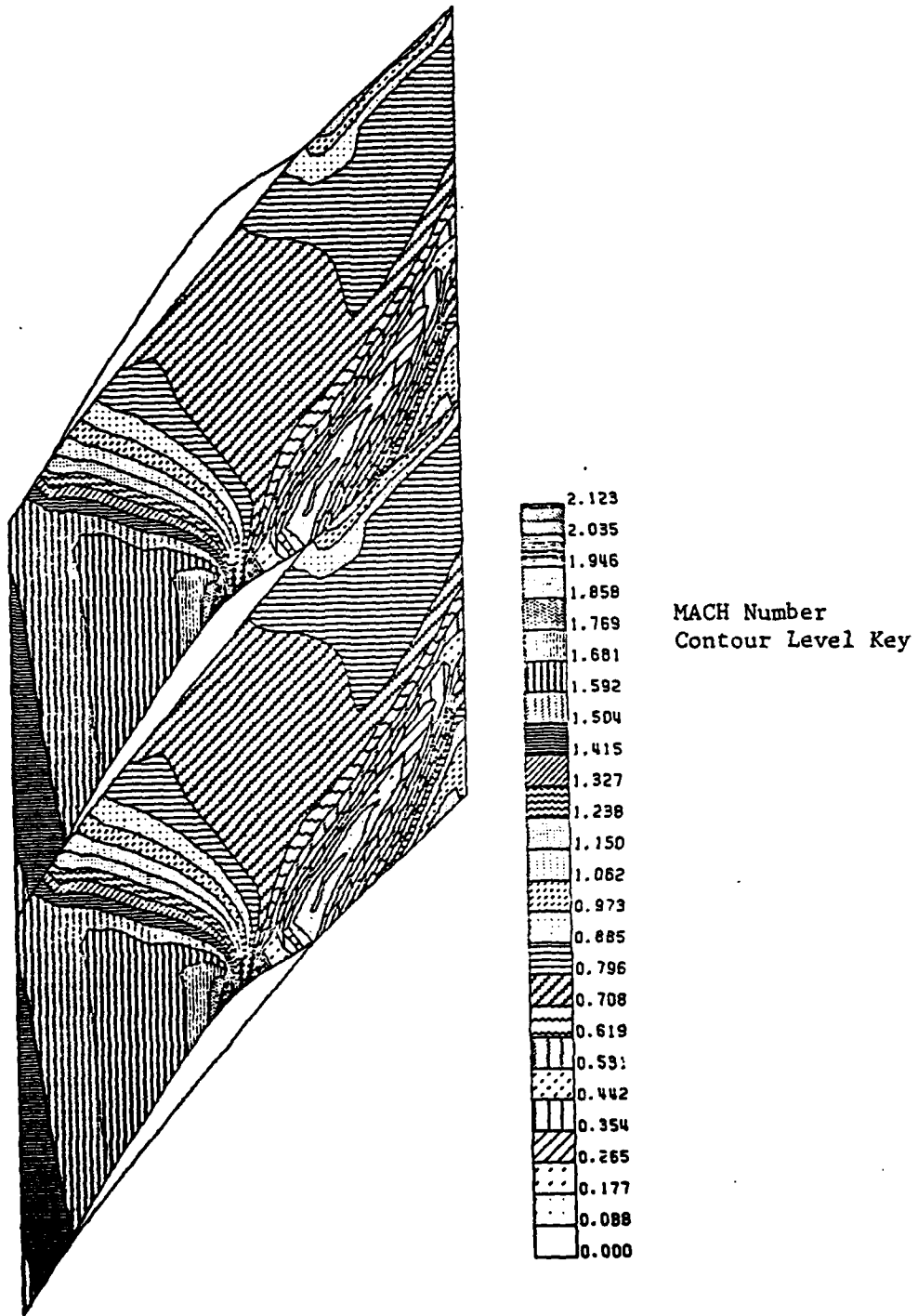


Figure 1.8 -- MACH Number Contour Levels for Reduced Stagnation Pressure Loss Blade Shape

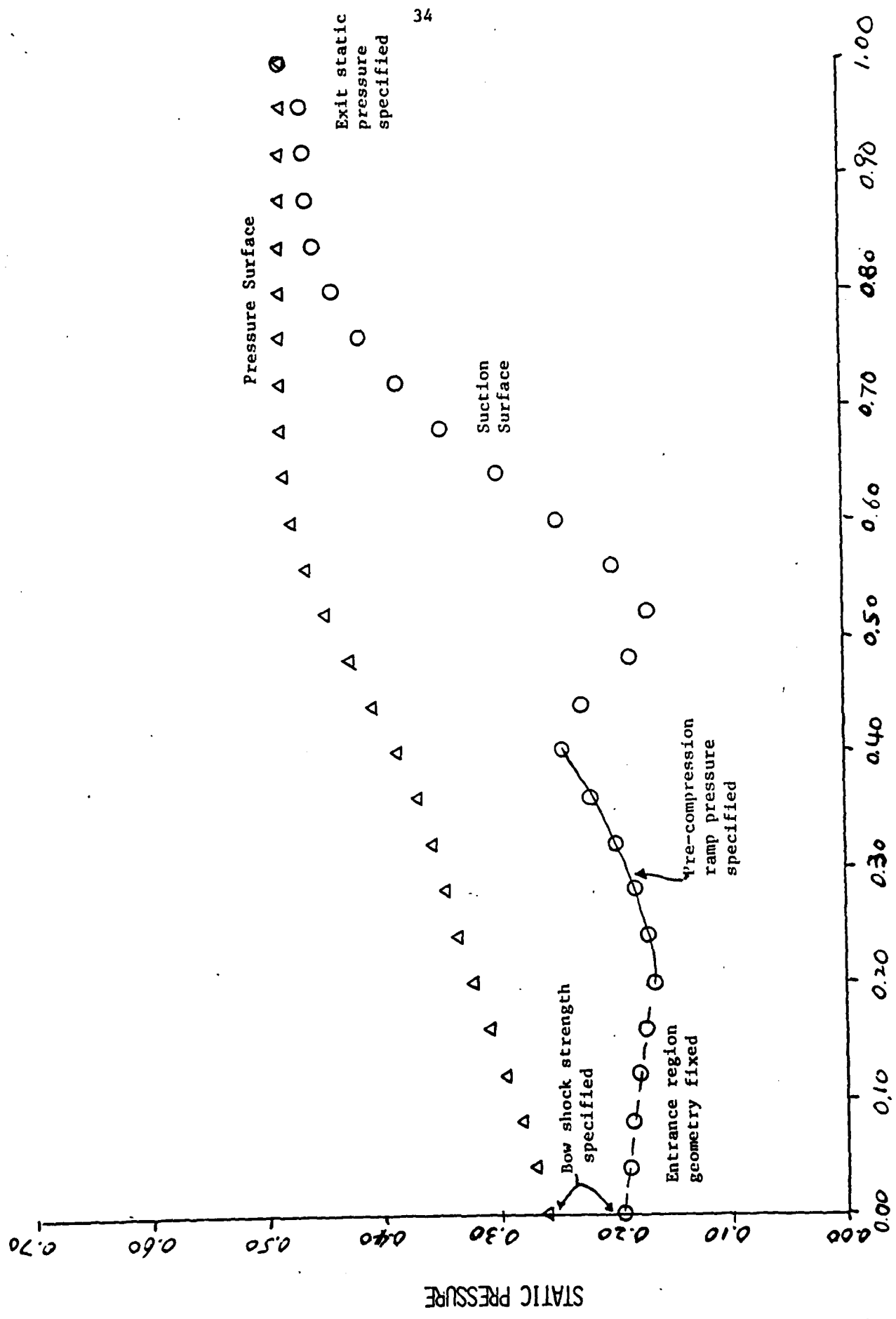


Figure 1.9 -- Target and Resultant Blade Pressure for Pre-Compression Type Design

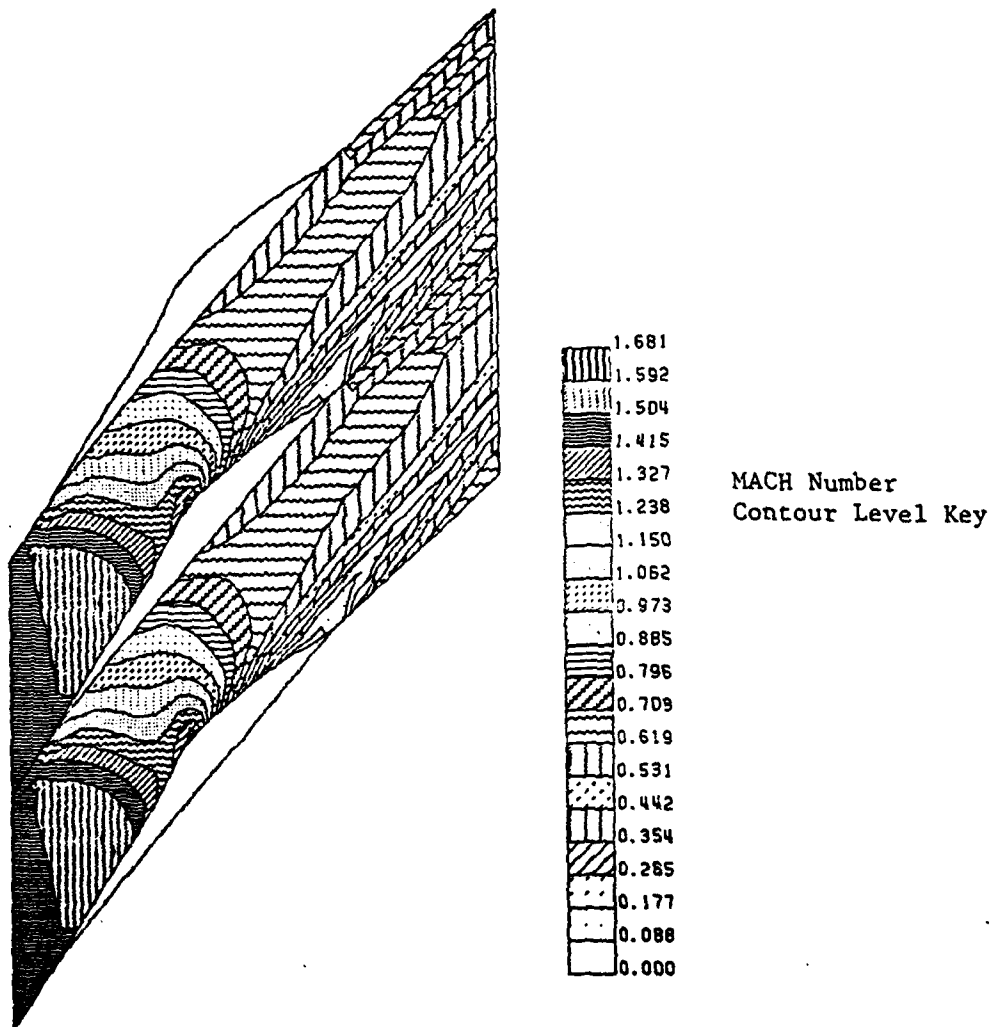


Figure 1.10 -- MACH Number Contour Levels for Pre-Compression Type Design

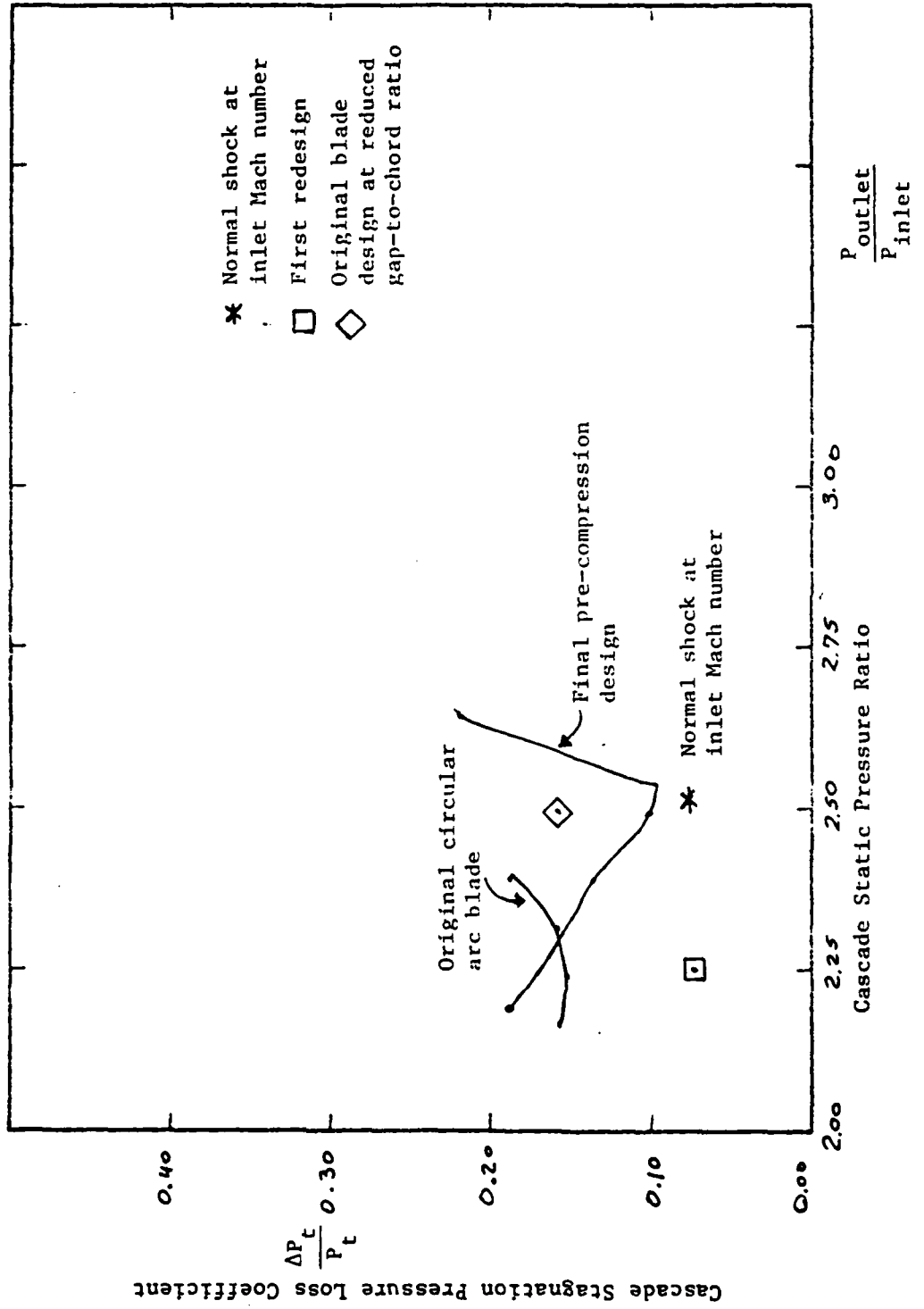


Figure 1.11 -- Computed Stagnation Pressure Loss Coefficient for a Range of Row Static Pressure Ratios

ADVANCED MEASUREMENTS

The MIT Gas Turbine Laboratory has developed an unique capability for measuring the time dependent three-dimensional flow field of transonic compressors. Using fast response semi-conductor diaphragm pressure transducers mounted on traversing probes, the time dependent flow fields upstream and downstream of the blade rows can be mapped. This had been done previously for the MIT stage and a NASA 20-inch diameter high aspect ratio compressor stage.^{1.11} In addition, as described below, the AFAPL 17-inch diameter through-flow stage is currently being studied. One aim of this data is to identify loss regions and mechanisms in transonic compressor stages.

In all of the above aerodynamic measurements, the efficiency of each stage was obtained by direct measurement of stagnation pressure together with a calculated stagnation temperature. This temperature was found using the Euler equation and the measured tangential Mach number. This calculation rests on the assumptions: 1) that the flow is steady in coordinates rotating with the rotor, and 2) that there is no exchange of energy between stream-tubes (in rotor coordinates) due to work done by viscous forces or due to heat transfer. Both of these assumptions are known from qualitative observations to be not completely correct, but in the absence of a direct measurement of the stagnation temperature at the rotor exit it has not been possible to relax the assumptions in treating the details of the rotor outflow.

For this reason, we have started work on a technique to measure the fluctuating total temperature in the Blowdown Compressor. This can be done by using an aspirating anemometer probe specially designed to be used in the Blowdown Compressor Facility. The general principle of the probe is as follows. The aspirating probe has a sonic nozzle. The mass velocity, (ρV) at the nozzle throat, is thus given by:

$$\rho V = P_T \sqrt{\frac{\gamma}{RT_T}} \left[\frac{M}{\left(1 + \frac{\gamma-1}{2} M^2\right)^{(\gamma+1)/2(\gamma-1)}} \right] \quad (1.34)$$

where:

- P_T is stagnation pressure
- T_T is stagnation temperature
- R is gas constant
- M is Mach number
- γ is ratio of specific heat

If the nozzle is choked and the gas concentration is uniform, then (ρV) depends only on the ratio $P_T/\sqrt{T_T}$. By using two hot wire sensors operated at constant temperature mode and at different overheat ratios, two signals are obtained from which the stagnation pressure and stagnation temperature can be resolved through a set of calibration curves. (As a consistency check, a total pressure probe can be used to measure the same flow field and compare to results obtained from the aspirating probe.)

During the past year we have carried out several steps toward the construction of a suitable probe. First an existing single wire aspirating probe has been tested in a known unsteady flow. This flow was created by the vortex street from a circular cylinder. The cylinder could be heated so that velocity and/or temperature fluctuations could be generated. A sketch of the probe is shown in Fig. 1.12A. As an example of the experimental results, Fig. 1.13 shows data taken behind a 0.010 inch circular cylinder. It can be seen that the probe gives a significant response to a vortex street with shedding frequency of 8 KHz.

Although the concept thus seemed promising it was found that the large L/D ratio of this existing probe gave rise to a thermal boundary layer and that the desired frequency response for temperature fluctuations could not

be achieved. To alleviate this problem the probe was redesigned to have an L/D of approximately two. A sketch of this probe is given in Figure 1.12E. Experiments with the redesigned probe have shown that we can now detect temperature signals with adequate response.

We have now also built a "model" of this probe which is twice scale in order to quantitatively examine the functional dependence of probe mass flow versus total pressure. This geometry is shown in Figure 1.14. This can be seen using the probe in a steady jet of known stagnation pressure. If the design concepts are correct Equation (1.34) and the King's law relationship for the hot wire imply that the relationship between jet total pressure and wire voltage should be essentially $V^2 \sim \sqrt{P_T}$. This is shown plotted in Figure 1.15. (In the figure the exponent used for P_T is actually 0.45 rather than 0.5 suggested by Collis and Williams^{1.12} It can be seen that the desired functional relationship is obtained within experimental uncertainty.

On the basis of the frequency response tests and the steady state model probe performance, we are thus reasonably confident that the actual dual wire probe, which we are starting to construct, will give us useful information on the time resolved temperature field in the Blowdown Compressor stage.

Measurements of AFAPL HTF Stage

Work has continued on testing of the AFAPL HTF Stage. High frequency response measurements have been taken in order to obtain total and stator pressure and tangential and radial flow angles. The reduction of this data is not yet complete, however.

Two problems have arisen in connection with this testing. The first concerns the new 4 way cylinder probe, which was constructed as a replacement for the 5 way sphere probe (Ref. 1.13). The cylinder geometry was chosen to reduce the size of the probe in the azimuthal direction in order to increase spatial resolution and also to permit incorporation of a third generation silicon pressure transducer with reduced thermal sensitivity. The new probe is greatly superior in this regard, exhibiting essentially no thermal drift. It does seem to be sensitive to transverse acceleration, however. This is a new problem with these probes and work is presently underway to resolve it.

The second problem is unique to the HTF Stage installation in the Blowdown Tunnel. The problem is that the stage operating point moves approximately 2-3% during a blowdown test. This is due to the relatively high work and low inertia of the HTF Stage. In other words, work is extracted (from the rotor) at such a high rate that the rotor, which is driven only by its own inertia, shows down faster than the square root of inlet total temperature ($\sqrt{T_{inlet}}$) drops. One solution to the problem is to reduce the inlet total pressure. This was done as much as was consistent with limitations of Reynolds' number and instrument sensitivity. The only other solution is to increase the moment of inertia of the stage by adding a flywheel. Because of the very limited space available, the flywheel must be constructed from a very dense metal, tungsten or uranium, neither of which is readily fabricated.

Notwithstanding the above problems, good high frequency data has been taken in the HTF Stage, a sample of which is shown in Fig. 1.16. Efforts

to be carried out during the coming year include fabrication and installation of the flywheel and further reduction of the data.

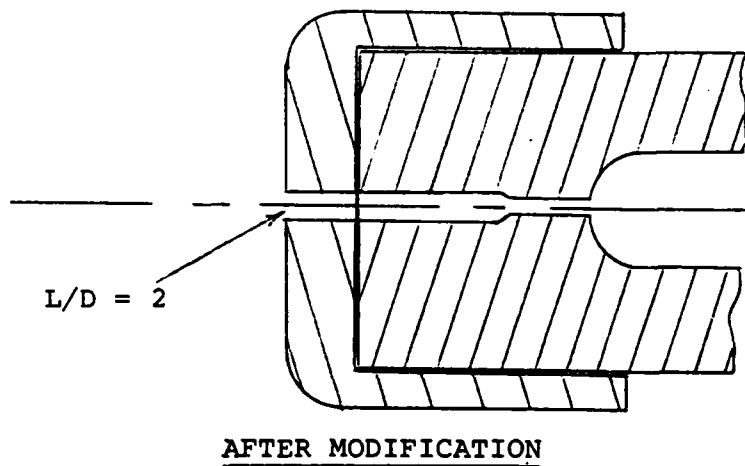
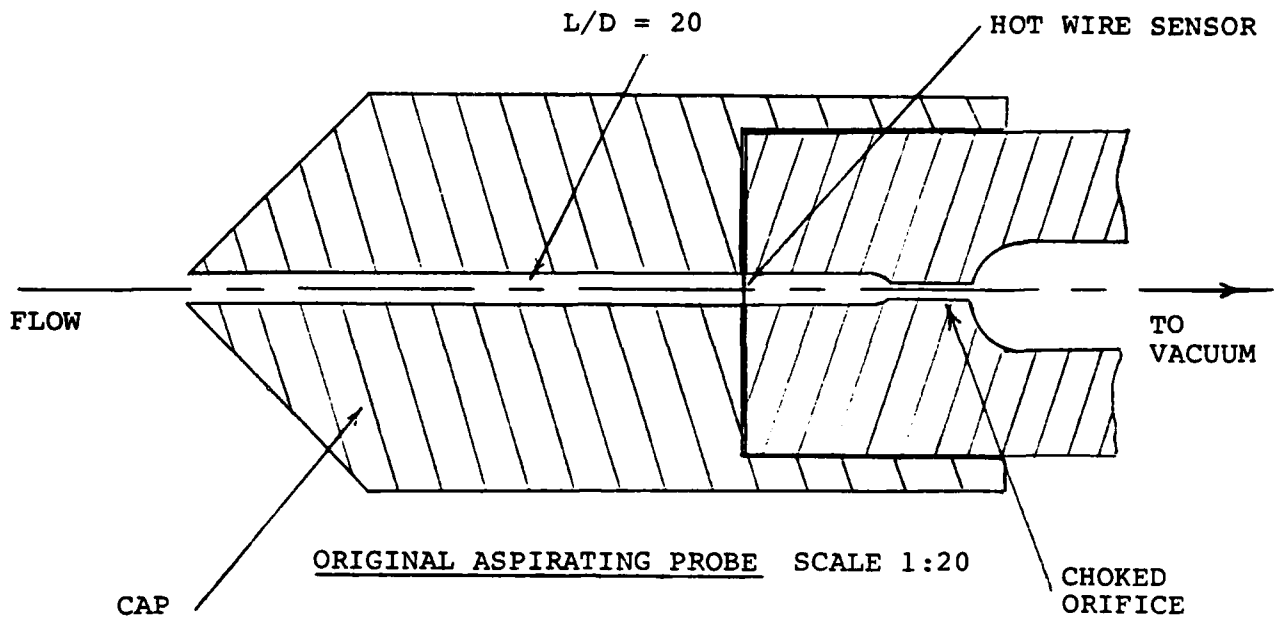
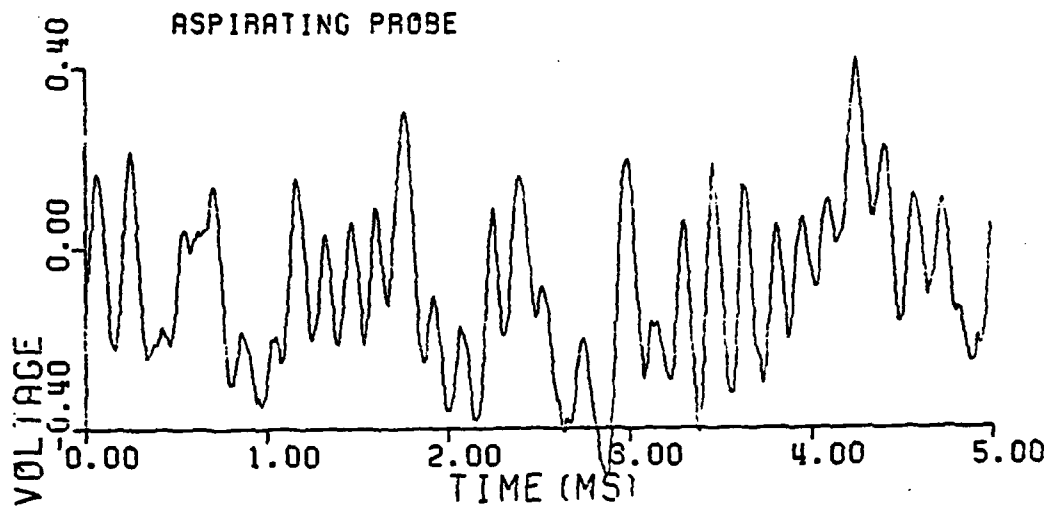
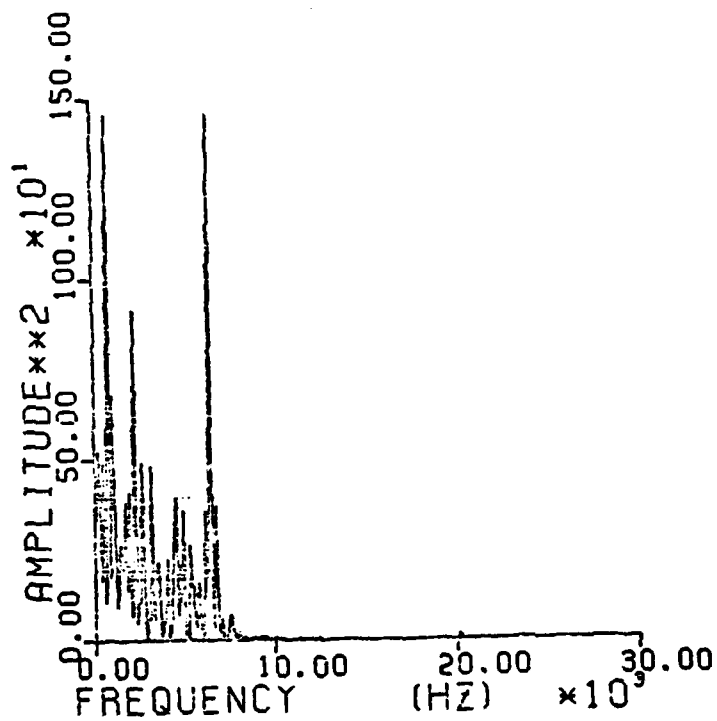


FIGURE 1.12: MODIFICATION OF EXISTING ASPIRATING PROBE



A) TIME HISTORY OF PROBE SIGNAL



B) POWER SPECTRUM DENSITY OF TIME HISTORY

FIG. 1.13: MEASUREMENTS OF WAKE SHEDDING FROM A RIGHT CIRCULAR CYLINDER MADE WITH SINGLE WIRE ASPIRATING PROBE. SHEDDING FREQUENCY IS 8 KHZ, $Re = 200$.

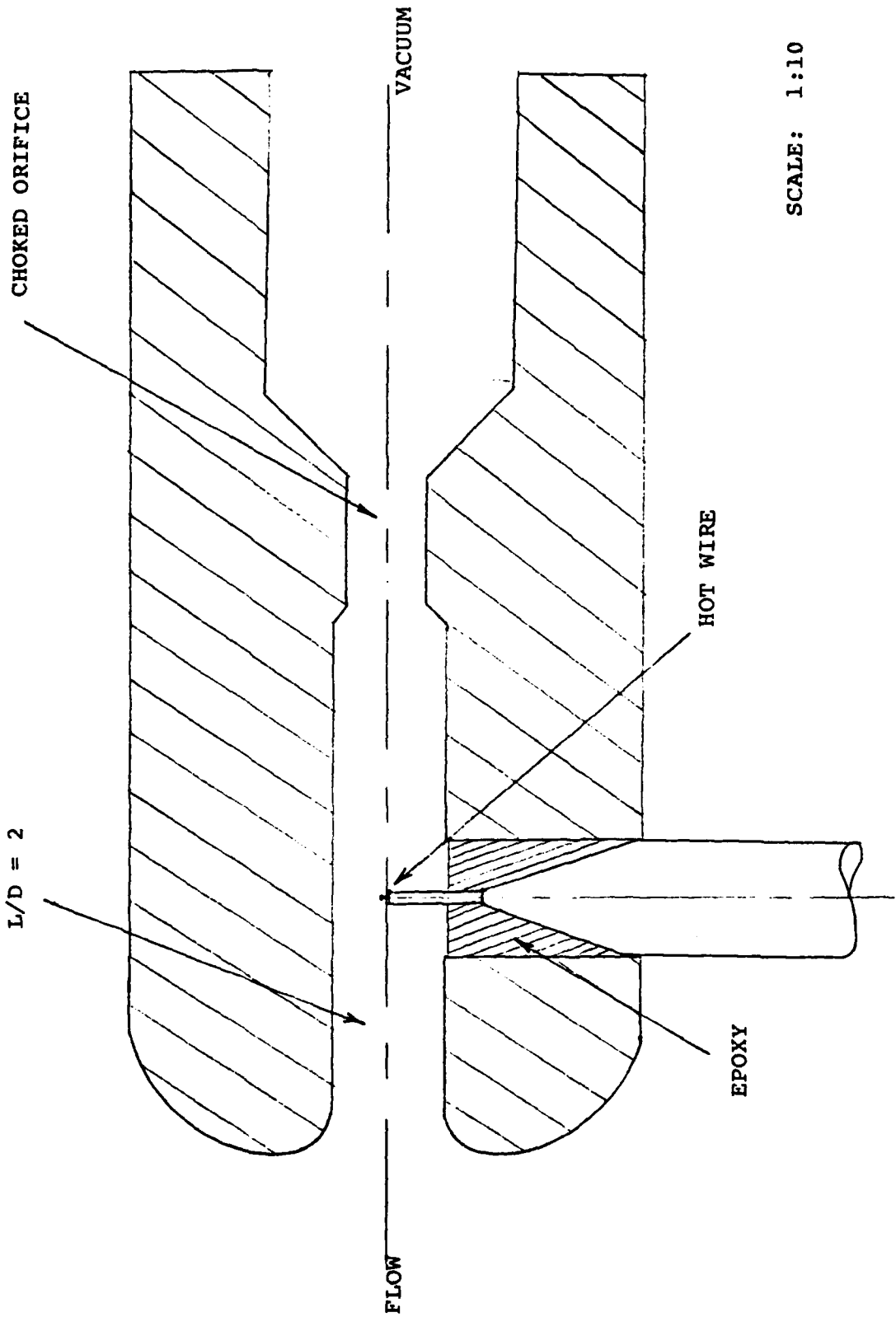
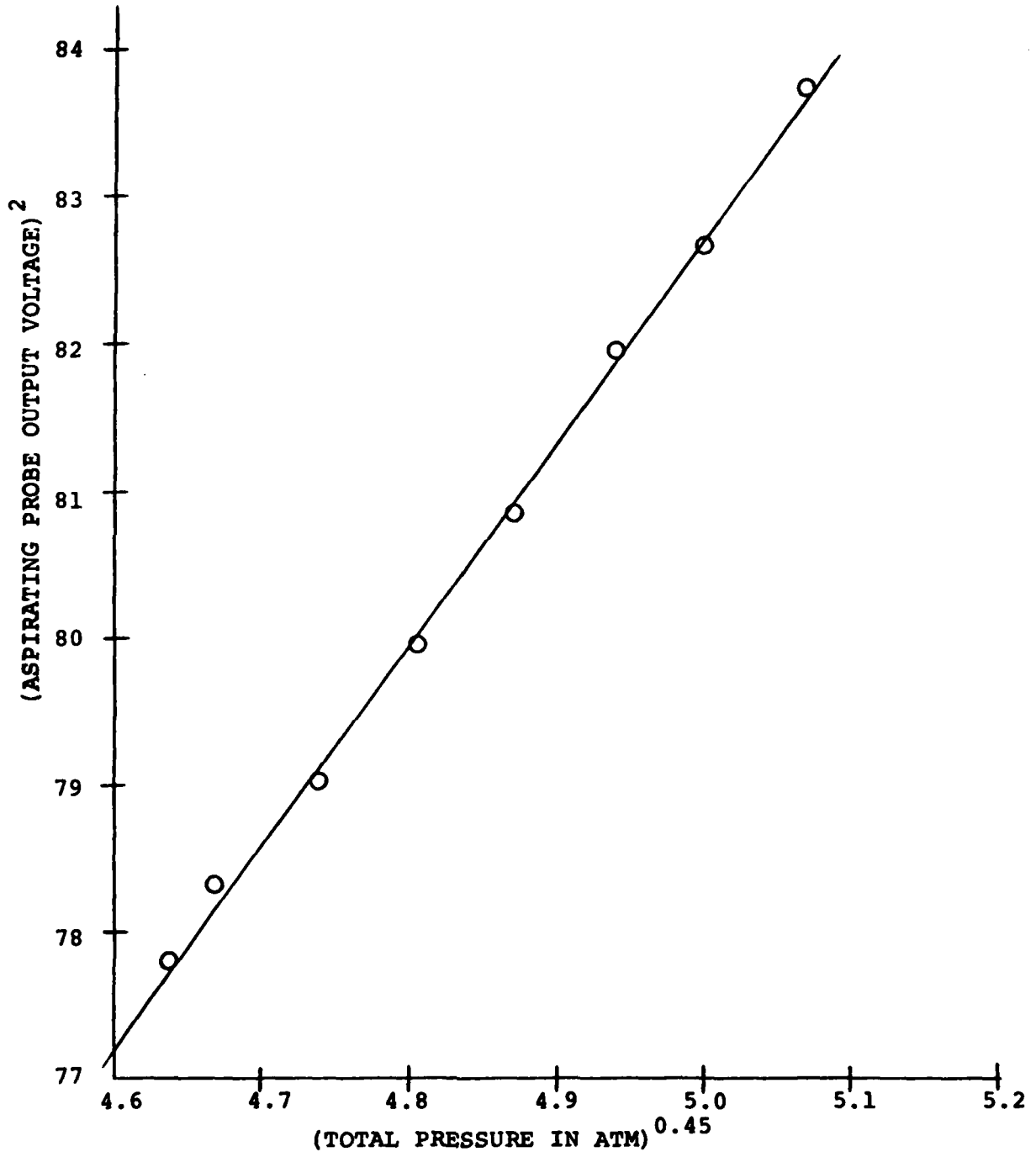


FIGURE 1.14 ASPIRATING PROBE MODEL

FIGURE 1.15: ASPIRATING PROBE OUTPUT VOLTAGE VS. FREE JET TOTAL PRESSURE.



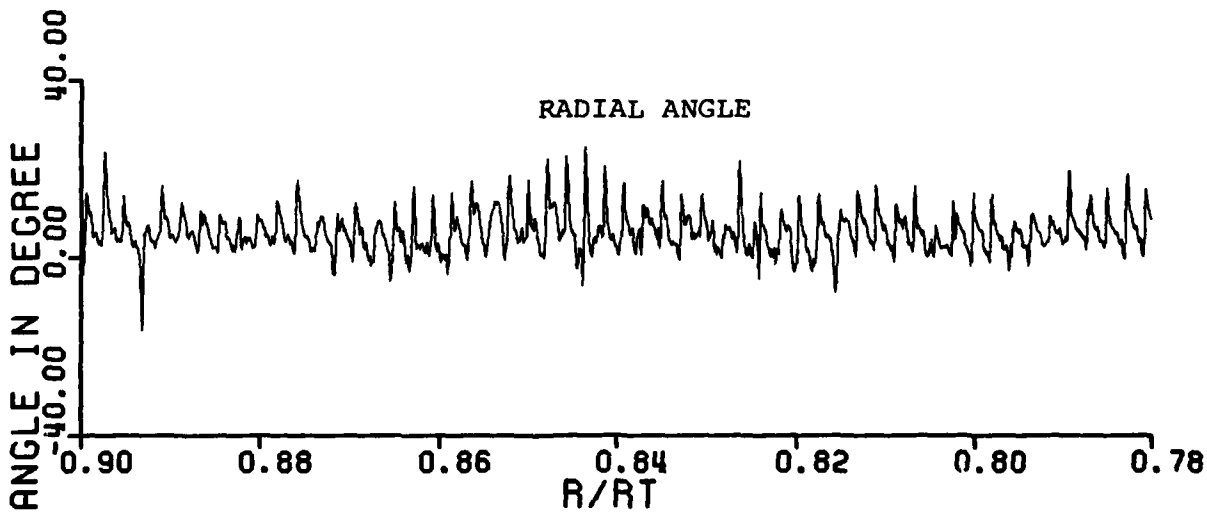
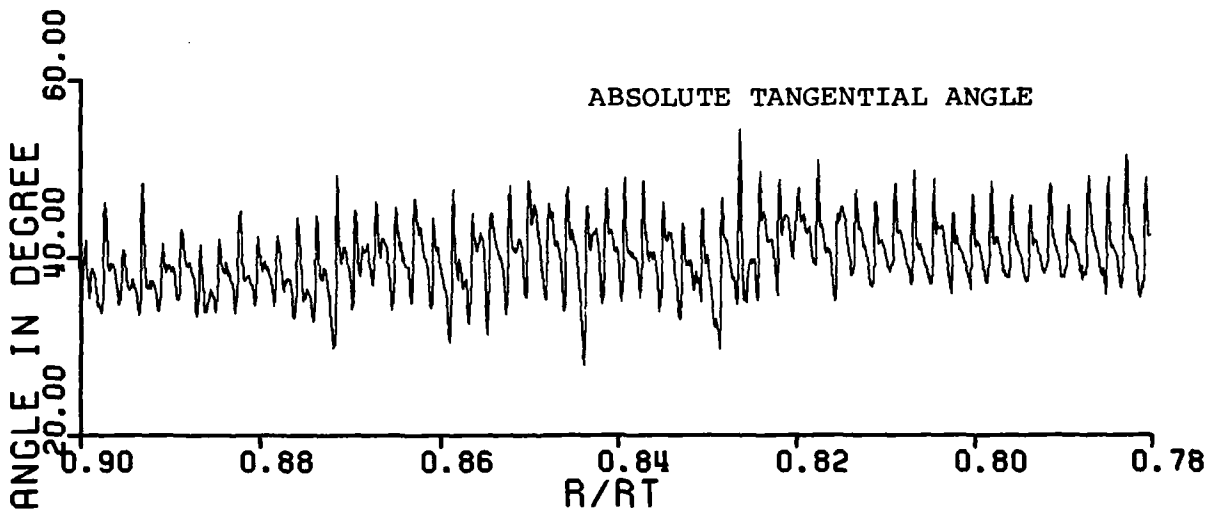
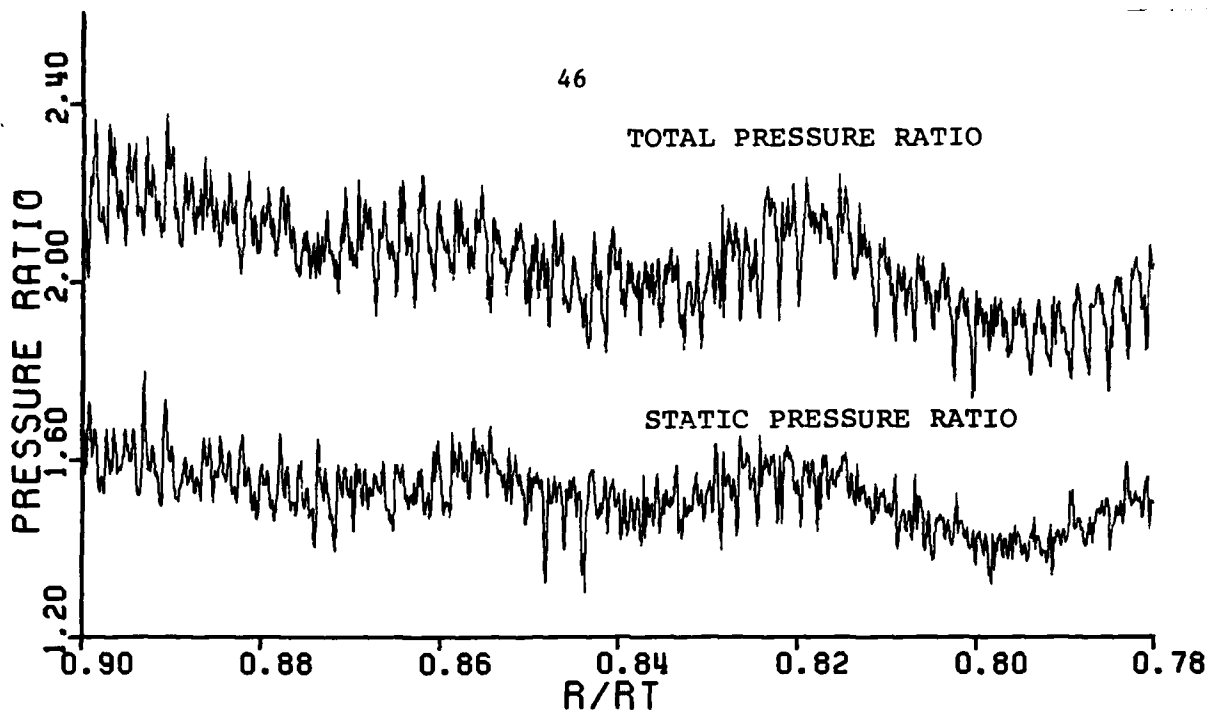


FIGURE 1.16: HIGH RESPONSE MEASUREMENTS FROM AFAPL HTF STAGE

30-NOV-81

REFERENCES

1. 1. Dulikravich, D.S., Sabieczky, H.: Shockless Design and Analysis of Transonic Blade Shapes. AIAA paper 81-1237, 1981.
1. 2. Fung, K.Y., Seebass, A.R., Dickson, L.J., and Pearson, C.F.: An Effective Algorithm for Shock-Free Wing Design. AIAA paper 81-1236, 1981.
1. 3. Carlson, L.A.: Transonic Airfoil Analysis and Design Using Cartesian Coordinates. Journal of Aircraft, 13, pp 349-356, May 1976.
1. 4. Henne, P.A.: An Inverse Transonic Wing Design Method. AIAA paper 80-0330, 1980.
1. 5. Shankar, V.: A Full Potential Inverse Method Based on a Density Linearization Scheme for Wing Design. AIAA paper 81-1234, 1981.
1. 6. Volpe, G. and Melnik, R.E.: The Role of Constraints in the Inverse Design Problem for Transonic Airfoils. AIAA paper 81-1233, 1981.
1. 7. Thompkins, W.T. and Tong, S.S.: Inverse of Design Calculations for Non-Potential in Turbomachine Blade Passages. ASME paper 81-GT-78, to appear in Journal of Eng. for Power.
1. 8. Viviani, H.: Conservation Forms of Gas Dynamic Equations. La Recherche Aerospaciale, No. 1, Jan. 1974, pp 65-68.
1. 9. MacCormack, R.W.: Computational Efficiency Achieved by Time Splitting of Finite Difference Operators. AIAA Paper No. 72-154.
- 1.10. Lord Rayleigh: On the Stability of Certain Fluid Motions. Proc. Math. Soc. London 11, 57, 1880.
- 1.11. Ng, W. F., "Detailed Time Resolved Measurement and Analysis of Unsteady Flow in a Transonic Compressor, GT&PDL Report No. 150, Aug. 1980.
- 1.12 Collis, D.C., Williams, M.J.: Two-Dimensional Convection from Heated Wires at Low Reynolds Numbers. J. Fluid Mech. 6, pp 357-389.
- 1.13 Kerrebrock, J.L., Epstein, A.H., Thompkins, W.T., "A Miniature High Frequency Sphere Probe," Proceedings of ASME Symposium Measurement Methods in Rotating Components of Turbomachinery, 1980.

TASK II: FLUID MECHANICS OF COMPRESSOR CASING AND HUB TREATMENTA. Introduction

It has been known for over a decade that the application of slots or grooves over the rotor tips in the casing of an axial flow compressor can lead to a significant improvement in the stall margin. Previous studies have indicated that a substantial reduction of the endwall boundary layer blockage in the rotor tip region and an interchange of fluid between the treatment and blade passage are associated with the operation of casing treatment. These effects are apparently due to the relative motion of the treatment and blades, and it is thus natural to ask whether a rotating treatment below a row of stator blades would also be effective in improving the stall margin of the stator. However there has been considerably less research on the subject of hub treatment, and to date it has not been conclusively demonstrated whether it is an effective means of inhibiting stator hub stall in an axial flow compressor. This has left a gap in our knowledge of the treatment phenomena, and further research is required in this area to enhance our understanding of the effects of treatment on compressor stall. A successful demonstration of hub treatment would also set the stage for experiments which could analyze the effect of treatment on the blade relative flow in the absolute frame, and would provide a different perspective from which to view the overall phenomenon.

A thorough review of the literature on casing treatment has been given by Smith (Ref 2.1) and many of the overall conclusions have been summarized by Greitzer et al (Ref 2.2). Thus, we will only briefly mention the work done on hub treatment. In particular, one recent investigation of stall margin improvement of a stationary row of blades via a rotating treatment

was done by Jansen, Carter, and Swarden (Ref 2.3) on the vaned diffuser of a centrifugal compressor. A skewed treatment similar to axial skewed slot casing treatment configuration was applied to the impeller rim, such that the treatment slots rotated under the forward portion of the diffuser vanes. The treatment application resulted in a significant increase in the stall margin (approximately 7%), and a large increase in the maximum flow. Thus it would seem that a substantial reduction in the flow blockage of the vaned diffuser, similar to that observed in the casing treatment studies, can be attributed to the treatment.

In the present study the rotor of a single stage axial flow compressor was fitted with an extended cylindrical hub which rotated under the tips of the cantilevered stator vanes. Experiments were run with a "baseline" smooth cylinder, and with a treated hub. The treatment employed consisted of axially oriented slots covering the middle 80% of the stator chord, skewed at an angle of 60° to the radial direction. This axial skewed treatment was chosen for its proven effectiveness in the casing treatment application.

In the design of the experiment several aerodynamic conditions are considered which can influence the effect of the treatment on stall margin. First it is desired that the compressor be stall limited at the stator hub. In this case the rotor is very lightly loaded at the stall point and acts only as a "flow generator" for the stator. The rotor loading is also tip biased, producing locally high loading at the stator hub. The treatment effectiveness may also depend upon whether a blade or wall stall is produced, as it has been established by Greitzer et al (Ref 2.2) that for some geometries casing treatment may not be effective in the presence of a dominant

blade stall. Since it can be difficult to accurately predict whether a given geometry will produce a blade stall or wall stall, this question must be examined experimentally.

B. Experiment Design

It is fundamental in the design of this experiment to ensure that the stator hub endwall is stall limiting. The design used is aimed at having rotor loading very low at the stator stall point so that the rotor acts only as a "flow generator" for the stator. Thus, in choosing the blade setting angles, it is desired that the rotor has a high stagger angle relative to the stator and that stage reaction be low. The requirement of high stator hub loading can be satisfied by using a rotor blade with very low twist. This creates only a small static pressure rise across the rotor hub relative to the tip, which in turn loads the stator hub. (It was fortunate that this requirement allowed the use of existing blades in which the rotor twist was only 9.5°.) In selection of the blade setting angles necessary for this series of tests it was also desired to have the stator discharge static pressure above ambient pressure at a flow somewhat above the stall point, so that the compressor would have adequate stable flow range.

The actual blade setting angles and radial load profiles were calculated using an axisymmetric compressor design program (Ref 2.4) which had been matched to data taken previously on this compressor by Gopalakishnan (Ref 2.5). The data match was accomplished by first determining an empirical relation of the departure of measured blade relative air angles from Carter's rule (Ref 2.6), or "x-factor," vs. radius ratio. Secondly it was assumed that

radial profiles of relative total pressure loss coefficient ($\bar{\omega}$) can be represented by an empirical relation of $\bar{\omega}$ and D-factor, and a radial loss multiplier to account for the endwall boundary layers. The D-factor relation used is similar to that suggested by Lieblien (Ref 2.7) and the endwall multiplier was determined from the total pressure profiles measured by Gopalakrishnan. This technique has been used previously in compressor design work and found to give satisfactory results.

Once the data was matched, the relations were applied to the present blading geometry to determine the air angles and loss profiles for various combinations of rotor and stator stagger at a flow coefficient near the stall point. If one adopts a nominal stall criterion, optimum blade angles can then be selected by comparing the computer runs and choosing the combination which best satisfied the design criteria.

The resulting design is described in detail in Ref 2.8. The computer solution estimated that the stage reaction would be approximately .5 and the resulting D-factor and $\Delta P/q$ profiles showed a very favorable stator hub load bias and rotor/stator load split as described in the previous progress report. The maximum D-factor and $\Delta P/q$ both occurred at the stator hub end-wall, and had values of .6 and .52 respectively at the 90% immersion streamline. It is of course desirable to have a $\Delta P/q$ as high as possible (relative to D-factor) at the stator hub since this condition increases the likelihood of wall stall. However, the calculations showed that a further increase in $\Delta P/q$ could only be achieved by an increase in stator solidity. It was therefore decided to run this experiment with the existing blades and resolve the question of blade or wall stall experimentally.

The experiment was conducted on a single stage research compressor driven by a variable speed D.C. motor. The compressor was equipped with inlet guide vane, a discharge diffuser/valve, and a circumferentially traversing outer casing. The compressor was modified for casing treatment as well as hub treatment as it is intended to be a vehicle for the study of both treatments. A cross sectional schematic of the compressor showing blading and treatment locations is given in Fig. 2.1. Details of the geometry and the experimental procedure are given by Prell (Ref 2.8).

The hub treatment consists of axial slots skewed at a 60° angle to the radial direction, which rotate under the middle 80% of the stator tip chord. The slot spacing is such that the open or slotted area is twice that of the solid or land area. The slot aspect ratio (axial length/tangential width) is 2.0, and the radial depth is 30% of the axial length. The actual dimensions and treatment geometry are shown in Fig. 2.2.

C. Experimental Results

The application of hub treatment to the compressor described above resulted in a reduction of the stalling flow coefficient of only 1-2% and an increase in the stator static pressure rise characteristic of approximately 5% at the stall point. Since the experimental error is also on the order of 1%, the improvement in stall flow due to treatment can be considered practically negligible. A comparison of the stator static pressure rise characteristics, as determined from the casing wall static taps just ahead of and just behind the stator, are shown in Fig. 2.3. The increase in static pressure rise across the stator due to the hub treatment is evident at all flow coefficients tested and is approximately 5% of the static pressure rise of the stator with the

untreated hub. The application of hub treatment has thus resulted in a small but measurable change in the stator aerodynamics.

A comparison of the rotor total pressure characteristic is given in Fig. 2.4. As expected there are no large differences in the rotor performance of the treated and untreated cases, and the negative slope of the characteristic indicates stable rotor operation throughout the flow range tested. The rotor stall point, although not precisely measured, was found to occur at a C_x/U of approximately .35, far below the stator stall point as designed. In contrast to the stator stall, which was very "soft" and could only be detected by the hot wire, the rotor stall was accompanied by an audible change in the compressor operation and a substantial vibration of the unit.

The point of stall inception was determined from observations of a hot wire anemometer probe located approximately 1 blade chord downstream of the stator trailing edge at an immersion of 75%. The wire axis was oriented perpendicular to the axial and radial dimensions. Stall inception was not sudden, that is, a fully developed instability did not set in as the stall flow was reached. Instead the stall first appeared as a transitory phenomenon which gradually became fully developed as the compressor was throttled. Figure 2.5 is an example of the stall signal downstream of the stator at five radial locations for the untreated case.* The figure shows a very flat signal at the 10% immersion position and only a slight indication of an instability at 25%. At 50% immersion, however, the stall is quite evident and increases in amplitude as the hub is approached. It thus appears as if the compressor is hub limited as desired, although the stall is not confined to the hub endwall region.

*These traces were retraced by hand to enhance their clarity.

We can also compare the measured radial profiles to the design. Figures 2.6 and 2.7 show this comparison at rotor exit. It is recalled that the design philosophy is to have substantially lower total pressure rise across the rotor hub, and consequent low axial velocity and static pressure, and high flow angle at the rotor hub discharge to facilitate a stator hub stall. In this context the actual performance is even "better" than expected since the data shows a somewhat higher radial P_T gradient than predicted (Fig. 2.6). In Fig. 2.7 the absolute air angle behind the rotor is also compared to prediction.

We can also comment on the flow through the stator. It was found that the stator total pressure drop in the treated and untreated configurations was essentially the same from the O.D. to $R/R_T \sim .9$ (40% immersion), but below this radial location there was a larger total pressure drop for the untreated case, especially in the midspan region. As previously discussed, casing treatment studies have shown that a significant reduction in losses and flow blockage is a characteristic of treatment. While these effects are most evident near the endwall, improvement of the midspan region has been observed for some configurations.

This improvement in the treated stator midspan is even more evident in a comparison of the treated/untreated stator exit air angles as shown in Fig. 2.8. As with the total pressure data, no improvement of stator turning is seen at the hub, but a substantial increase in turning (5°) due to treatment is seen in the midspan. It is noted here that the increase in treated stator static pressure rise discussed previously may be due to the midspan improvement.

We can also examine the circumferential traverses of the stator wakes for the treated and untreated configurations at the stall point in an attempt to understand the nature of the stall in both cases. Since the question of wall stall vs blade stall appears to be of importance in the understanding of treatment effects (see Ref 2.2), we will first seek to characterize the stall in this regard. Again, the details are given by Prell, and we can only show selected examples. One of these is the stator wake profile at several immersions. This is useful in addressing the question of a limiting stator hub. Circumferential traverses at 10%, 50%, 75% and 90% immersion for the untreated stator are shown in Figs. 2.9. We see a fairly narrow wake near the casing, but a substantially thicker wake at immersions of 50% and greater. In addition the level of total pressure loss increases as we approach the hub endwall. Thus it appears as though the stator loading is indeed biased to the hub as desired.

We have also used the axisymmetric compressor design program to determine the radial profiles of D-factor, $\Delta P/q$, C_x/U , and $\bar{\omega}$ (at the stall point) that are implied by the treated and untreated data. Figures 2.10 and 2.11 show a comparison of the untreated rotor/stator D-factor and $\Delta P/q$ profiles derived from this analysis. The D-factor profiles in Fig. 2.10 show a fairly flat rotor load profile, with the normal increase at endwalls. This profile is typical of a lightly loaded rotor operating near the design point, with no portion of the blade having an excessively high aerodynamic loading. The stator D-factor profile, however, is highly biased at the hub. Comparison of the D-factor profiles to the design curves shows a higher level of D-factor for both rotor and stator, and a somewhat smaller rotor/stator load split for the test data. The higher load level at

stall is due to the conservative stall criterion used for the design case, and the relatively higher rotor load due to an underestimate of the stator deviation in the design. Comparison of the stator D-factor profile to design also shows a higher hub bias for the test data (this was indicated previously in a comparison of the rotor total pressure profile to design [see Fig. 2.6]). The stator $\Delta P/q$ profile shown in Fig. 2.11 also shows the high hub bias, but the level is substantially below the D-factor, thus indicating the possibility of a blade stall. The rotor $\Delta P/q$ as well is sufficiently low as to exclude any apparent aerodynamic difficulty. Thus from this comparison it appears as if the design objective of a substantial rotor/stator load split and a high stator hub load bias has been met.

The effect of the treatment on the radial distribution of axial velocity can be seen in Fig. 2.12. As we might expect from some of the previous comparisons, the treatment results in an increase in axial velocity in the midspan and a slight reduction at the endwalls. Figure 2.13 shows the effect of treatment on the implied \bar{w} profiles. Here again the treatment has apparently improved the flow in the midspan. The computer analysis is thus consistent with the experimental results which indicate that the application of stator hub treatment to the geometry tested in this experiment results in a reduction of flow blockage not at the hub endwall, but in the midspan of the blade row.

D. Recommendations for Future Work

Continued research in the subject of stator hub treatment should examine the question of its effect on stator stall with a wall stall configuration, as well as seek to determine the mechanism responsible for the

midspan improvements. Concerning the question of stall margin improvement, an experiment should be conducted in which the stator hub endwall is the sole "source" of stall, i.e., no blade stall. As discussed above, the existence of a blade stall in this experiment is felt to be the key reason for the ineffectiveness of the treatment on stall margin. Thus, a clear wall stall experiment would be very informative as to the hub treatment stall effect. For the present compressor configuration we have pushed about as far as possible toward achieving this. However, with the installation of an exit fan, we are now no longer limited by the requirement of greater than ambient static pressure at exit and can thus consider configurations with a higher stator stagger, in order to increase the $\Delta P/q$ relative to D-factor. An increase in the solidity of the present blades would also be helpful in dropping D-factor, and blade stall might be inhibited by an increase in stator camber also. These effects should be examined and the compressor rebuilt in a configuration that is much more clearly in a wall stall situation. It should be emphasized that the criteria for wall stall vs blade stall are still not certain and that the obtaining of a definite wall stall is regarded as one of the more uncertain features of the experiment.

As previously mentioned, the improvement in the stator midspan flow could be due to the action of a secondary flow induced by the treatment, in which low energy fluid in the stator suction surface boundary layer is entrained radially towards the hub. By taking stator wake traverses very close to the stator trailing edge, it may be conclusively determined if the treatment results in a thinning of the suction side of the midspan wakes, an expected consequence of the above hypothesis. Hot wire surveys

of the stator passage and boundary layers could also serve to identify changes in the secondary flow characteristics due to treatment.

It would also be of interest to examine the slot flow itself and compare it to the well known observations of the casing treatment slot flows. This could best be accomplished via hot wire surveys of the stator endwall boundary layer region. Pressure and velocity traverses of the stator channel with a five hole probe as previously used by Smith (Ref 2.1) could also contribute significantly to our understanding of the hub treatment effects.

FIGURE 2.1.1 COMPRESSOR CROSS SECTION

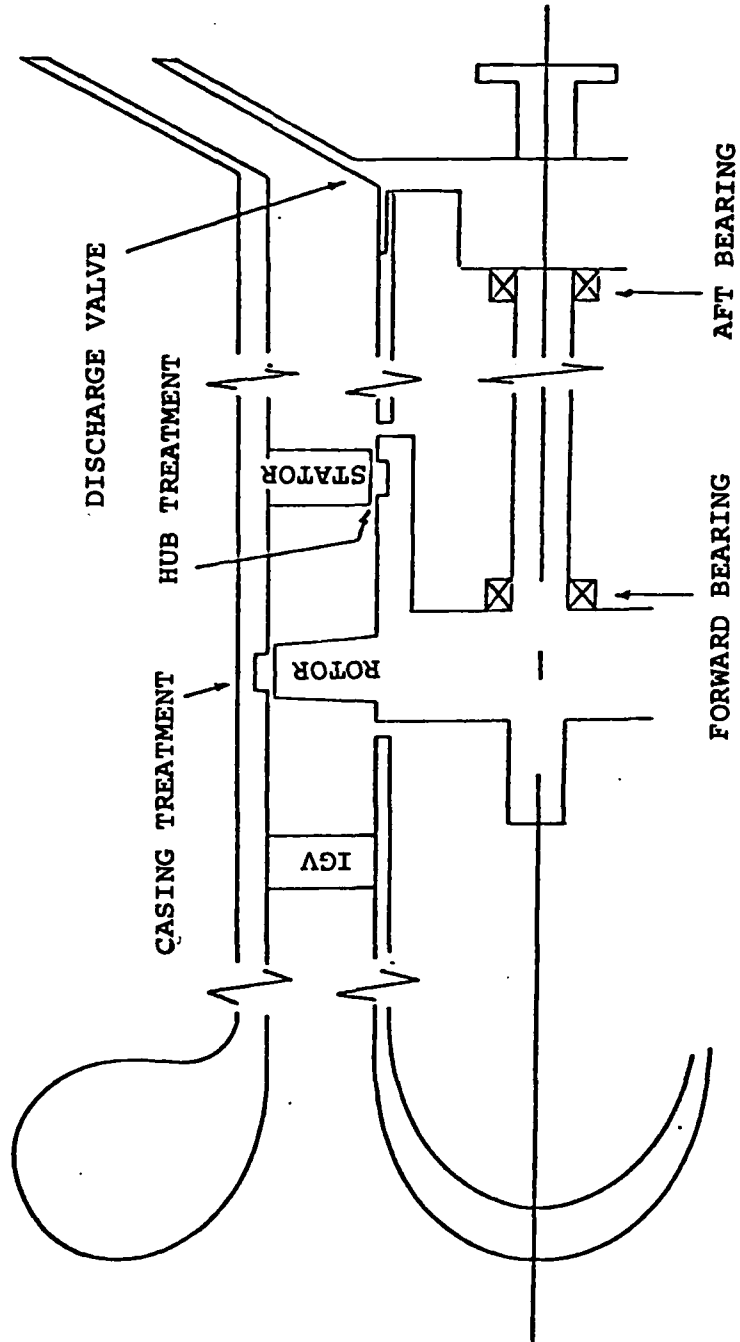
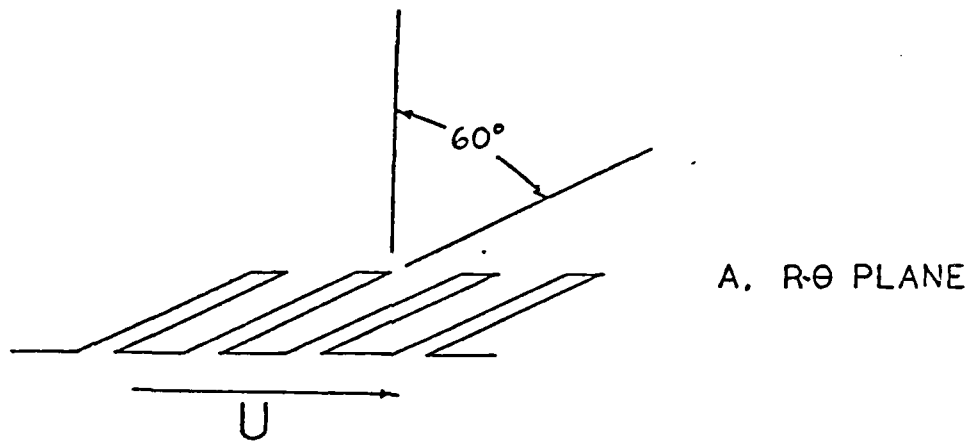
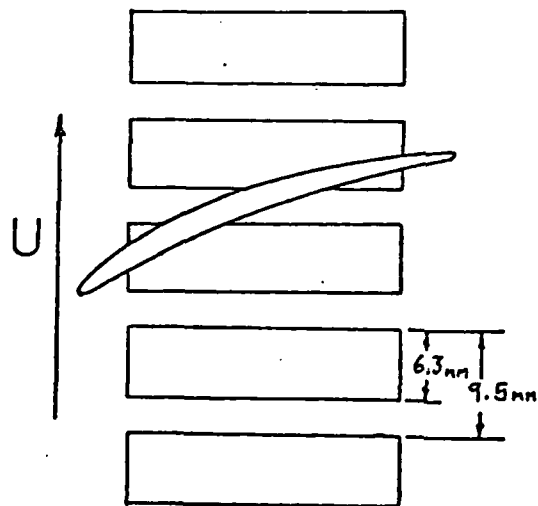


FIGURE 2.2 HUB TREATMENT GEOMETRY



B. X-θ PLANE



C. X-R PLANE

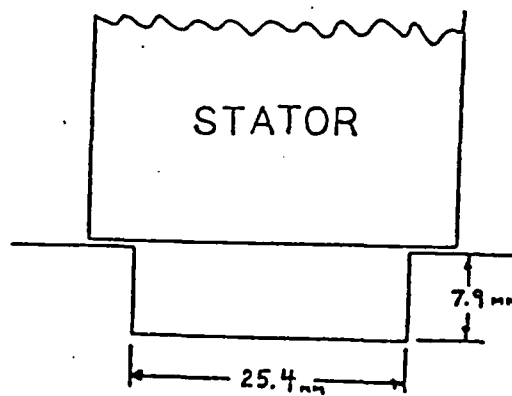


FIGURE 2.3 STATOR STATIC PRESSURE RISE CHARACTERISTIC

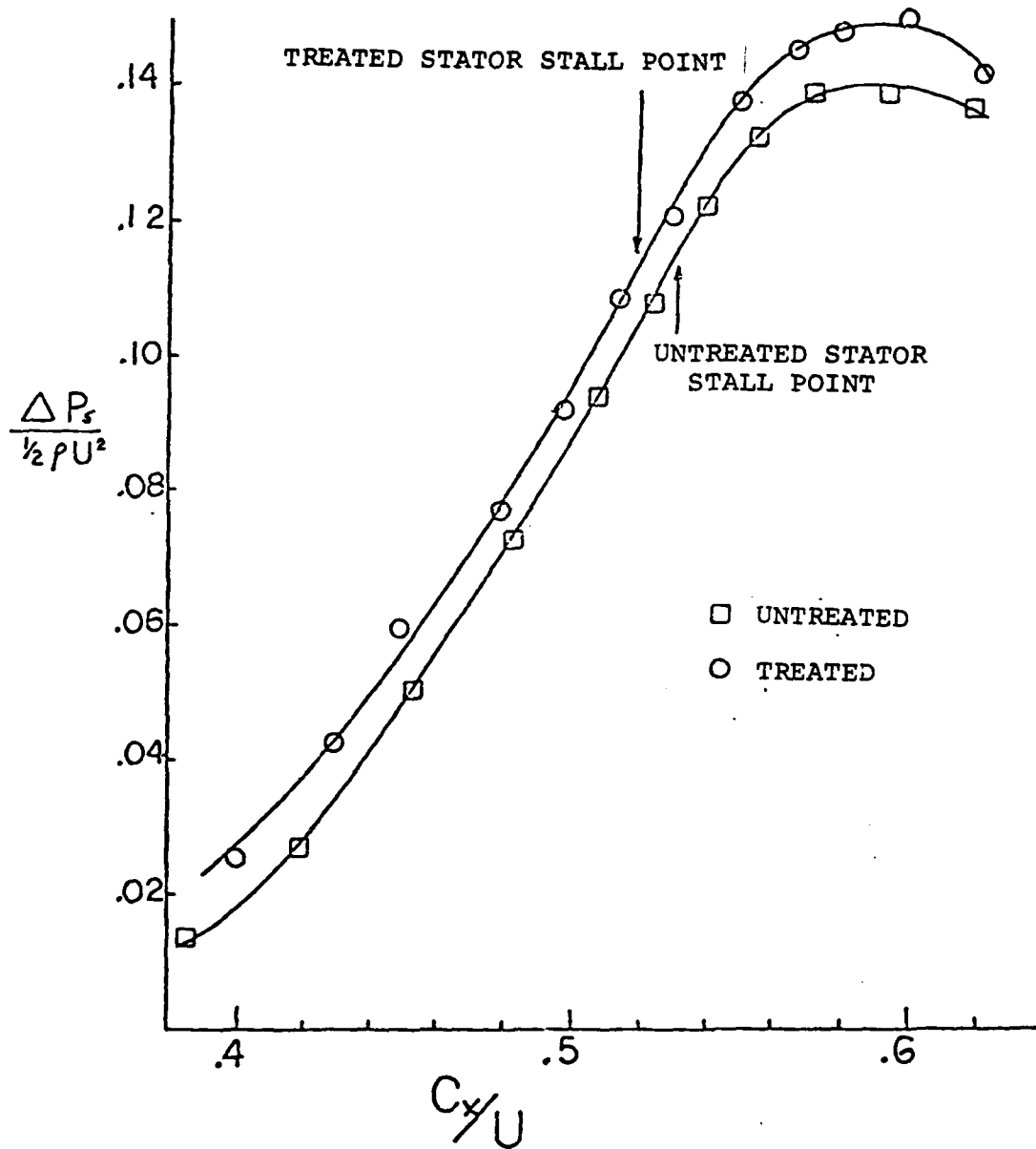


FIGURE 2.4 ROTOR TOTAL PRESSURE RISE CHARACTERISTIC

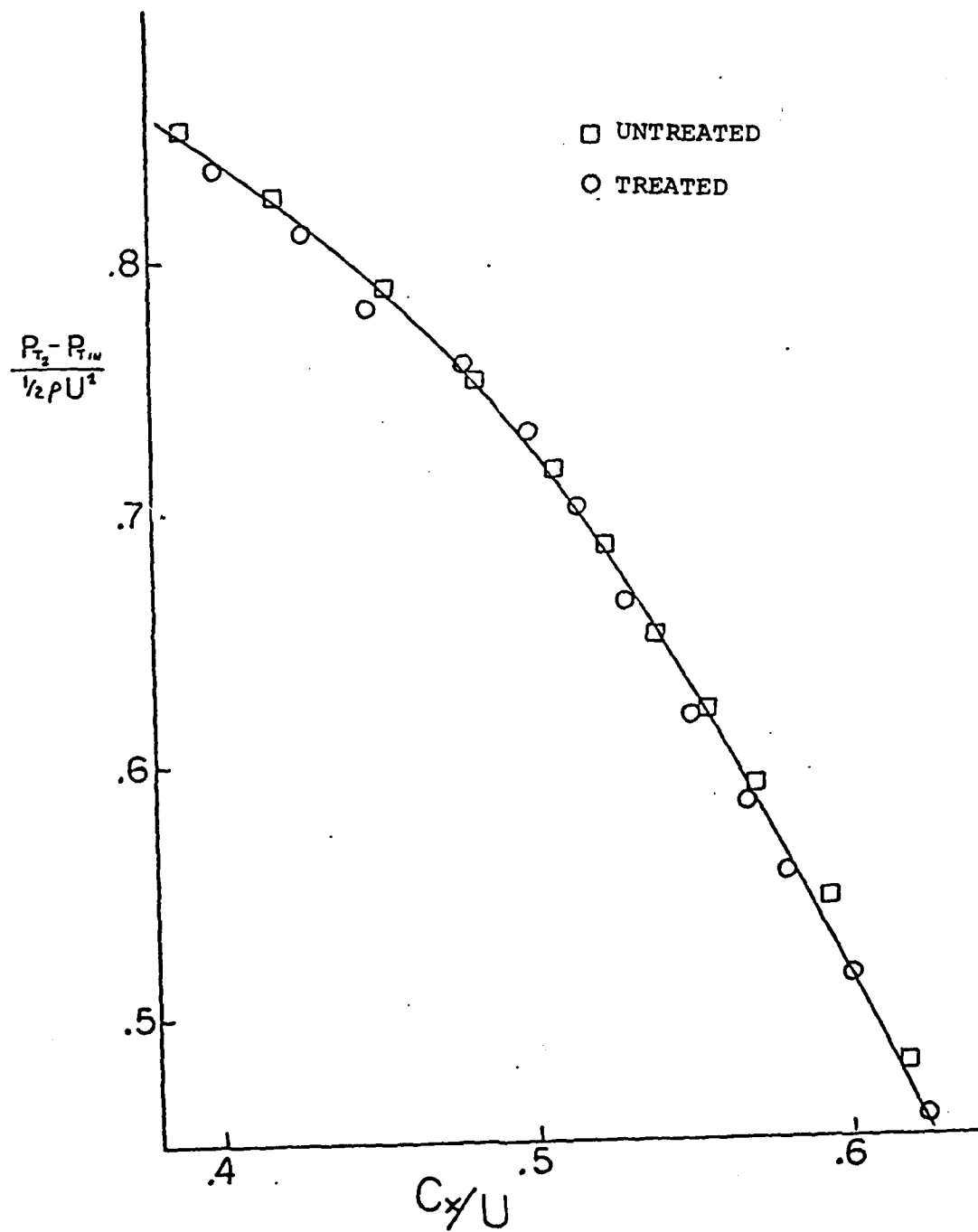


FIGURE 2.5 HOT WIRE SIGNAL AT UNTREATED STATOR DISCHARGE,
STALL POINT

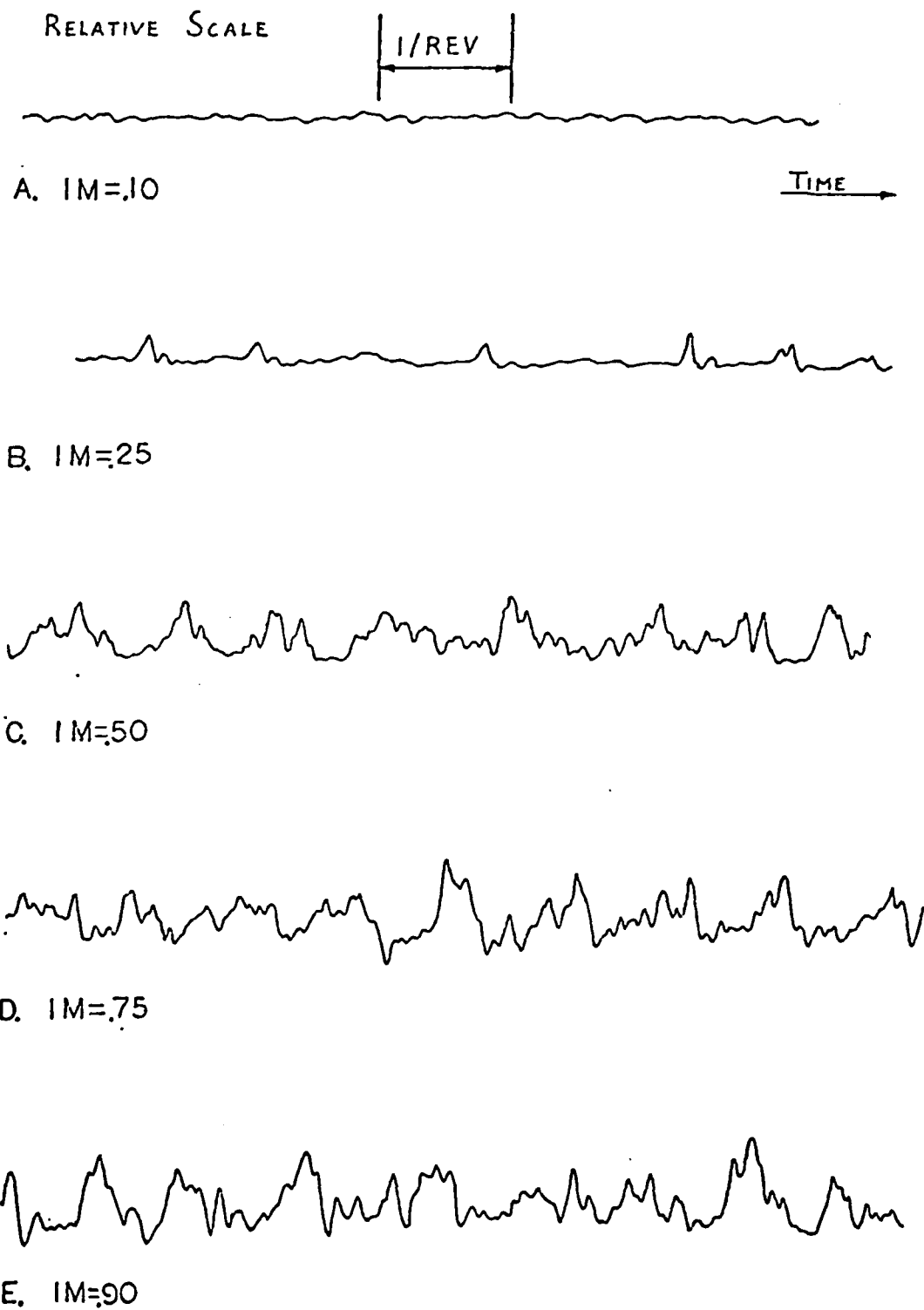


FIGURE 2.6 ROTOR EXIT TOTAL PRESSURE PROFILE VS. DESIGN, STALL POINT

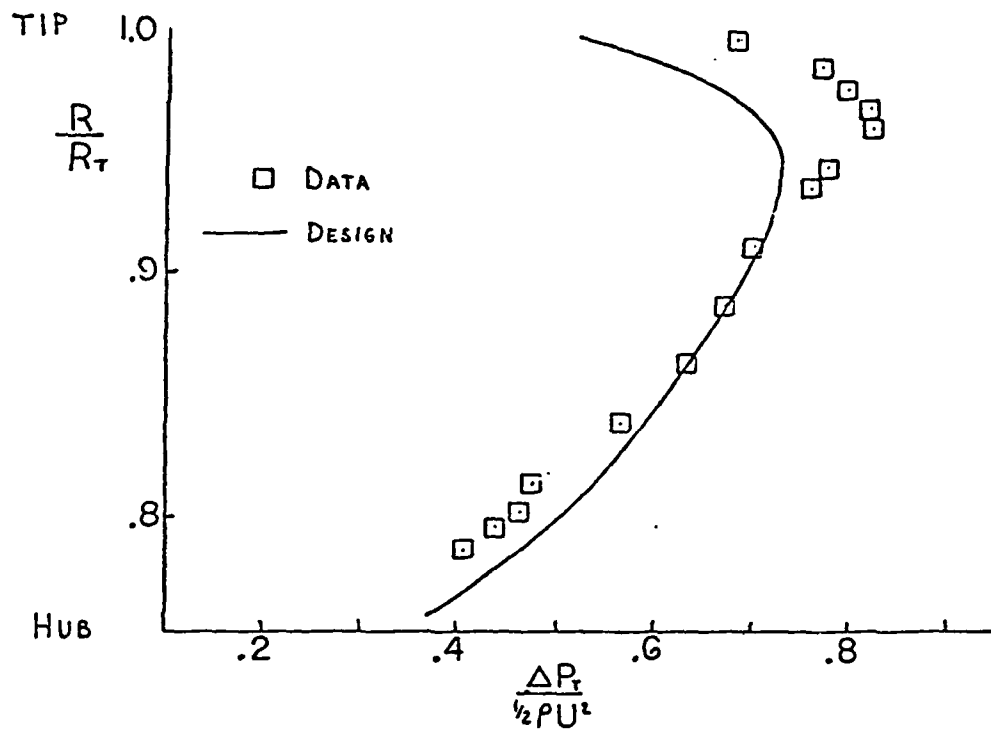


FIGURE 2.7 ROTOR EXIT AIR ANGLE PROFILE VS. DESIGN, STALL POINT

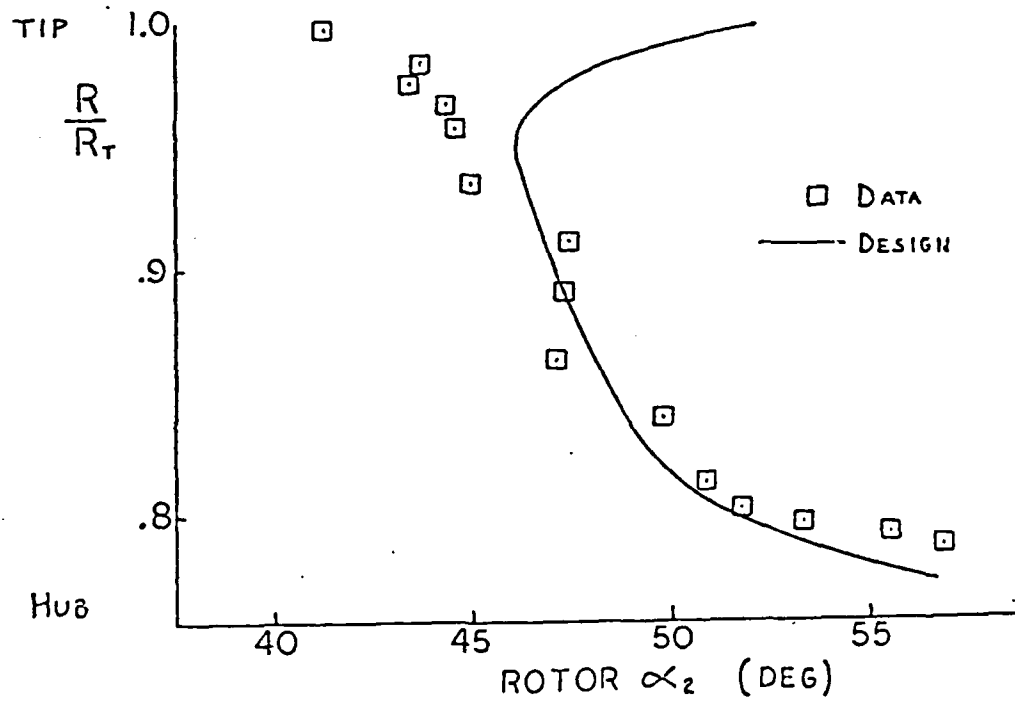


FIGURE 2.8 STATOR EXIT AIR ANGLE PROFILE AT STALL POINT,
TREATED VS. UNTREATED

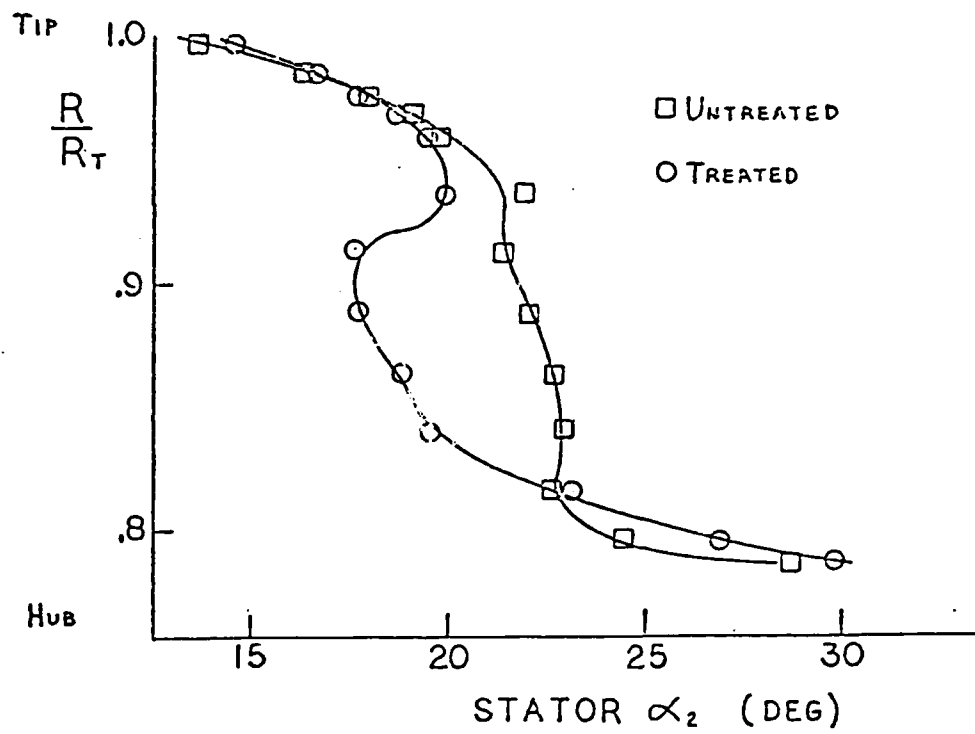


FIGURE 2.9 UNTREATED HUB: STATOR WAKE TOTAL PRESSURE TRAVERSE AT STALL POINT

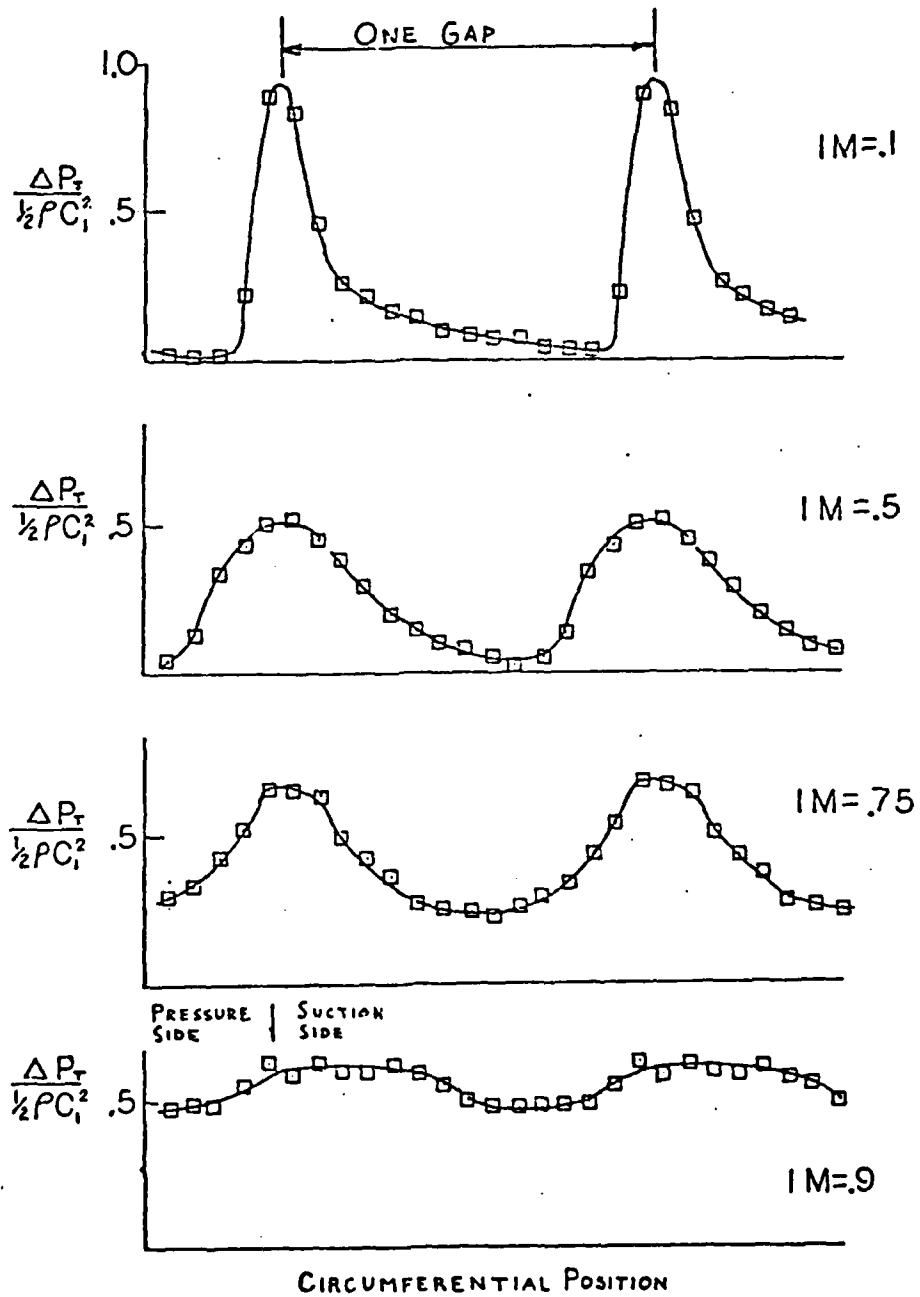


FIGURE 2.10 UNTREATED HUB: ROTOR AND STATOR D-FACTOR PROFILES AT STALL (BASED ON AXISYMMETRIC CALCULATION)

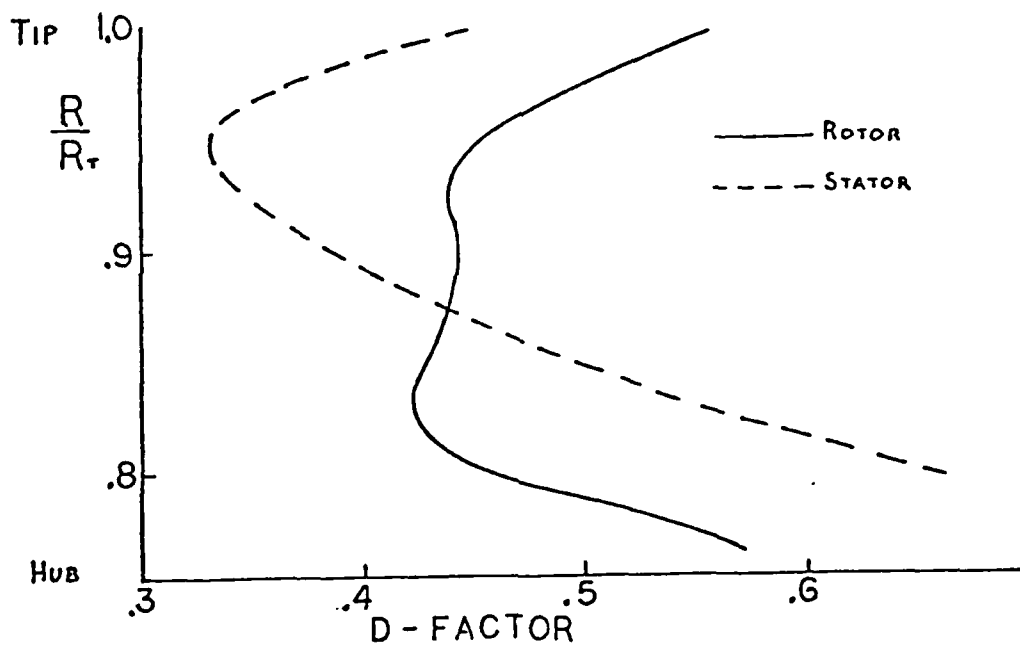


FIGURE 2.11 UNTREATED HUB: ROTOR AND STATOR $\Delta P/Q$ PROFILES AT STALL (BASED ON AXISYMMETRIC CALCULATION)

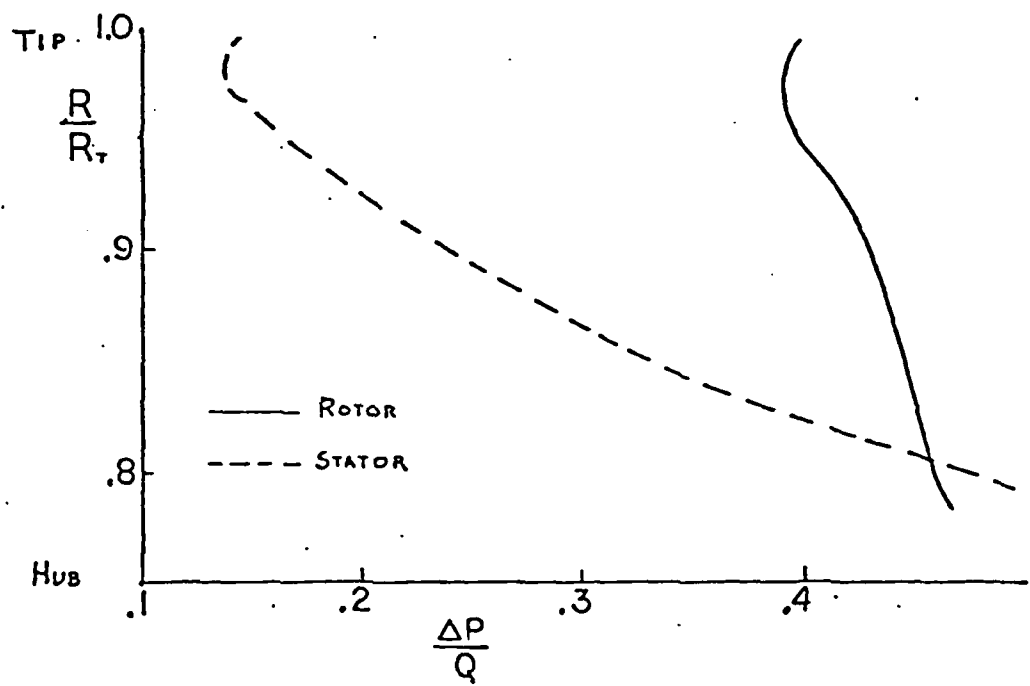


FIGURE 2.12 STATOR AXIAL VELOCITY PROFILE AT STALL, TREATED VS. UNTREATED (BASED ON AXISYMMETRIC CALCULATION)

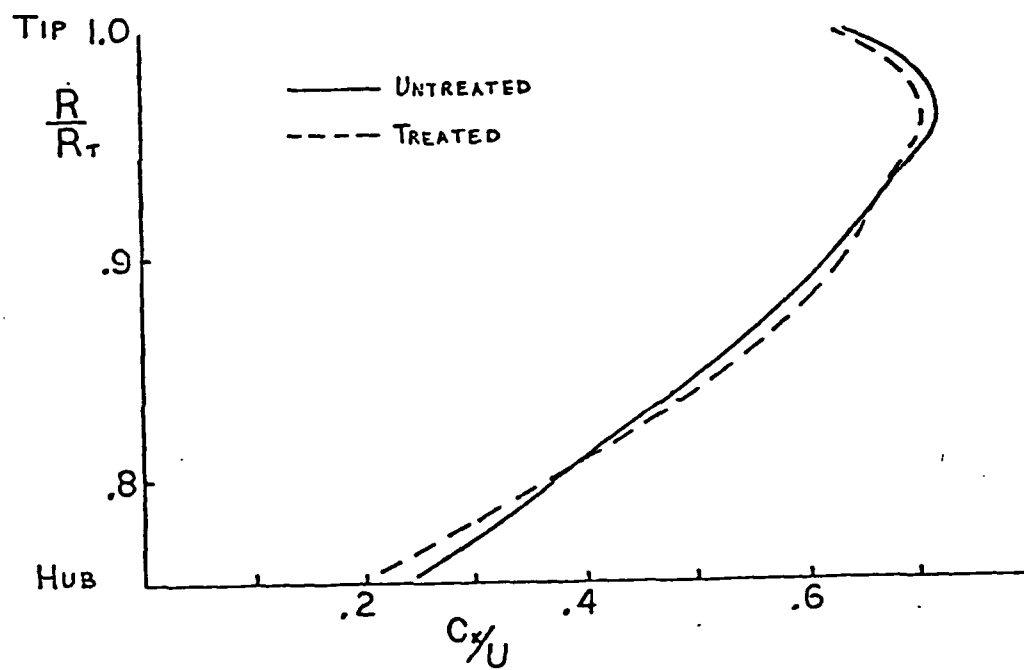
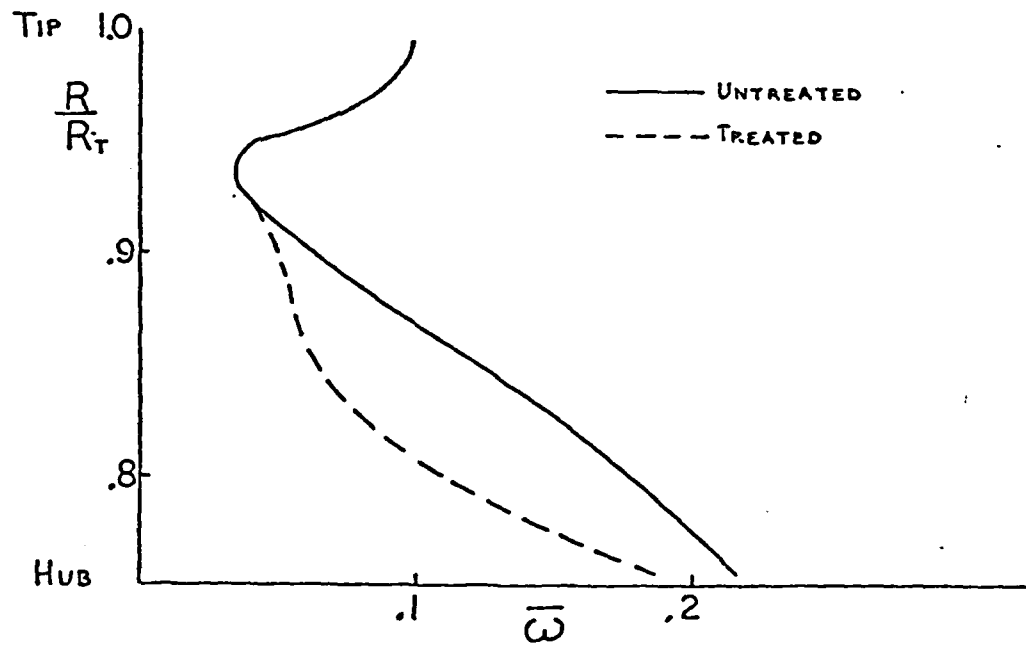


FIGURE 2.13 STATOR RELATIVE TOTAL PRESSURE LOSS COEFFICIENT PROFILE AT STALL, TREATED VS. UNTREATED (BASED ON AXISYMMETRIC CALCULATION)



REFERENCES

- 2.1 Smith, G. D. J., "Casing Treatment in Axial Compressors", Doctoral Thesis, Engineering Department, University of Cambridge, April 1980.
- 2.2 Greitzer, E. M., Nikkanen, J. P., Haddad, D. E., Mazzawy, R. S., and Joslyn, H. D., "A Fundamental Criterion for Application of Rotor Casing Treatment," ASME Journal of Fluids Engineering, June 1979, Vol. 101.
- 2.3 Jansen, W., Carter, A. F., Swarden, M. C., "Improvements in Surge Margin for Centrifugal Compressors", presented at AGARD 55th Specialists' Meeting, "Centrifugal Compressors, Flow Phenomena and Performance", Brussels, Belgium (1980).
- 2.4 Hearsey, R. M., "A Revised Computer Program for Axial Compressor Design", Vol. 1 and 2, ARL-TR-75-001, Aerospace Research Laboratory, Wright Patterson Air Force Base, Ohio, 1976.
- 2.5 Gopalakrishnan, S., "An Unconventional Blade Design for Axial Compressors", M.I.T., Gas Turbine Laboratory Report No. 98, May 1969.
- 2.6 Horlock, J. H., "Axial Flow Compressors, Fluid Mechanics and Thermodynamics", pp 56-63.
- 2.7 Lieblien, S., "Experimental Flow in Two-Dimensional Cascades", Aerodynamic Design of Axial Flow Compressors, Chapter VI, NASA SP-36, 1975.
- 2.8 Prell, M. E., "An Experimental Investigation of Stator Hub Treatment in an Axial Flow Compressor," GT & PDL Report No. 161.

TASK III: INLET VORTEX FLOW DISTORTIONSA. Introduction

When a gas turbine engine is operated near a ground plane at static or near static conditions, a strong vortex is often observed to form between the ground and the inlet. This so-called inlet or ground vortex can cause severe operational difficulties. For example, it can cause loose debris to be picked up from the ground and drawn into the engine. More importantly, the presence of a vortex at the engine face can be associated with a flow distortion that adversely affects the aerodynamic stability of the engine compression system.

An inlet vortex produces a flow which has a large amplitude flow angle and velocity distortion over a considerable extent of the engine face, with, however, a significant total pressure defect only over a small fraction of the inlet flow-through area, i.e., only in the vortex core. Thus the decrease in stall margin due to this type of distortion cannot be predicted by present analyses of compressor response to non-uniform inlet flow, since these are all aimed at roughly uni-directional motions with large extent total pressure distortions.

Initially because of the ingestion problem, but more recently due to the effect on engine stability, the inlet vortex phenomenon has been examined by many investigators. These have included small scale experiments (e.g., Refs 3.1, 3.2, 3.3, 3.4, 3.5) full-scale tests with engines (Refs 3.6, 3.7), panel method calculations of the velocity field associated with a potential vortex and inlet combination (Ref 3.8), and two-dimensional free streamline potential flow models of an inlet near ground plane (Ref 3.9). A discussion

of these various studies is given in Ref. 3.10, but we can summarize the main conclusions presented in the existing literature as follows. First, it is assumed that an inlet vortex can form only if ambient vorticity exists in the fluid drawn into the inlet. By the term "ambient vorticity" we mean vorticity created at a far upstream location, where the existence of the vorticity is essentially independent of the presence of the inlet. The second conclusion is that the existence of a stagnation point on the ground near the front of the inlet is believed to be required for the phenomenon to appear. In addition, the inlet vortex, which can be part of a system of vortices, may be unsteady. Further, the thin boundary layer due to the inlet (sink flow) alone is not essential in the vortex formation. The following parameters have been used to characterize this phenomenon: inlet throat velocity to ambient wind velocity ratio, V_i/V_∞ , centerline height to inlet diameter ratio, H/D , wind direction, and the ratio of the inlet velocity to the product of far upstream wind velocity gradient and inlet diameter (this is a rough measure of the magnitude of the ambient vorticity). In particular, increasing the first ratio or decreasing the second and fourth has been found to result in either an increased tendency for a vortex to form, or the strengthening of an existing vortex.

In spite of the work that has been done on this topic, the fundamental fluid mechanic processes responsible for the generation of the inlet vortex are still not well understood. The initial aim of the present study is thus to clarify the basic fluid dynamics associated with the inlet vortex phenomenon. A second, no less important, goal is then to assess the response of an axial compressor to this type of inlet distortion.

In order to study this topic, an experimental and theoretical study of the inlet vortex flow field has been carried out. The results of this study showed that there are two quite different mechanisms of vortex formation. One of these is the intensification of ambient vorticity referred to above. For this to occur the ambient flow in which the inlet is immersed is, of course, rotational. However, there is another mechanism which, contrary to what has been supposed previously, can produce a vortex in a flow that is irrotational upstream of the inlet (for example, uniform at a far upstream location). This feature appears not to have been described before. The two mechanisms were illustrated by a series of flow visualization experiments carried out with a model inlet in a low speed water tunnel, as well as by a numerical study of the vorticity field in an inlet/ground plane configuration.

We will discuss the results of the latter first, and then describe the experiments that were carried out.

B. Secondary Flow Approach to the Vorticity Field

The flow we consider is incompressible, constant density, inviscid, and free of body forces. In this situation the vortex filaments are always composed of the same fluid particles, i.e., they move with the fluid. Also for a vortex filament of fixed identity, the ratio of the vorticity to the length of the filament remains constant as time proceeds. Thus if a vortex filament is stretched, the vorticity associated with it increases. The vorticity is also inversely proportional to the cross-sectional area of the vortex filament, since the circulation round a given material curve is invariant. As a result, the evolution of the vorticity between far upstream and the engine compressor face can be deduced from the deformation undergone by vortex filaments in their motion toward the engine.

To calculate the movement of vortex filaments requires the velocity field to be determined. The flow under consideration is clearly rotational, not only in a thin layer as in many aerodynamic applications, but throughout the flow domain, and is strongly three-dimensional. However, since the basic concept to be studied is the intensification of vorticity due to the stretching of the vortex filaments as they are drawn into the inlet, a useful simplification can be made by viewing the problem as a "small shear, large disturbance flow," as described by Hawthorne (Ref 3.11). In this approximation which has been utilized, for example, to calculate secondary flows in turbomachines, the flow is assumed to be composed of an irrotational primary flow and a weak shear flow. The vortex filaments associated with this shear are regarded as being deformed by this primary flow only. In other words, the additional influence of the so-called "secondary" velocities on the convection of vortex filaments is neglected. The primary flow can be determined using potential flow theory and, in particular, advantage can be taken of the fact that many numerical methods exist to compute potential flows.

The actual steps used in investigating the vorticity field were as follows. First, an inlet-ground plane geometry was selected and the overall parameters describing the inlet vortex formation given typical values. Second, the three-dimensional potential flow about the inlet is determined numerically. Third, selected vortex lines (material lines) are (numerically) tracked from far upstream to the inlet. By examining the stretching and "tipping" they undergo it is possible to predict the vorticity pattern at the engine face due to a given far upstream vorticity distribution. A further step would then consist of computing the secondary flow produced at this location by the calculated vorticity distribution.

C. Flow Geometry Used in the Analysis

The specific flow geometry that is analyzed can be seen in Fig. 3.1. It consists of a cylindrical inlet and its image, which is introduced to simulate the ground plane. For the general situation the inlets are set at an angle of incidence, α , in a uniform stream (with direction parallel to the plane of symmetry between the inlet and its image) and magnitude V_∞ . In the case to be discussed first, α is zero. The operating condition for a given inlet at a given H/D (height to diameter ratio) is hence defined by a single non-dimensional parameter; the ratio of inlet velocity to far upstream velocity, V_i/V_∞ .

The inlet geometry used in this study had no centerbody: the internal machinery which controls the amount of fluid entering the inlet is taken to be far enough from the inlet lip for its effect to be lumped into a single parameter, mass flow through the inlet. Additionally, in order to minimize the influence of the fluid exiting the engine on the flow near the forward part of the inlet, the inlet walls have to be extended as far as possible downstream. This is also required for good accuracy in the numerical calculation of the potential flow about the inlet.

D. Three-Dimensional Potential Flow Calculation Procedure

The approach taken requires the potential flow about the geometry described above to be computed. Many different methods exist to calculate potential flow about three-dimensional bodies. It is not within the scope of this report to describe them in detail and a complete coverage of these matters can be found in the abundant literature, for example, Refs 3.12-3.15. The computational method used in the present study was the constant strength source and dipole method developed by Hess, Mack and Stockman (Ref 3.16) to solve flow about arbitrary bodies.

E. Results of Calculations

The drift of the material lines has been examined to show directly the convection and amplification of the vortex filaments. For the general situation the inlet is at a yaw angle α to the mean flow. However, we will here first discuss the case of zero yaw, since in this configuration one of the basic mechanisms can be most clearly seen. Thus let us consider the behavior of different material lines in the flow into an inlet that is facing directly upstream. In doing this it is useful to resolve the far upstream (ambient) vorticity into three components respectively: 1) streamwise, 2) transverse to the flow direction and parallel to the ground plane (horizontal), and 3) transverse to the flow direction and normal to the ground plane (vertical).

Figure 3.2, taken from Ref 3.10, gives one example of the results of this type of calculation. The figure shows the different positions of a vortex line which is vertical far upstream and 0.60 inlet heights (0.75 inlet diameters) from the x,z plane. The figure shows the projections on a plane perpendicular to the inlet axis with the numbers corresponding to different times. It can be seen that from this view there is a distinct lack of symmetry between the behavior in the top and bottom halves of the inlet. This is associated with the flow near the stagnation streamline. It can be seen that the lower part of the filament at the latest time shown ("9") has drifted considerably closer to the midplane of the inlet (in fact, to the location of the stagnation streamline) than has the upper part. (Note that since vortex lines cannot end in the flow, the lines tracked in this figure actually extend to infinity. However, those portions of the material lines outside the capture surface which do not enter the inlet are not shown.)

The above is just one example of this type; however, the extensive calculations that were carried out (Ref. 3.10) give a good insight into mechanisms of inlet vortex formation due to amplification of ambient vertical vorticity. Based on these calculations, we can in fact form the following conceptual picture of the configuration (in particular the ultimate positions) of the vertical vortex lines as they are convected into the inlet.

This is shown in Fig. 3.3, which presents the suggested deformations of vertical material lines within the capture surface. A far upstream uniform distribution of vertical vortex lines evolves into a configuration in which the upper legs of the lines are "fanned out" over the upper part of the inlet while the lower legs are concentrated around the stagnation streamline associated with the stagnation point S_1 in the figure. (Although the stagnation points are never reached in an actual flow, these trends will still remain valid.) The predicted concentration is accompanied by an increase of the associated circulation per unit area. Note that in the calculation, in which all viscous effects are neglected, the stretching of both "legs" of the vortex line is actually infinite. The difference, however, lies in the spatial distribution of the associated vorticity amplification, as can be seen in (Ref. 3.10), where calculations are shown for fluid particles close to the "foot" and "head" of the vortex line.

This is the situation at zero yaw. Calculations were also carried out at forty-five degrees of yaw to see if there was any indication of vorticity concentration due to initially horizontal vortex filaments. The calculation of convection of material lines showed that there did not appear to be any situation of this kind.

We have thus presented one possible mechanism for the formation of an inlet vortex. In the next section we will discuss the experiments that were

set up to examine this possibility, and show that not only is this mechanism a real one, but that the experiments lead us to identification of another, completely different, physical process for vortex formation.

F. Experimental Studies of the Inlet Vortex Flow Field

The flow visualization studies were carried out in the 6,000 gallon capacity MIT Ocean Engineering Water Tunnel. A schematic of this facility is shown in Fig. 3.4. The 1.5 m long, 0.5 m square test section is equipped with four interchangeable 0.038 m thick plexiglass windows. In this investigation, it was run with a free surface. Details of the facility are given in Ref. 3.17.

The engine inlet is modeled in this investigation using a plexiglass pipe, with the suction provided by a downstream centrifugal pump. Three different inlet configurations were studied in some detail: an inlet at zero degrees to the mean flow far upstream; an inlet at ninety degrees to the mean flow far upstream, and a twin inlet configuration at ninety degrees to the mean flow, with inside diameters of 0.044 m, 0.05 m and 0.025 m, respectively. All three inlets are (platinum) wired for hydrogen bubble flow visualization in order to determine the location of the vortex in the inlet. The inlets were tested in both a shear flow and a uniform i.e. irrotational, upstream flow. The different shear profiles that were generated are shown in Fig. 3.5. These are created using honeycomb of non-uniform lengths. The velocities have been deliberately shown in dimensional form to indicate the actual range of velocities at which the hydrogen bubble technique was employed. Note that the first two profiles have vortex lines which are horizontal, while the latter two have vortex lines which,

outside of a thin boundary layer, are vertical, i.e. perpendicular to the ground plane and to the mean flow.

Using the hydrogen bubble technique, with a long wire stretched either vertically or horizontally across the tunnel, one can essentially mark material lines and examine their behavior as they are convected to the inlet. Since, for this flow, vortex lines can to a good approximation be regarded as moving with the fluid, if we mark a material line that is, far upstream, either vertical or horizontal, we are thus marking a vortex line. We can thus see directly the deformation (stretching and tipping) of vortex filaments in order to understand the vorticity amplification process associated with the formation of an inlet vortex.

The results of the experimental study can be broken into two parts; namely the tests with an inlet at zero degrees to the mean flow, i.e., with the inlet pointing upstream, and tests with the inlet at ninety (or two hundred seventy) degrees to the mean flow. The results are given in detail in DeSiervi (Ref 3.17), and we will only summarize the main conclusions of the tests. For the zero degree case the flow with vertical vortex filaments showed an inlet vortex flow field much like that implied by the theoretical calculations. There was a strong vortex at approximately six o'clock. The swirling flow region associated with this vortex appeared to start on the ground plane slightly in front of the vortex. The sense of the vortex was determined by the sense of the ambient vorticity. Thus when we created an upstream flow with an ambient vorticity of the opposite sign (by reversing the honeycomb), the resulting flow field was quite similar in nature, except that the sense of the swirl was reversed. The secondary flow approach therefore does seem to be a reasonable method of describing the fluid motions encountered in this configuration. A photograph of the vortex in this configuration is shown in Fig. 3.6 .

In the tests with the inlet at ninety degrees to the mean flow, however, the situation was quite different. A clockwise (looking into the inlet) vortex was produced irrespective of the sense of the ambient vorticity. Diagnostic tests revealed that this was not due to any asymmetry or clockwise bias produced by the tunnel geometry, and it thus appeared to be due to the basic asymmetry inherent in the three-dimensional flow around the inlet. The presence of this clockwise rotation bias with the ninety degree inlet configuration motivated an examination of the inlet flow field with initially uniform upstream flow.

G. Single Inlet in Irrotational Flow at Ninety Degrees of Yaw

For an inlet oriented at ninety degrees to the mean flow, a strong steady vortex was observed in the lower part of the inlet at approximately the 6:00 location. The sense of the rotation was clockwise when viewed looking into the inlet. Examination of the flow field also revealed a further, previously undetected, feature. This was a trailing vortex from the downstream side of the inlet lip region. The relative position and size of this trailing vortex, compared to the inlet vortex, is shown in Fig. 3.7; which is drawn from extensive observations (and videotapes) of the hydrogen bubble flow visualization. Relative to the inlet vortex, the trailing vortex is considerably larger, with the diameter of the vortical region being approximately 0.9 inlet diameters. The sense of rotation was clockwise, when viewed from the upstream section of the tunnel.

Based on the preceding, we see that the inlet vortex is, in the case of an irrotational upstream flow, part of a vortex system, with the pattern of vortex lines as sketched in Fig. 3.8. Note the similarity with (half of)

the vortex system of a finite wing. In both circumstances it is the "spanwise" change in circulation that gives rise to a trailing vortex, although in the present case the circulation would be said to have a large value at the "tip" of the inlet and would be approximately zero at the location corresponding to midspan. Further discussions of this aspect are given in Ref. 3.17.

The change in circulation along the length of the inlet could be observed using the flow visualization technique, by examining the separation of the flow from the outside of the inlet. The change in circulation was associated with a skew in the separation line, which appeared as shown in Fig. 3.9 (which is also drawn from observations). At Station 1, which represents a location far from the inlet lip, the flow separated at approximately 12:00 and 6:00, with the dividing streamline impinging on the inlet at 9:00. This symmetry implies that there is a near zero circulation at this location, similar to the two-dimensional results for a cylinder near a ground plane at the present H/D value. Proceeding along the inlet (parallel to the axis) towards the inlet lip (Station 2) one finds an increasing asymmetry in the locations of the separation points. The upper point of separation moves further in the clockwise direction than the lower point moves in the counter-clockwise direction, so that at Station 2 the separation points are located at 4:00 and 6:00. In addition, as one approaches the lip, the velocities increase. The combination of the shift in the position of the separation and the increase in the velocity as one nears the lip imply a pronounced (clockwise) circulation around the inlet in the neighborhood of the lip. Presumably the asymmetric flow separation,

and the clockwise circulation, are due to the non-symmetrical pressure field resulting from the ground plane and cylinder interaction when there is a large ratio of inlet to far upstream velocity. However, whatever the detailed mechanism, it is clear that the variation of circulation with distance along the inlet length is directly linked to the generation of the trailing vortex system, and thus to the inlet vortex formation.

H. Experiments with Twin Inlets: The Role of the Ground Boundary Layer

We have been focusing so far on the overall picture of the inlet vortex system. Another basic fluid mechanic question concerns the role of the ground boundary layer in the creation of this vortex. It is true that the ground boundary layer can be the source of the vorticity which exists in the core of the inlet vortex, and which is convected along the axis of the vortex into the inlet. However, the overall features of the velocity field outside of the viscous regions might not be expected to be greatly dependent on the characteristics of this ground boundary layer, or even perhaps on whether there is a ground boundary layer. In order to investigate this, we examined a twin inlet configuration, at ninety degrees and two hundred seventy degrees to the mean flow. The centerline "height" to diameter ratio for each inlet was 1.4, i.e., the center to center distance was 2.8, as with the single inlet. The inlets were identical and the (downstream) resistance characteristics of each were made high enough so that the flow would exhibit a plane of symmetry between them at the same geometrical position as the ground plane, i.e., the ground plane was "replaced" by the symmetry plane. Flow visualization showed that the streamlines were indeed quite symmetrical with respect to this plane.

The replacement of the ground plane, and its boundary layer by this (inviscid) plane of symmetry allows us to study the inlet vortex formation with no ambient vorticity upstream of the inlet.

The investigation of the double inlet configuration at ninety degrees of yaw revealed a steady, strong, clockwise (when viewed looking down on the tunnel) vortex, which stretched between the two inlets. A trailing vortex was evident from each of the inlets. The inlet vortex enters the top and bottom inlets at approximately 6:00 and 12:00, with clockwise and counterclockwise rotation, when viewed looking into the inlets, respectively. The center of the vortex core was often apparent due to cavitation along its length.

The streamlines for this configuration were thus as sketched in Fig. 3.10, which also shows the relative scale of the trailing vortex and of the vortex between the inlets. The overall flow field for each inlet was thus similar to that for the single inlet situation. A sketch of the vortex lines for the double inlet configuration is shown in Fig. 3.11, in which the similarity to the vortex system of a finite wing is apparent. Observations of the hydrogen bubbles showed that the circulation around the inlet was found to vary with axial distance from the inlet lip, as in the single inlet configuration.

Tests were also carried out with the inlet at two hundred seventy degrees of yaw. The result was that the same type of vortex system was present, with a reversed sense of rotation. This again indicates that the phenomenon is not due to any lack of symmetry of the tunnel, i.e., the ambient conditions, but rather to the asymmetry produced by the effect of the inlets on the flow. A detailed discussion of the fluid mechanics of the formation of this vortex is given in (Ref. 3.17).

I. Summary and Discussion

In the preceding we have presented two different mechanisms for inlet vortex formation. The first of these, the intensification of ambient (vertical) vorticity is essentially an inviscid phenomenon, with the role of viscosity being primarily to limit the vorticity amplification in regions of high rates of stretching. It thus appears that many of the overall features of this type of flow can be predicted using an inviscid calculation procedure, perhaps coupled with an approximate description of the effects of viscosity.

In the second mechanism the appearance of an inlet vortex is linked directly to the variation in circulation along the length of the inlet. Viscous effects are much more central in creating this type of flow, since the circulation distribution round the inlet is determined by the separation of the three-dimensional boundary layers on the outer surface of the inlet.

There are still several aspects of this problem that are unresolved and that we hope to pursue. The foremost is the quantification of the fluid dynamic process that set the circulation round the inlet and hence that determines the strength of the vortex generated by the second mechanism. If this can be done, one is then in a position to state which of the two mechanisms is important in a given situation, as well as how serious the vortex problem will be.

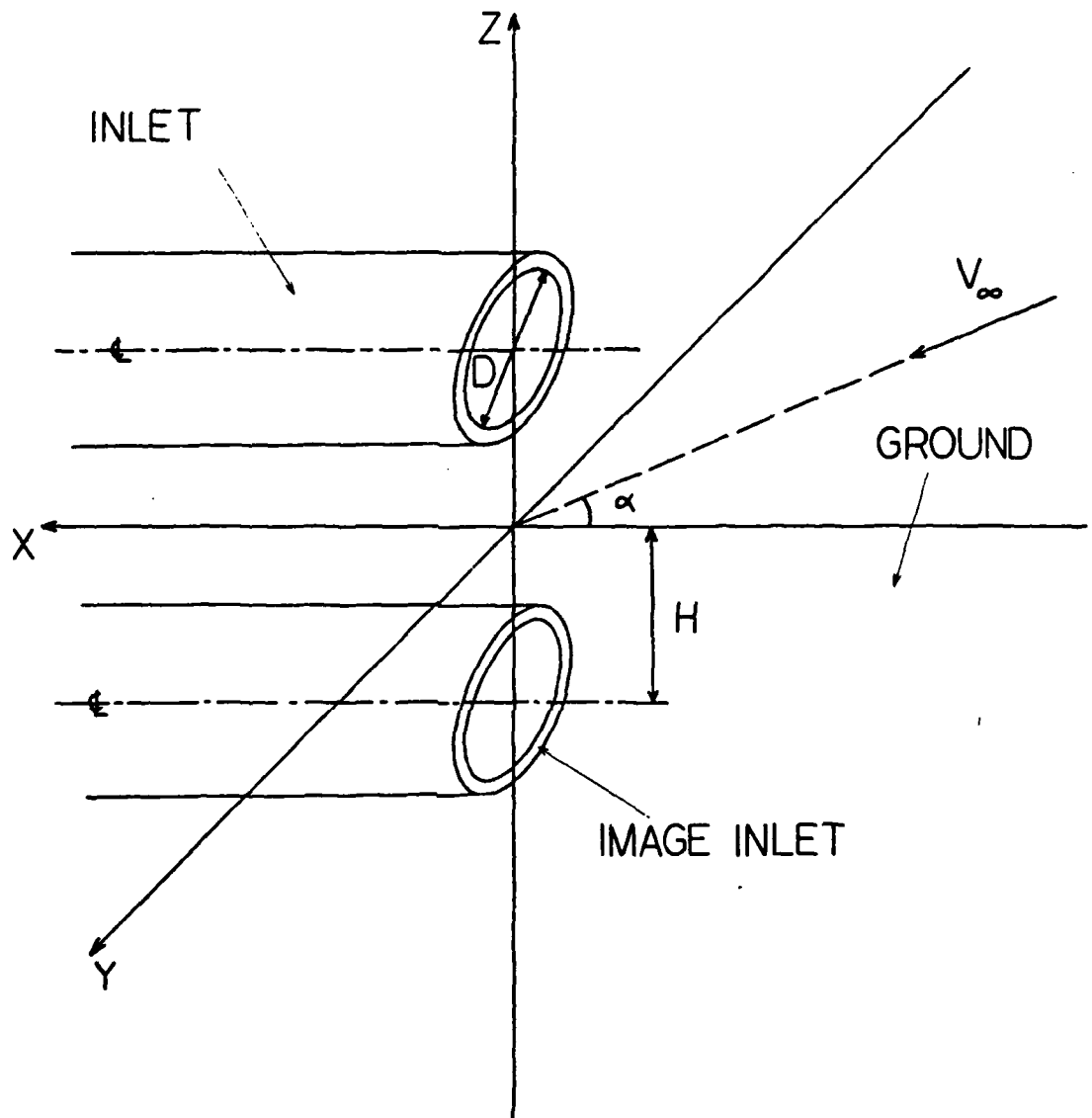


FIGURE 3.1 FLOW GEOMETRY

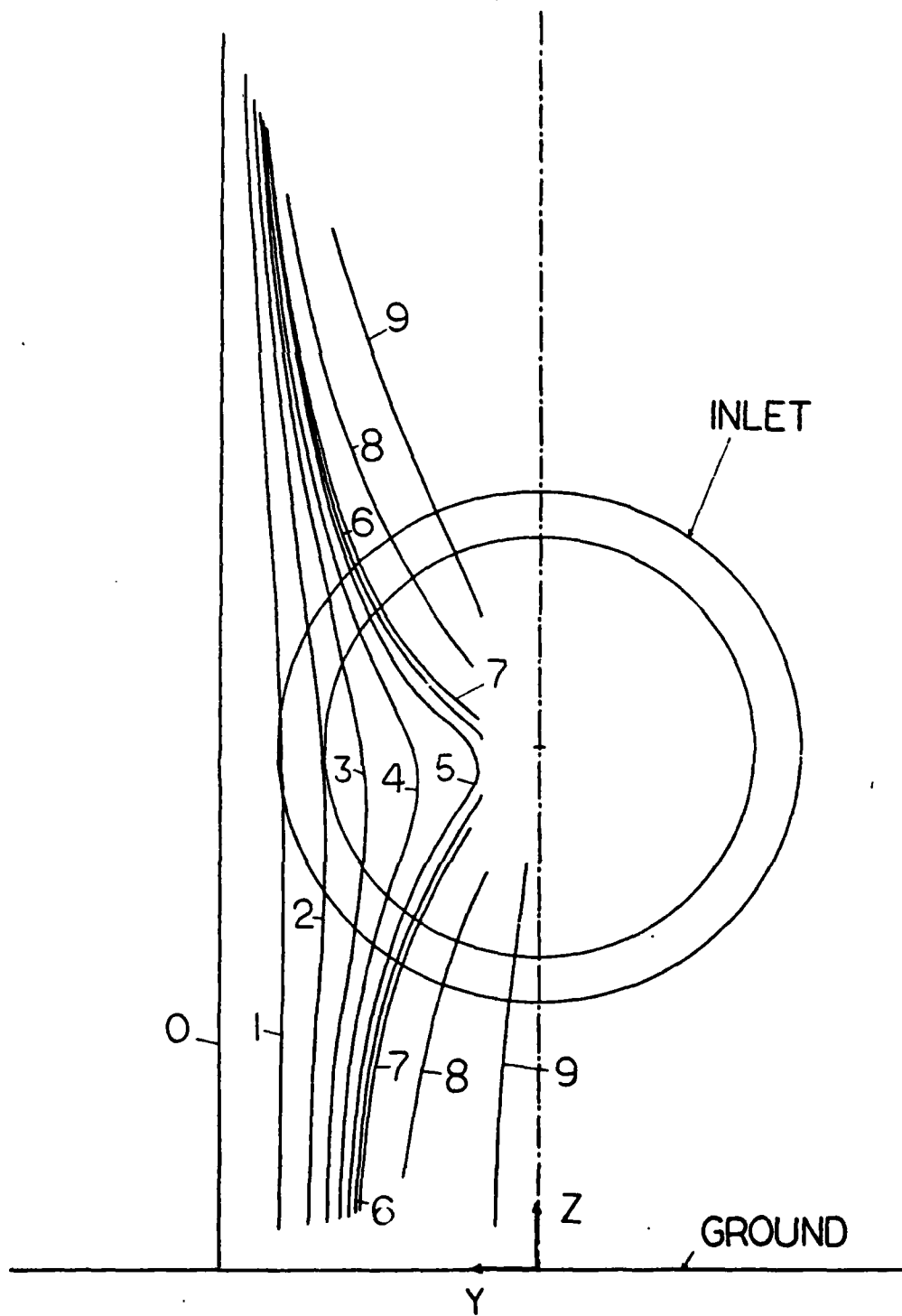


FIGURE 3.2 PROJECTIONS OF MATERIAL LINES SHOWN IN FIGURE
ON Y, Z PLANE

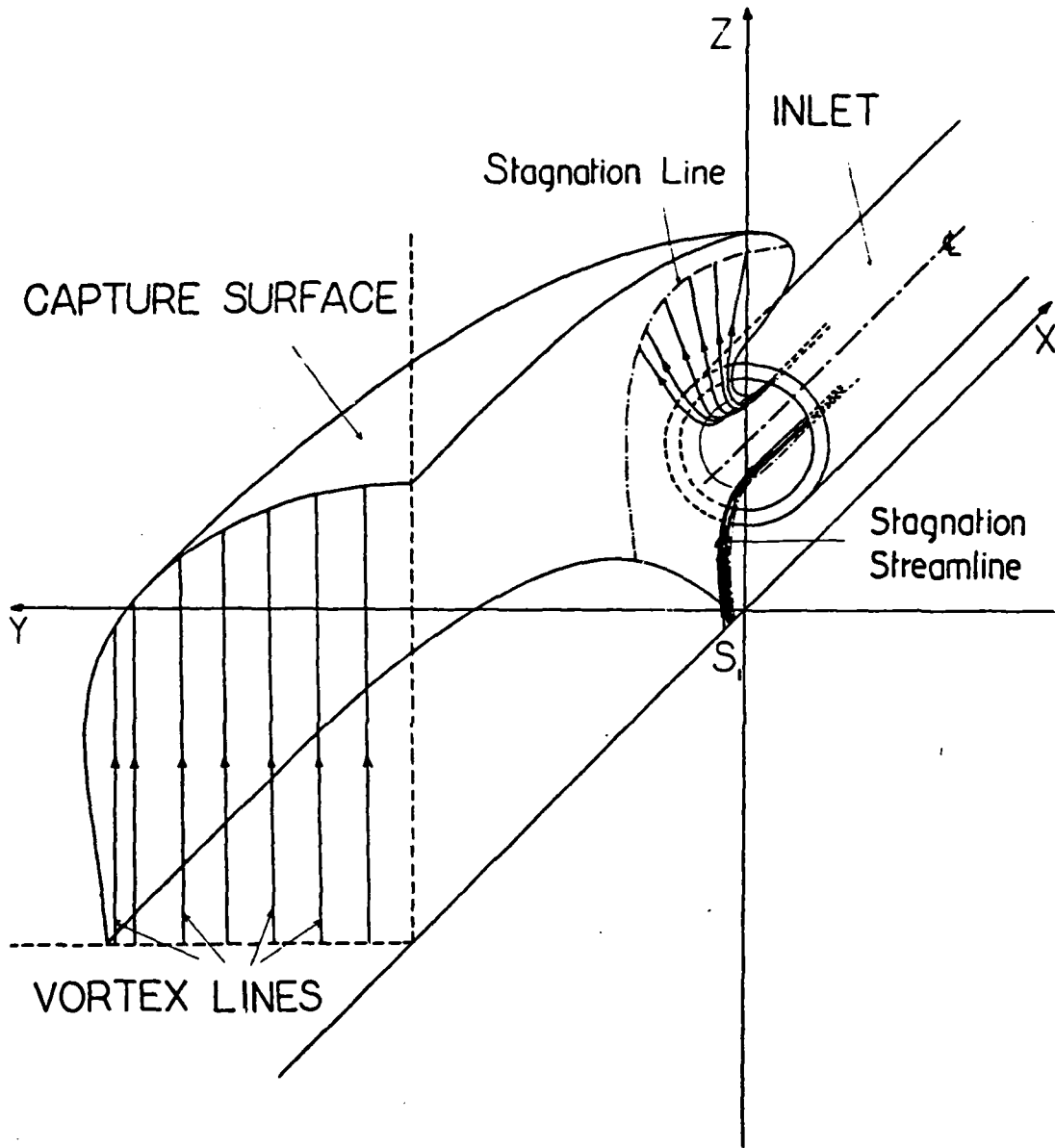


FIGURE 3.3 SUGGESTED DEFORMATION OF A FAR UPSTREAM UNIFORM DISTRIBUTION OF VERTICAL VORTEX LINES

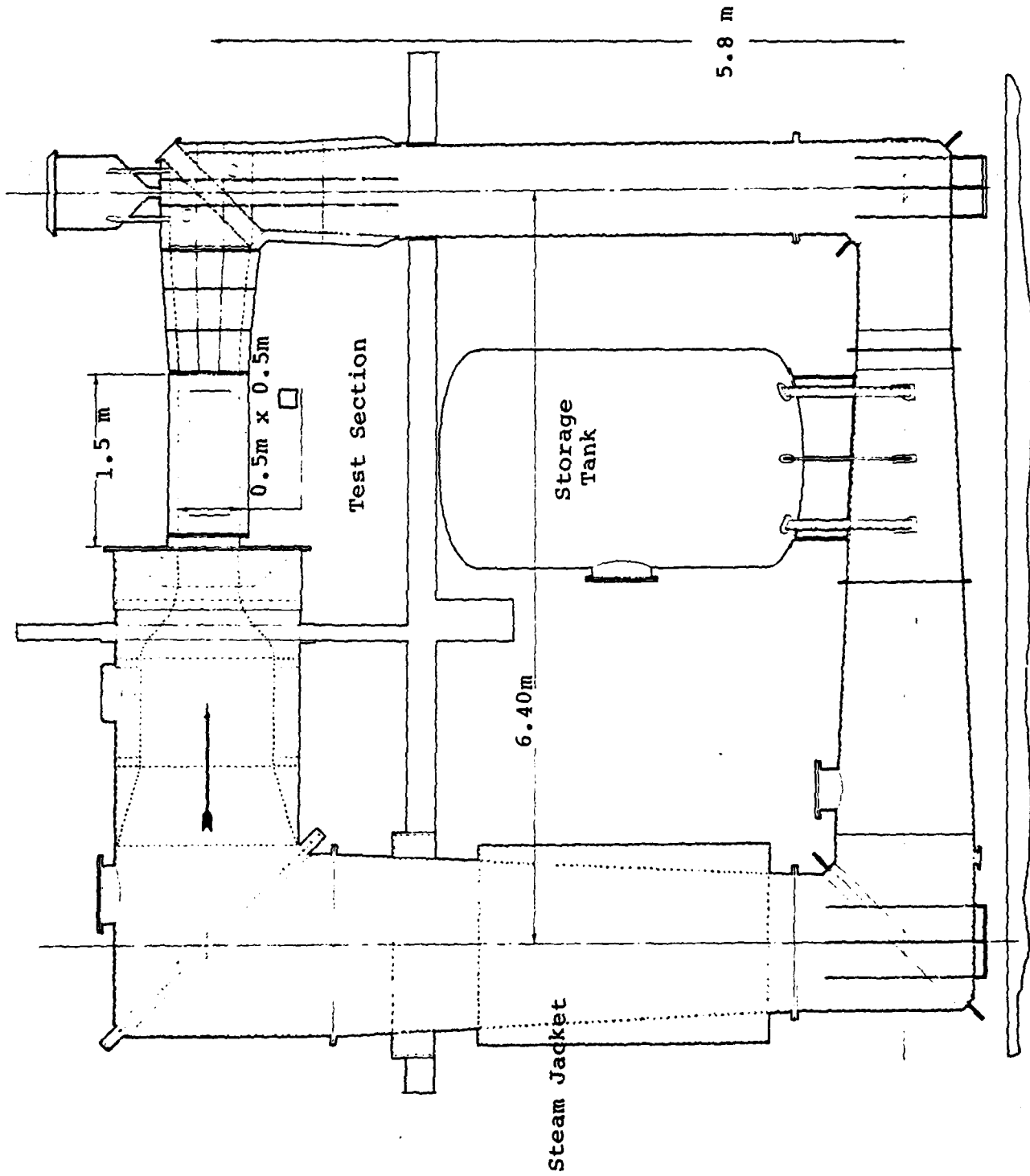
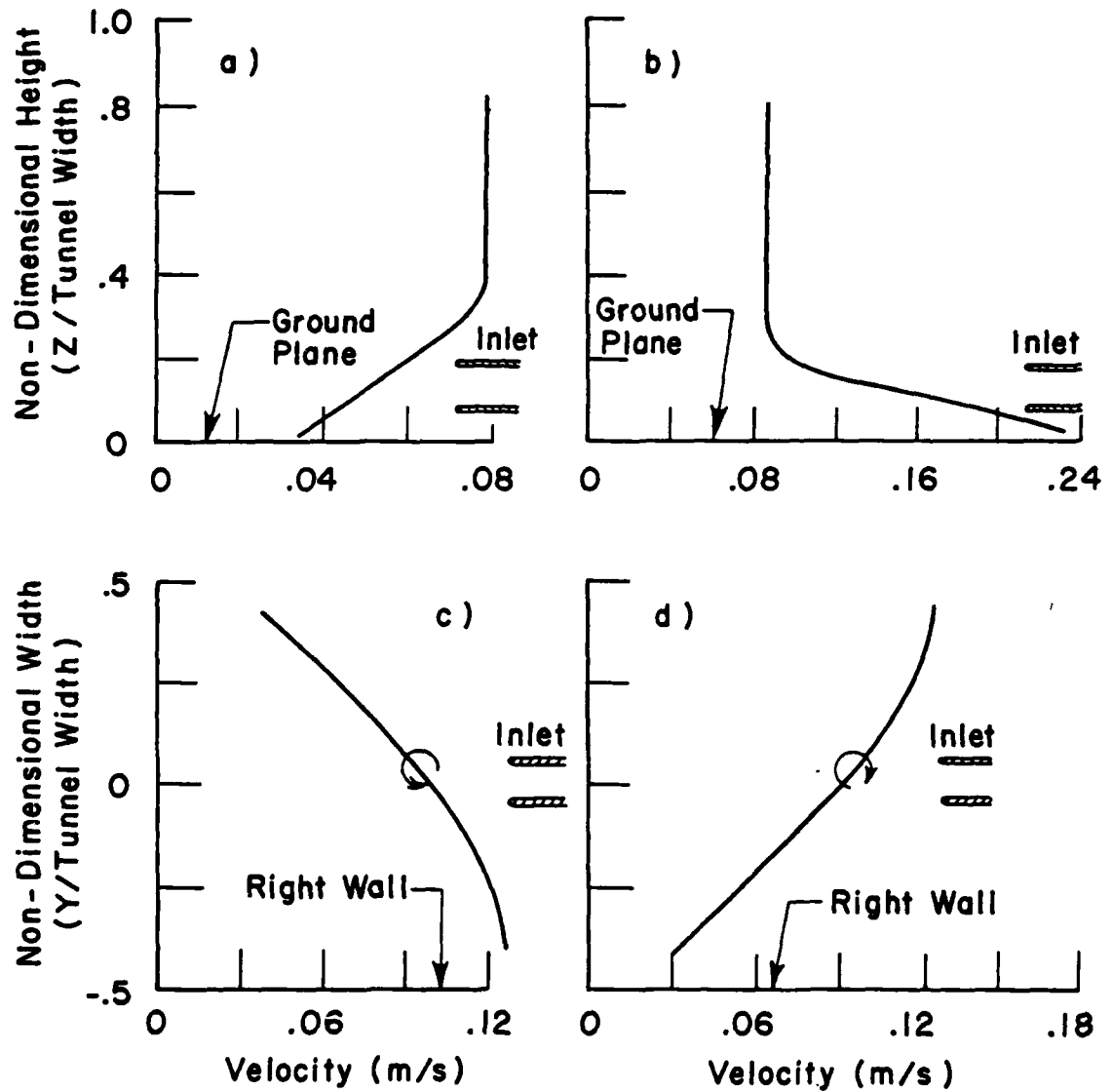


FIGURE 3.4 MIT OCEAN ENGINEERING WATER TUNNEL

A) BOUNDARY LAYER TYPE PROFILE

B) JET TYPE PROFILE



C) LEFT TO RIGHT WINDSHEAR PROFILE ; D) RIGHT TO LEFT WINDSHEAR PROFILE

FIGURE 3.5 VELOCITY PROFILES (CALCULATED FROM HYDROGEN BUBBLE FLOW VISUALIZATION)

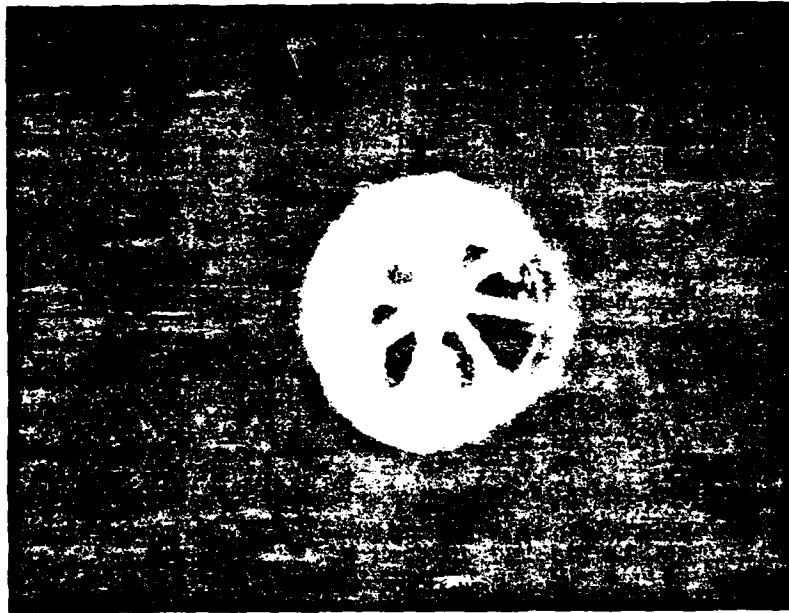


FIGURE 3.6 INGESTION OF A VERTICAL VORTEX LINE (LEFT-RIGHT SHEAR INTO A 0° INLET - VIEWED LOOKING UPSTREAM THROUGH A MIRROR. (PHOTOGRAPH OF HYDROGEN BUBBLE FLOW VISUALIZATION).

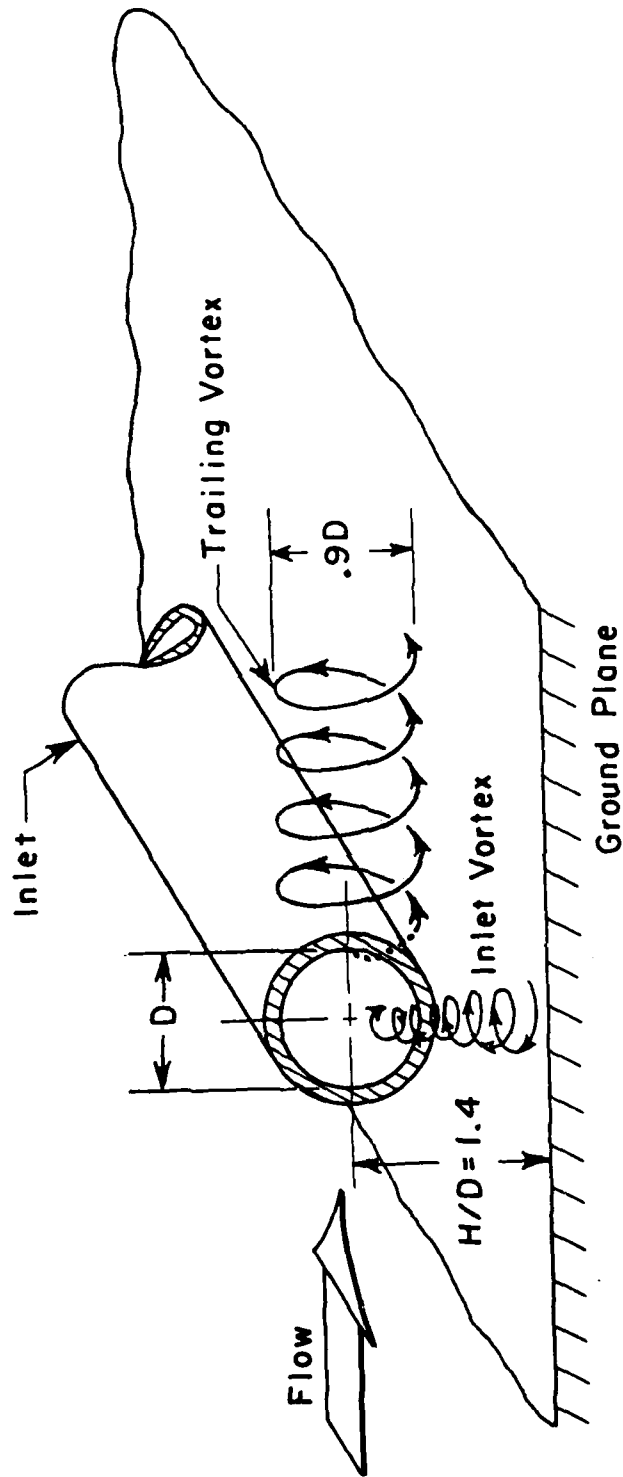
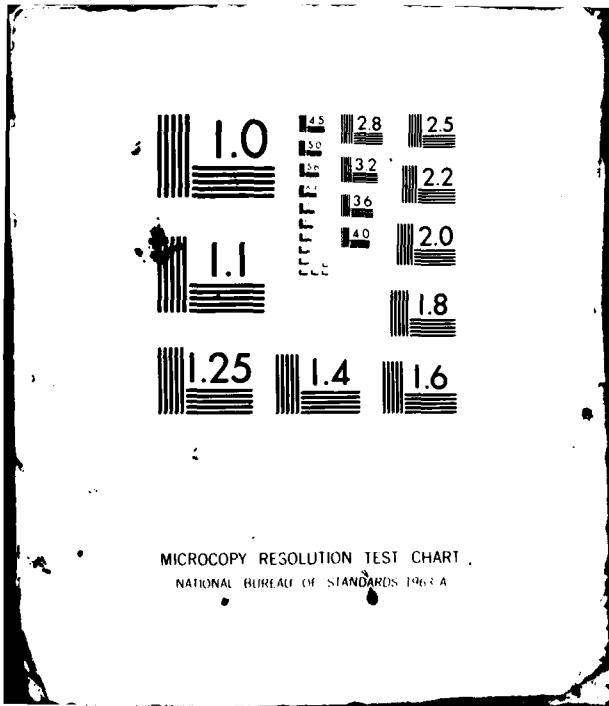


FIGURE 3.7 STREAMLINES ASSOCIATED WITH INLET AT 90° OF YAW
IN AN IRRATIONAL UPSTREAM FLOW (DRAWN FROM
HYDROGEN BUBBLE FLOW VISUALIZATION)



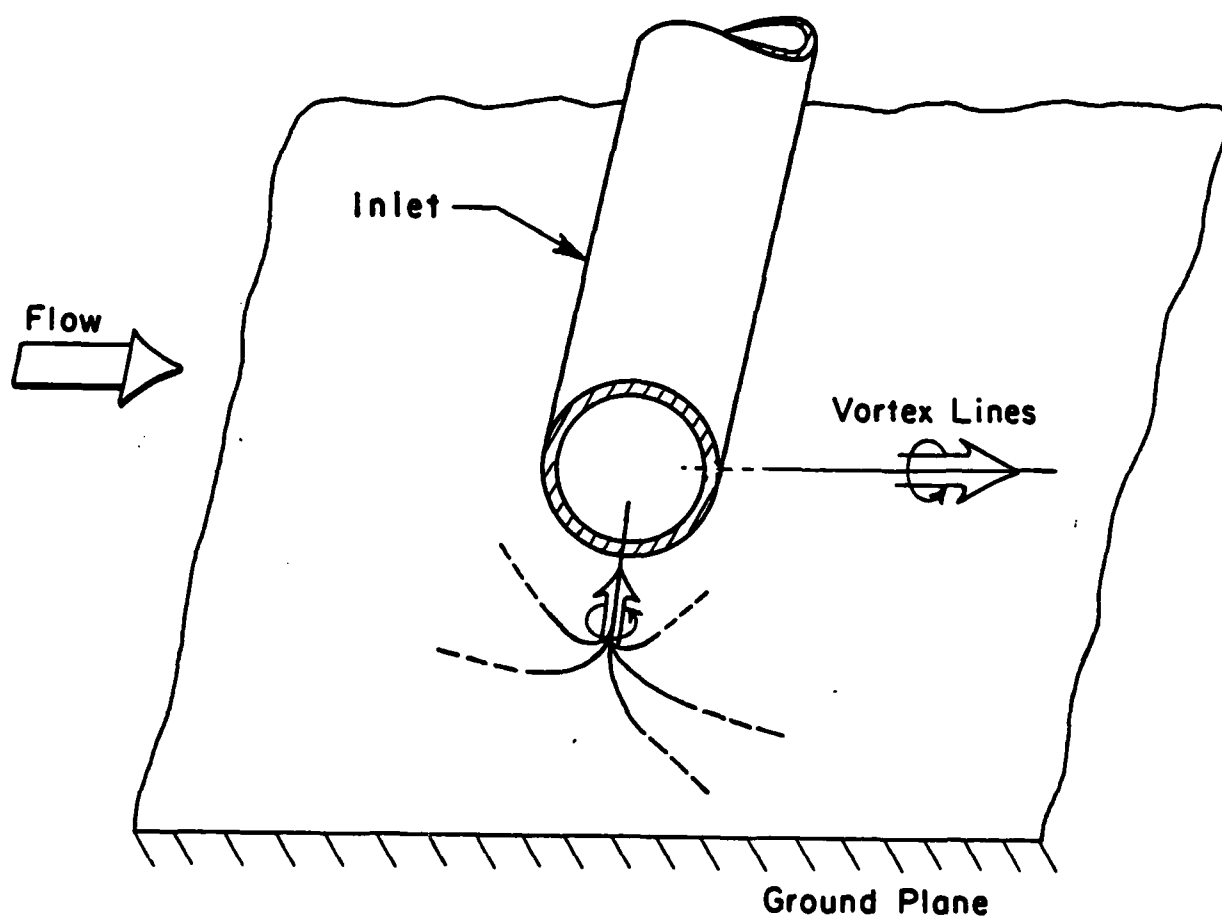
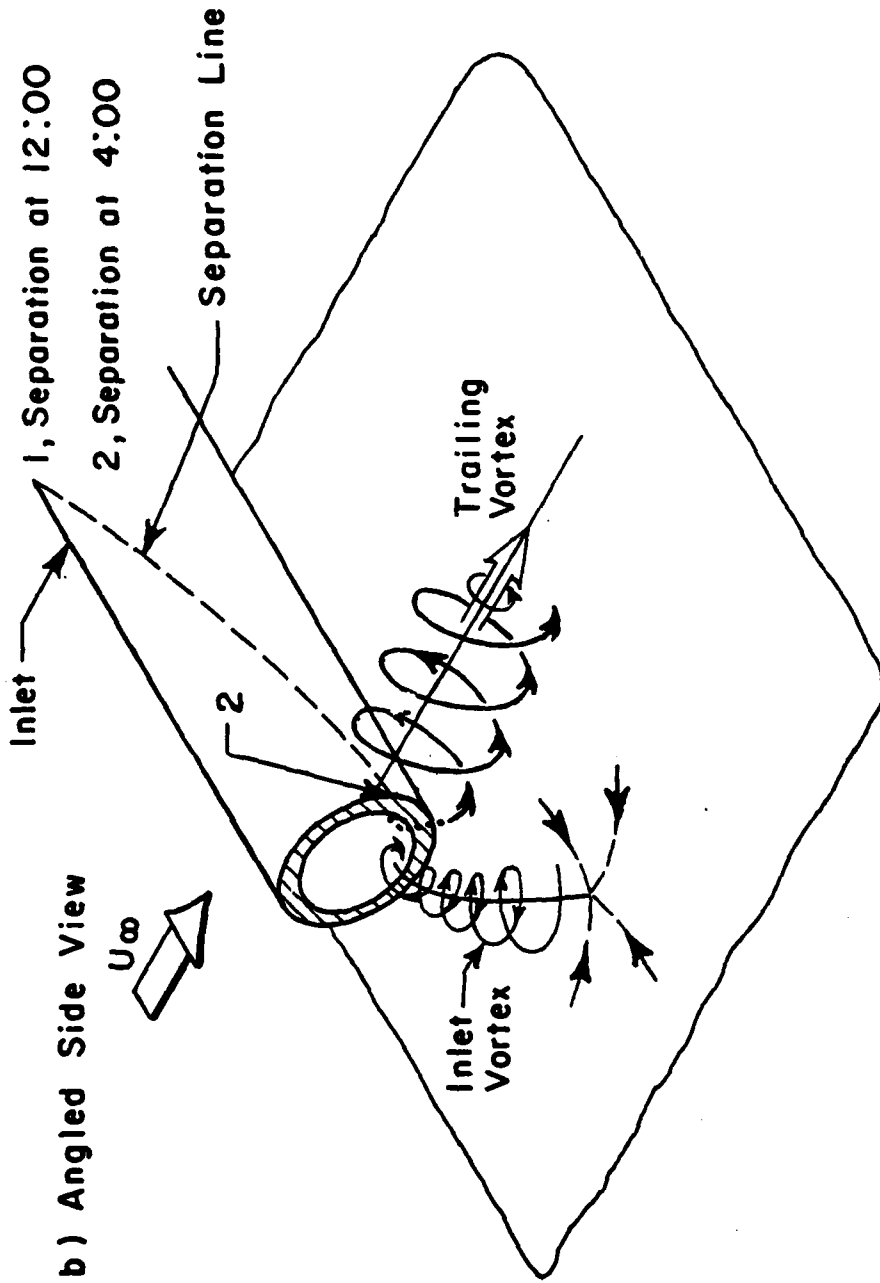


FIGURE 3.8 VORTEX LINES ASSOCIATED WITH AN INLET AT 90° OF YAW IN AN IRROTATIONAL UPSTREAM FLOW (DRAWN FROM HYDROGEN BUBBLE FLOW VISUALIZATION)



b) Angled Side View

FIGURE 3.9 ANGLED SIDE VIEW

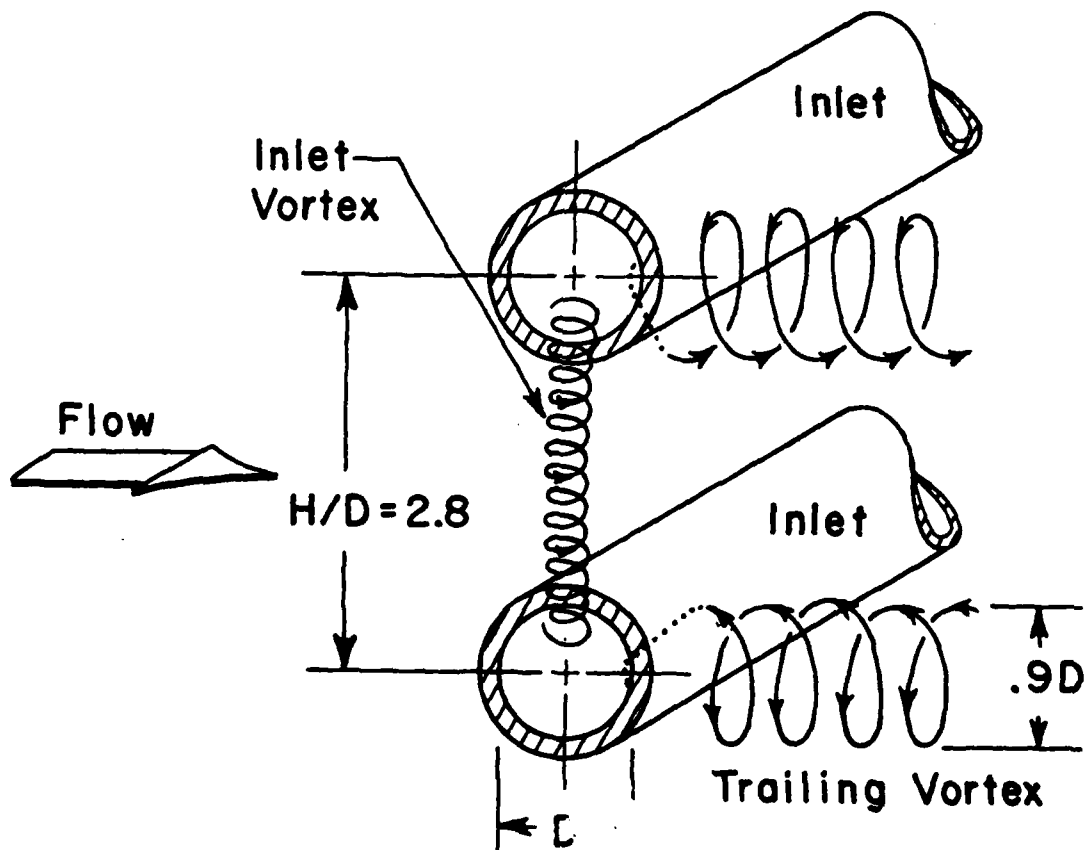


FIGURE 3.10 STREAMLINES ASSOCIATED WITH TWIN INLETS AT 90° OF YAW IN AN IRRATIONAL UPSTREAM FLOW (DRAWN FROM HYDROGEN BUBBLE FLOW VISUALIZATION)

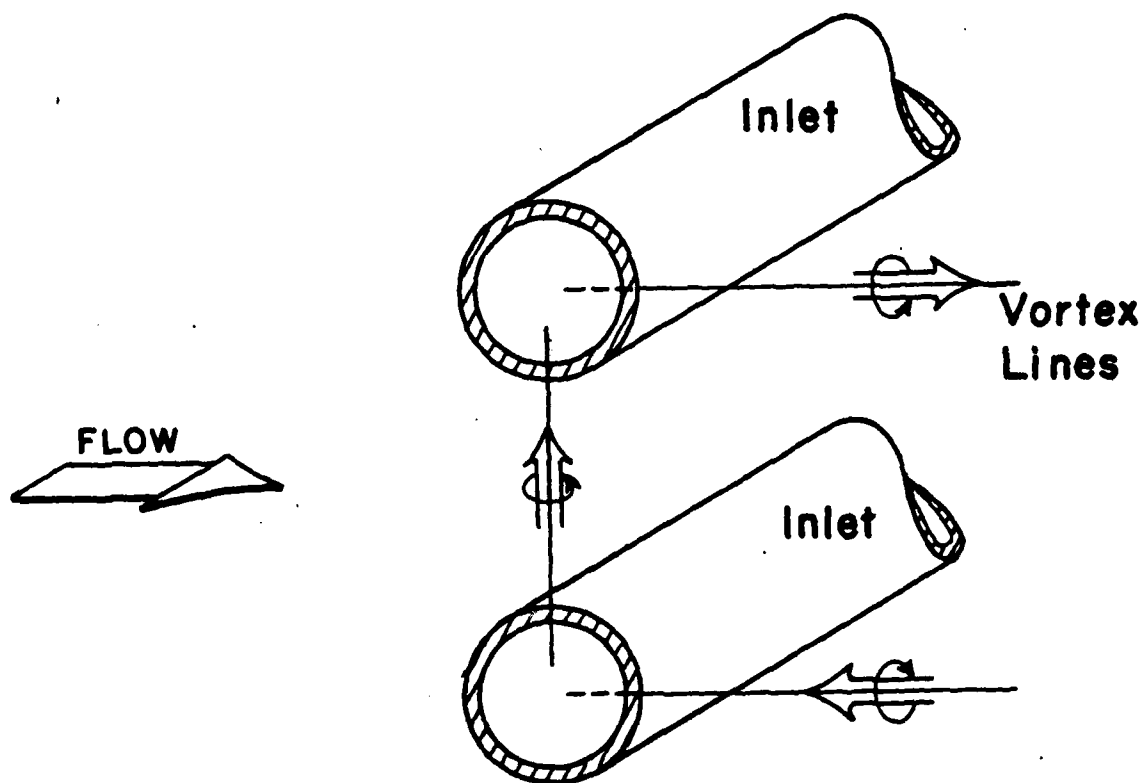


FIGURE 3.11 VORTEX LINES ASSOCIATED WITH TWIN INLETS AT 90° OF YAW IN AN IRROTATIONAL UPSTREAM FLOW (DRAWN FROM HYDROGEN BUBBLE FLOW VISUALIZATION)

COMBINED RADIAL/CIRCUMFERENTIAL FLOW DISTORTIONIN TURBOMACHINES

During the contract period, we have successfully used Clebsch-Hawthorne (3.18) formulations of the flow field to solve two different problems. These are: the three-dimensional flow field resulting from the passage of a combined radial/circumferential distortion through a highly-loaded annular blade-row, and the effects of compressibility on the behavior, in a three-dimensional swirling flow, of non-axisymmetric disturbances created by the introduction of a distortion in stagnation pressure/or temperature at a far upstream station or at the exit of an annular blade row. The analysis is a linearized one so that closed form solutions are possible.

In the case of combined radial circumferential distortion, the radial variation of an upstream stagnation pressure distortion will give rise to the presence of tangential vorticity. As the tangential vorticity passes through the blade-row, a component of streamwise vorticity will be created. The presence of such streamwise vorticity will induce a secondary flow pattern, and would lead to a finite value of radial velocity at hub and tip. Since this cannot occur, the blade circulation in the neighborhood of the hub and tip casing must readjust itself so that trailing vorticity is shed into the downstream flow in such a way as to yield a zero radial velocity at these locations. Because of this effect, the analysis of (Ref. 3.19) must be modified considerably to describe these flows. This modified analysis is fully documented in the M.S. Thesis of Mr. A. Lifshits (3.20). In the thesis several numerical examples are worked out to compare with the results obtained using a strip theory based on taking two-dimensional "slices" at different radial stations. Typical comparisons are shown in Figs. 3.12 to 3.15. It is seen that there is a significant difference between the two results, and only the three-

dimensional theory can adequately describe the effect of the combined radial circumferential distortion through a highly-loaded blade row. This is because a 3-D description properly includes both the centrifugal effects together with the two distinct types of vorticity: the Beltrami vorticity and the vorticity associated with a stagnation pressure gradient.

When compressibility effects become significant, it is necessary to transform the equation governing the flow in the physical flow field into a reduced flow field (3.21), before the Clebsch-Hawthorne Technique is employed to describe the non-axisymmetric disturbances resulting from the introduction of an inlet distortion. The use of the flow transformation technique, and the resulting analytical formulation of compressible asymmetric swirling flow theory, will be documented in a forthcoming Gas Turbine Lab report. From the analysis, it is concluded that one may consider the use of (asymmetric) non-uniformities in stagnation pressure/temperature as a useful alternative measure of the flow non-uniformity (rather than entropy and vorticity). The formulation also shows that for a stationary system, variations in the stagnation temperature do not contribute to any disturbances, in accord with the Munk and Prim (3.22) substitution Principle. (This states that all flows with different stagnation temperature distribution, but the same distribution of stagnation pressure, have the same geometrical configuration of streamlines).

Three cases of numerical examples are worked out. In the first two cases, the distortion in stagnation pressure is introduced far upstream of: 1) a stator and 2) a rotor, while in the last case the distortion is introduced immediately downstream of a stationary blade-row. Some numerical examples are shown in Figures 3.16 to 3.20. They show that the compressibility effects can have a strong influence on the magnitude and downstream evolution of flow disturbances. In particular, at higher Mach number, the amplitude of the disturbance in the hub region (with high swirl) can oscillate with decreasing

modulation in the downstream region; and in the case of a rotor, the amplitude of the downstream stagnation pressure in the tip region can increase strongly with Mach numbers. The numerical examples also show that at sufficiently high Mach number the potential disturbance is dominant in the immediate neighborhood of the blade-row and the phase speed of the disturbance (in tangential - axial space) can be negative in the downstream region close to the blade row before becoming positive again further downstream.

Finally, it should be emphasized out that in agreement with earlier work (3.23, 3.24, 3.25) the results presented here show that in an environment of swirling flow, the entropy, vorticity and the pressure disturbances are strongly coupled. Thus, in addition to the convected and potential disturbances, non-convected disturbances can also arise in a swirling flow. It is this non-convected disturbance which yields a static pressure field that persists downstream with modulation in amplitude.

2 Three-dimensional theory
 1 Two-dimensional theory

Stator:
 Hub-to-tip ratio=0.4
 K = 0.4
 Inlet distortion.

$$(P_t^4 - \bar{P}_t^4) / \rho \bar{V}_z^2 = 0.2 \sin\left(\pi \left(\frac{1-z}{1-h}\right)\right) \cdot \cos \theta$$

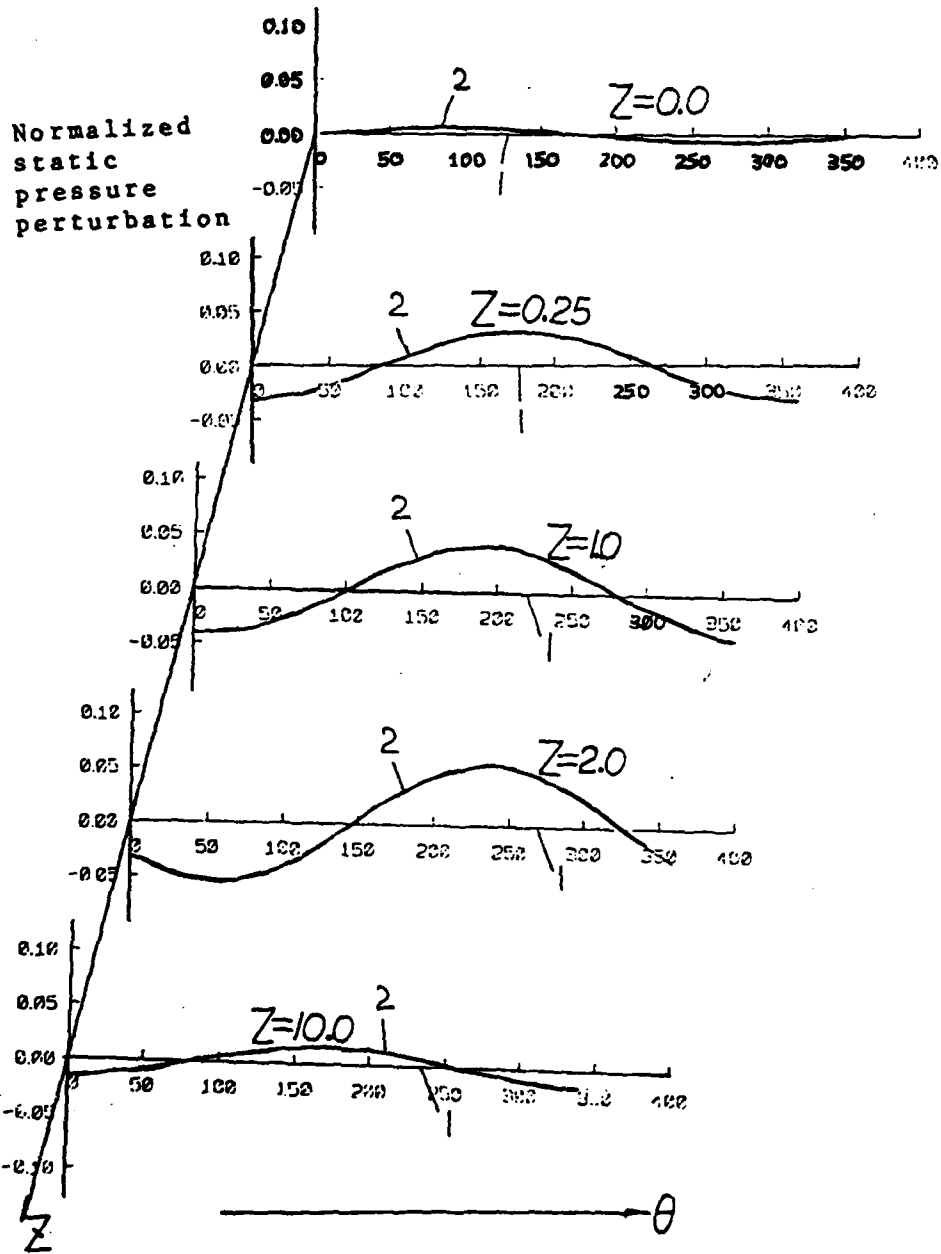


FIG. 3.12. TWO-DIMENSIONAL AND THREE-DIMENSIONAL PREDICTIONS OF DOWNSTREAM STATIC PRESSURE PERTURBATION AT DIFFERENT AXIAL STATIONS AT THE HUB.

2 Three-dimensional theory
 1 Two-dimensional theory

Rotor:
 Hub-to-tip ratio=0.4
 K =0.4
 Rotor tip speed = 1.7
 Inlet distortion.

$$(P_t^u - \bar{P}_t^u) / \rho \bar{V}_z^2 = 0.2 \sin\left(\pi \left(\frac{1-z}{1-h}\right)\right) \cdot \cos \theta$$

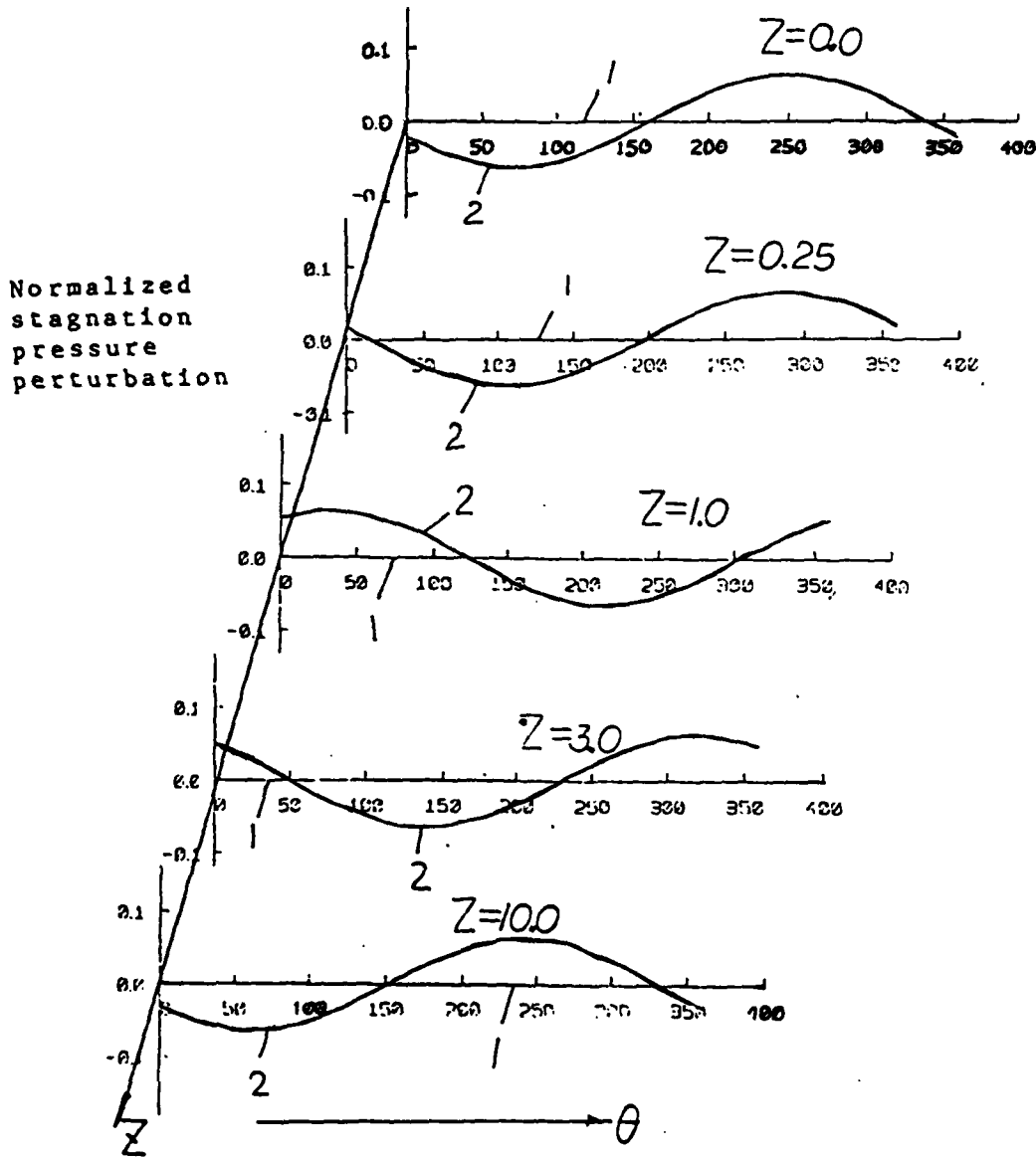


FIGURE 3.13;
 TWO-DIMENSIONAL AND THREE-DIMENSIONAL
 PREDICTIONS OF UPSTREAM STAGNATION PRESSURE
 PERTURBATION AT DIFFERENT AXIAL STATIONS AT THE HUB.

2- Three-dimensional theory
 1- Two-dimensional theory

Rotor:
 Hub-to-tip ratio=0.4
 K =0.4
 Rotor tip speed = 1.7
 Inlet distortion,

$$(P_t^4 - \bar{P}_t^4) / \rho \bar{V}_z^2 = 0.2 \sin(\pi(\frac{1-z}{1-h})) \cdot \cos \theta$$

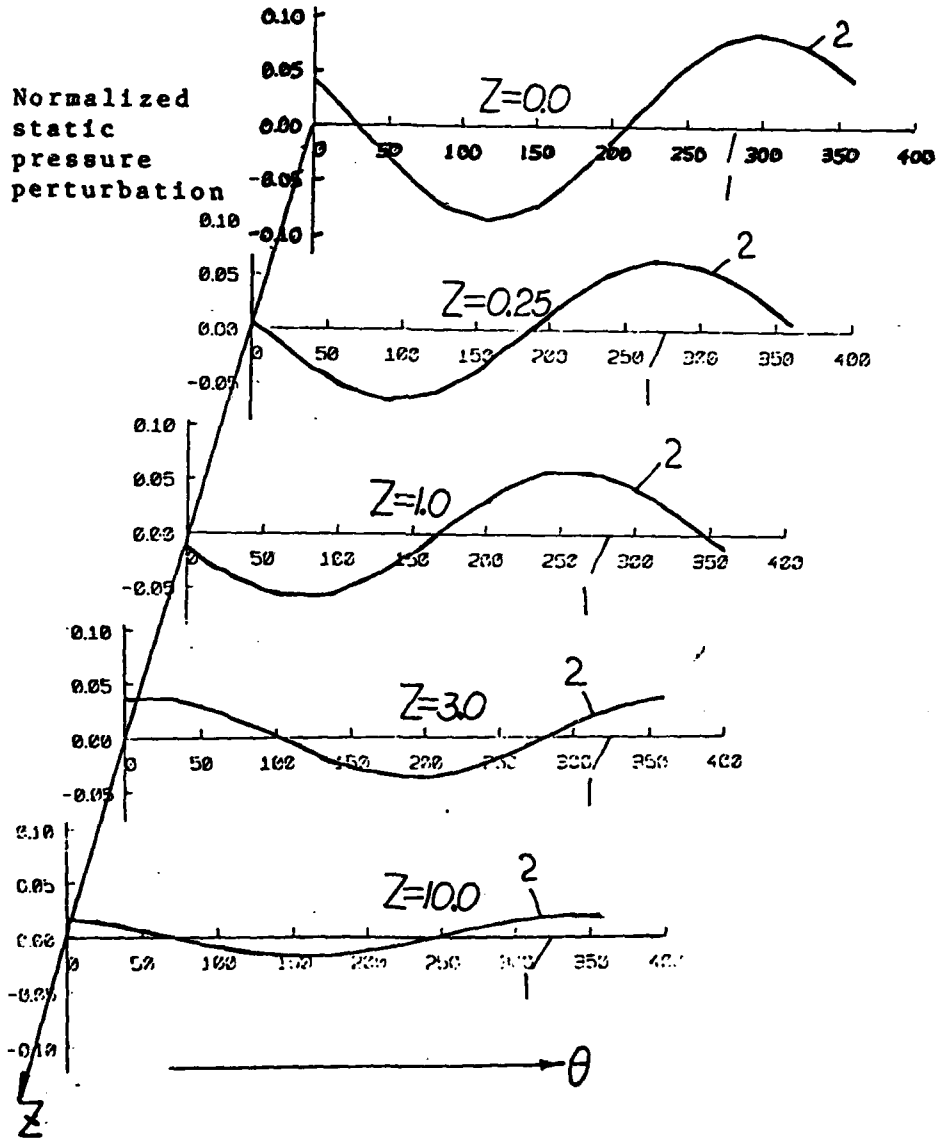
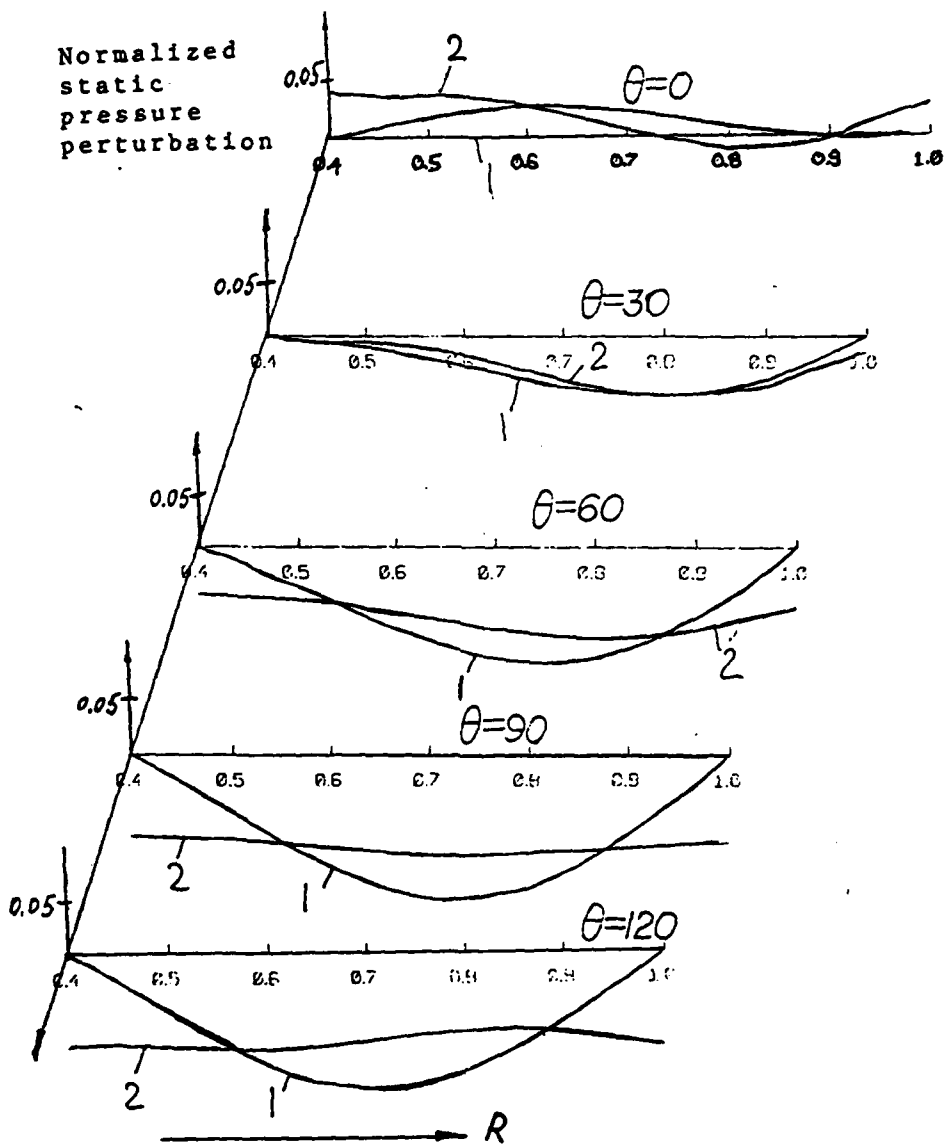


FIG: 3.14: TWO-DIMENSIONAL AND THREE-DIMENSIONAL PREDICTIONS OF DOWNSTREAM STATIC PRESSURE PERTURBATION AT DIFFERENT AXIAL STATIONS AT THE HUB.

2-Three-dimensional theory
 1-Two-dimensional theory

Rotor:
 Hub-to-tip ratio=0.4
 K=0.4
 Rotor tip speed = 1.7
 Inlet distortion,

$$(P_t^u - \bar{P}_t^u) / \rho \bar{V}_z^2 = 0.2 \sin\left(\pi \left(\frac{1-z}{1-h}\right)\right) \cdot \cos \theta$$



FIG; 3,15: TWO-DIMENSIONAL AND THREE-DIMENSIONAL PREDICTIONS OF DOWNSTREAM STATIC PRESSURE PERTURBATION AT DIFFERENT ANGLES FOR Z=0.0

NOMENCLATURE FOR FIGURES 3.16 - 3.20

HR	hub to tip ratio
K	$r\bar{v}_\theta$ (product of radius and mean tangential velocity)
W	angular velocity of blade row
PT	amplitude of upstream stagnation pressure distortion
M	far upstream axial Mach number
Z	axial distance
R_T	tip-radius
R	radius normalized by the tip radius R_T

FIGURE 3.16 AXIAL EVOLUTION OF THE AMPLITUDE OF TANGENTIAL VELOCITY PERTURBATION FOR STATOR

AT $M = 0.01$.

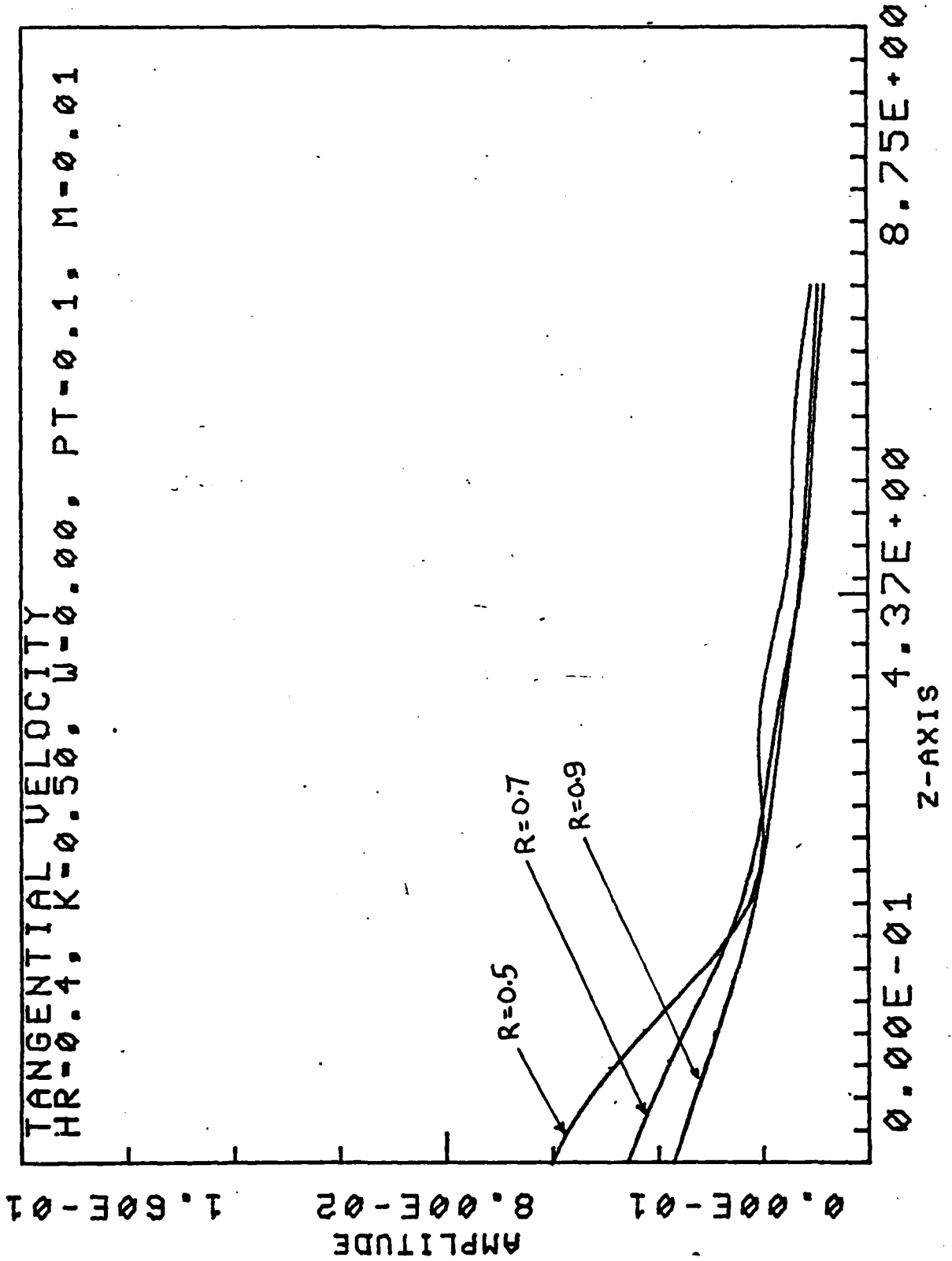


FIGURE 3.16B: AXIAL EVOLUTION OF THE AMPLITUDE OF TANGENTIAL VELOCITY PERTURBATION FOR STATOR AT $M = 0.5$

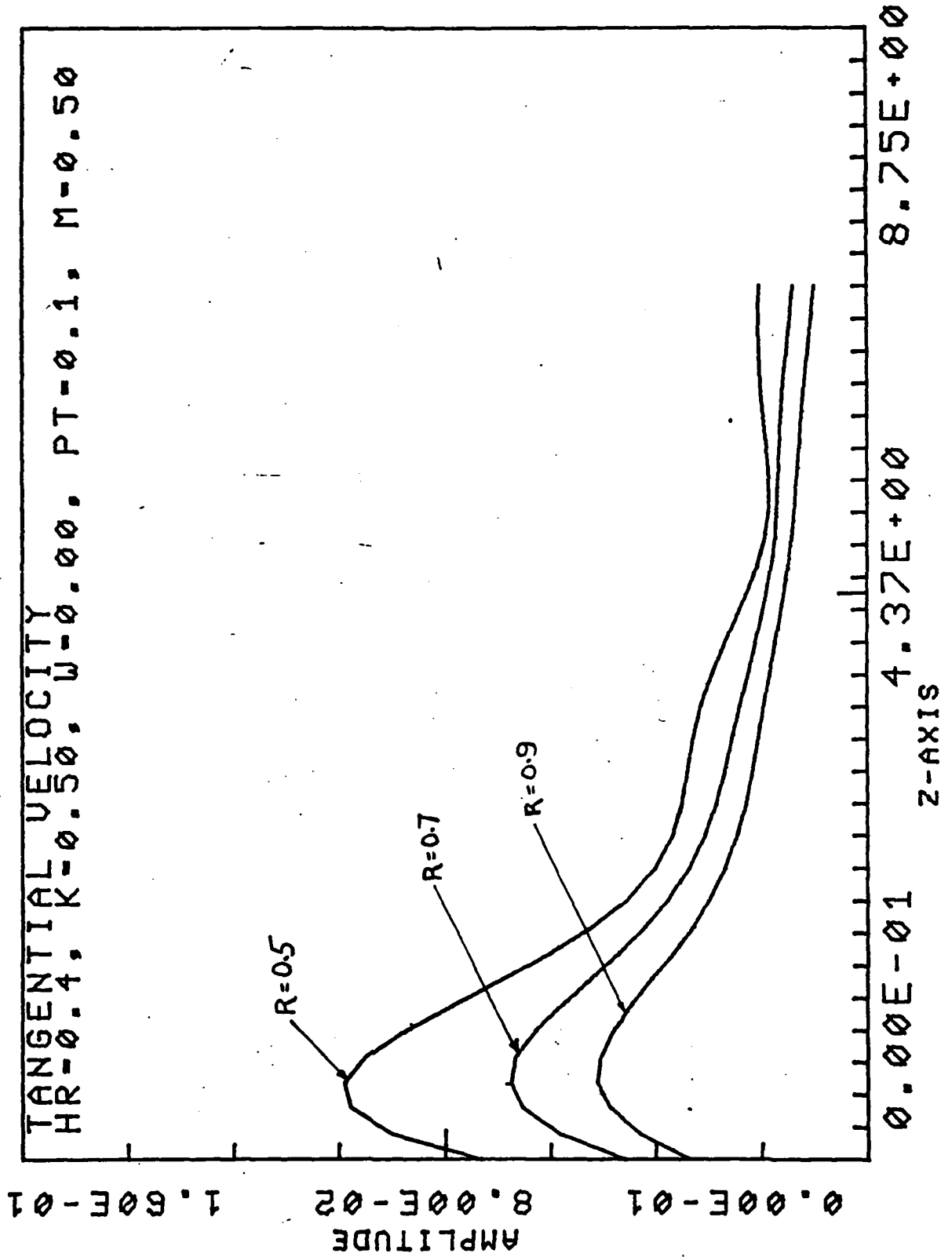


FIGURE: 3.17A

DOWNSTREAM AXIAL EVOLUTION
OF STATIC PRESSURE
PERTURBATION FOR STATOR
AT $M = 0.01$
 $R = 0.5$
 $HR = 0.4$
 $K = 0.5$
 $W = 0.0$
 $PT = 0.1$

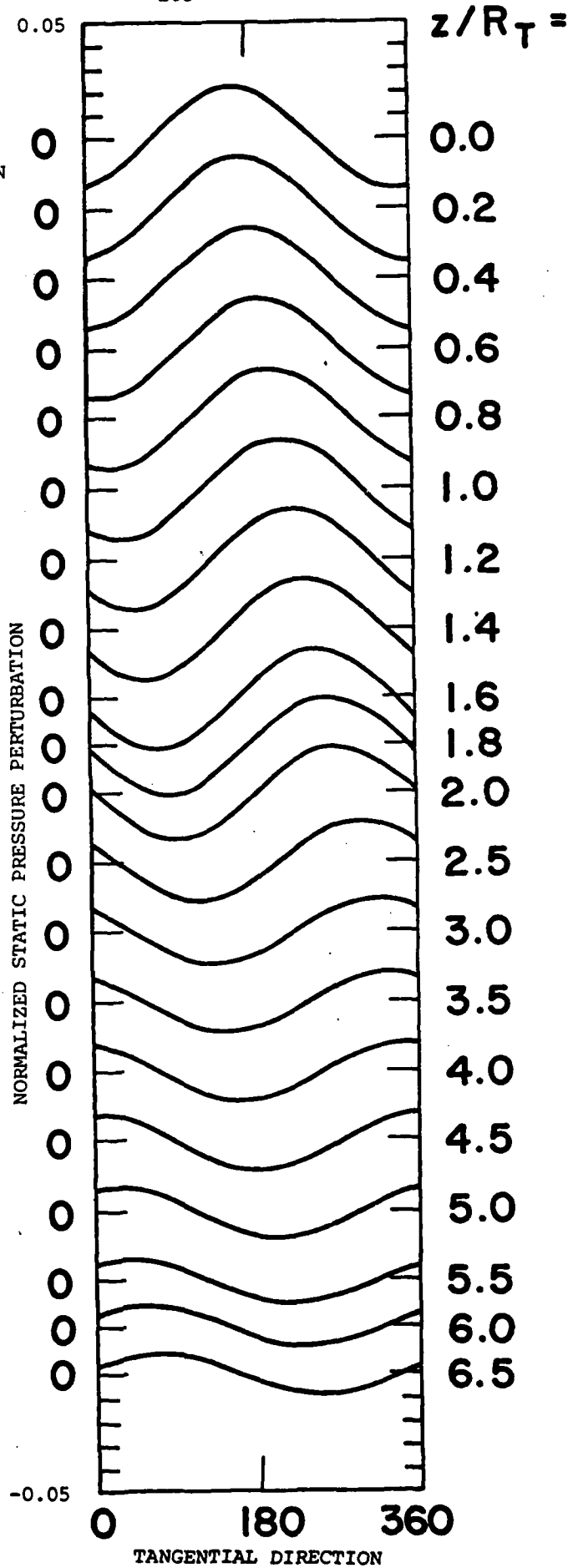


FIGURE 3.17B:

DOWNSTREAM AXIAL EVOLUTION
OF STATIC PRESSURE
PERTURBATION FOR STATOR

AT $M = 0.5$
 $K = 0.5$
 $HR = 0.4$
 $W = 0.0$
 $PT = 0.1$

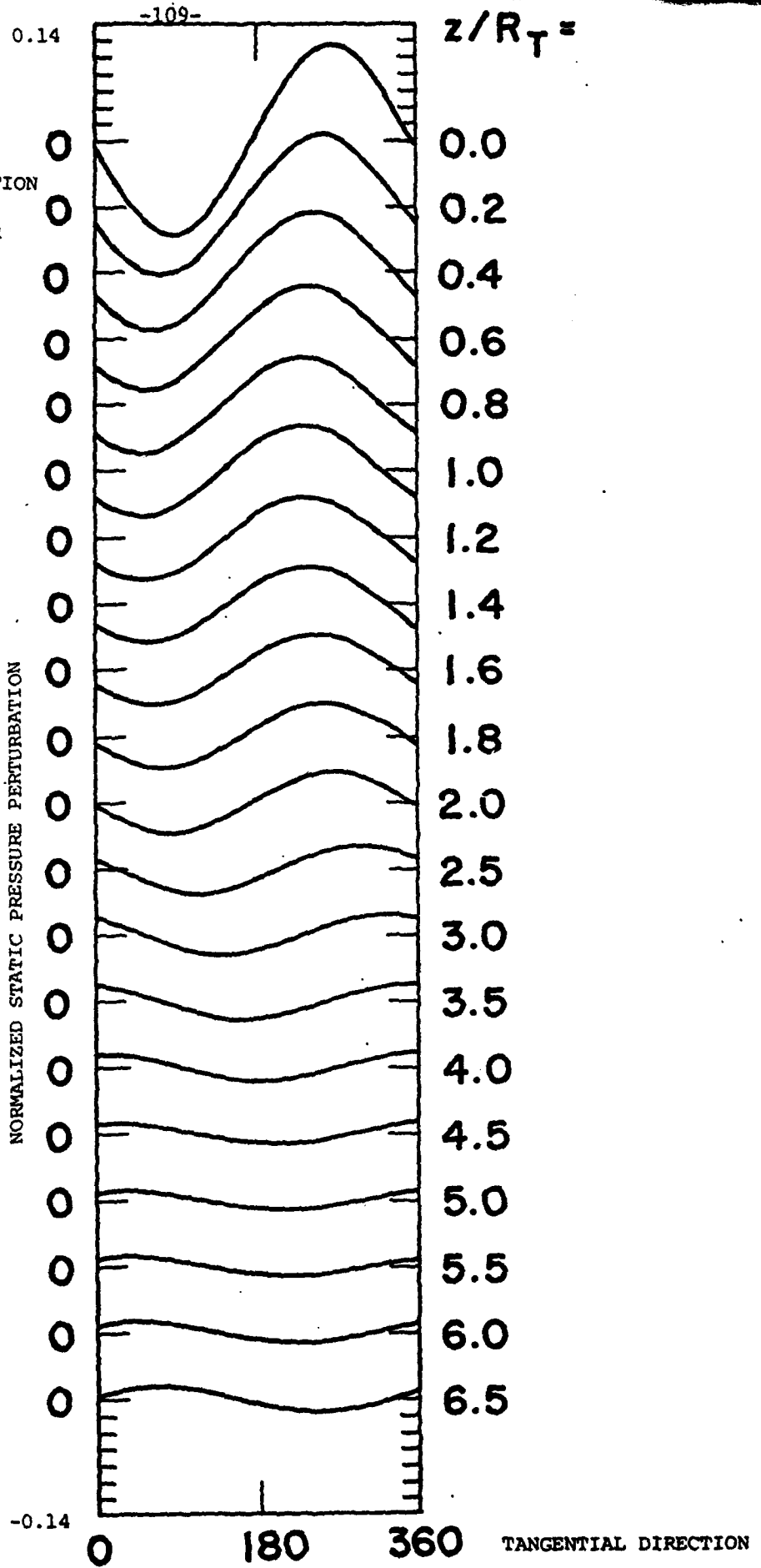


FIGURE 3.18A: AXIAL EVOLUTION OF AMPLITUDE OF STATIC PRESSURE PERTURBATION FOR ROTOR AT $M = 0.1$

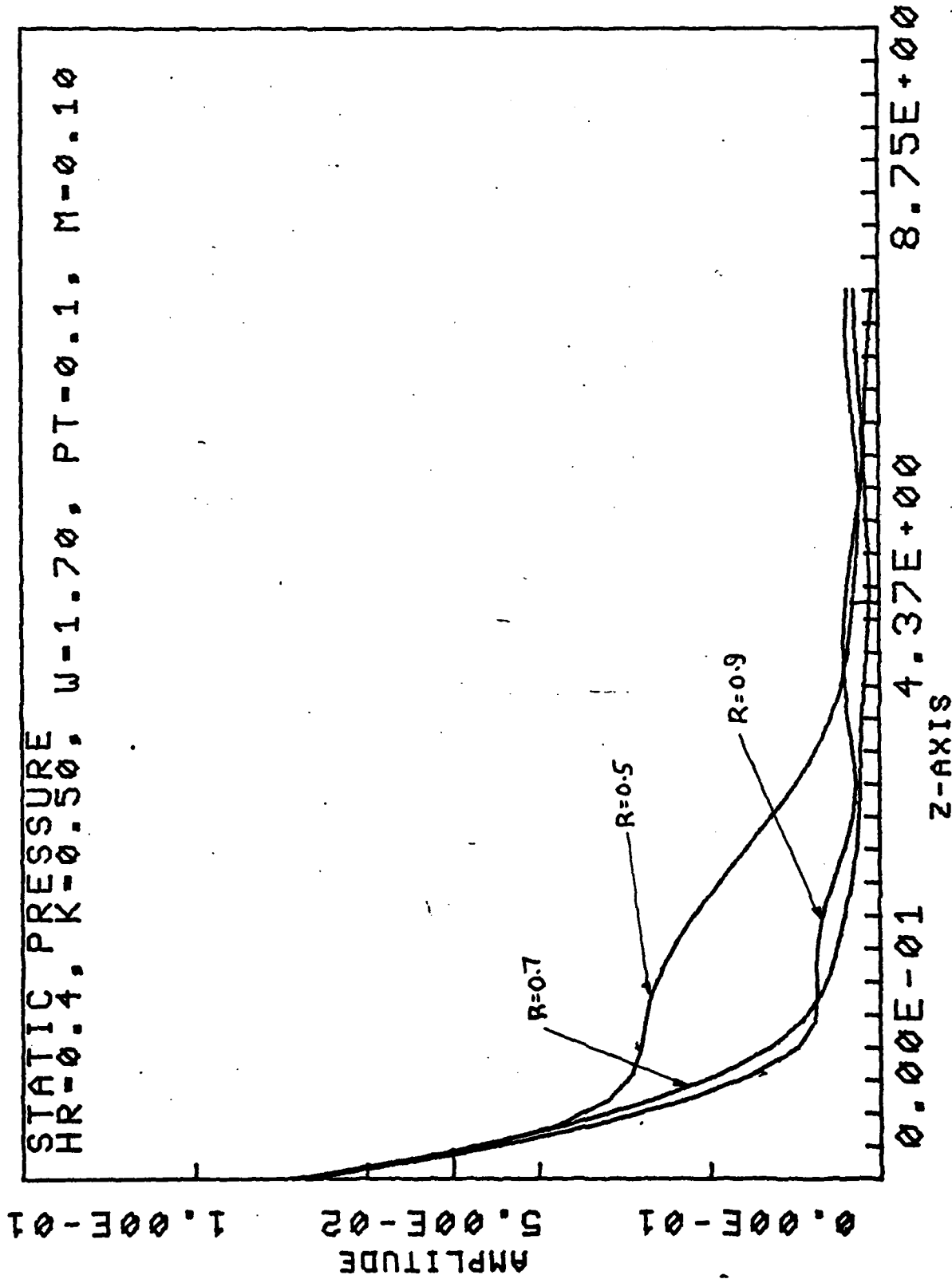


FIGURE 3.18B: AXIAL EVOLUTION OF AMPLITUDE OF STATIC PRESSURE PERTURBATION AT $M = 0.50$

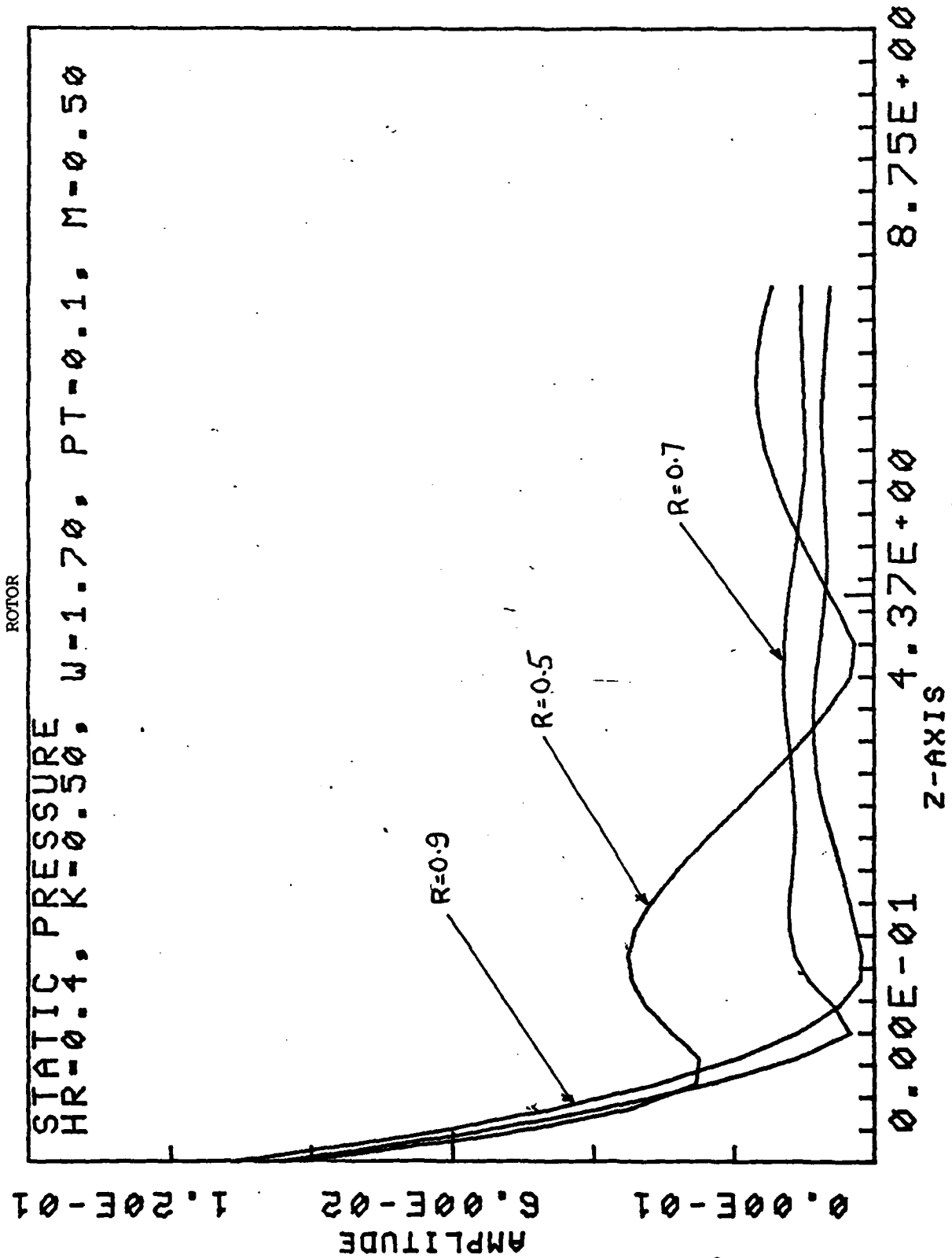


FIGURE 3-19: DEPENDENCE OF DOWNSTREAM STAGNATION PRESSURE DISTORTION ON MACH NUMBERS (ROTOR)

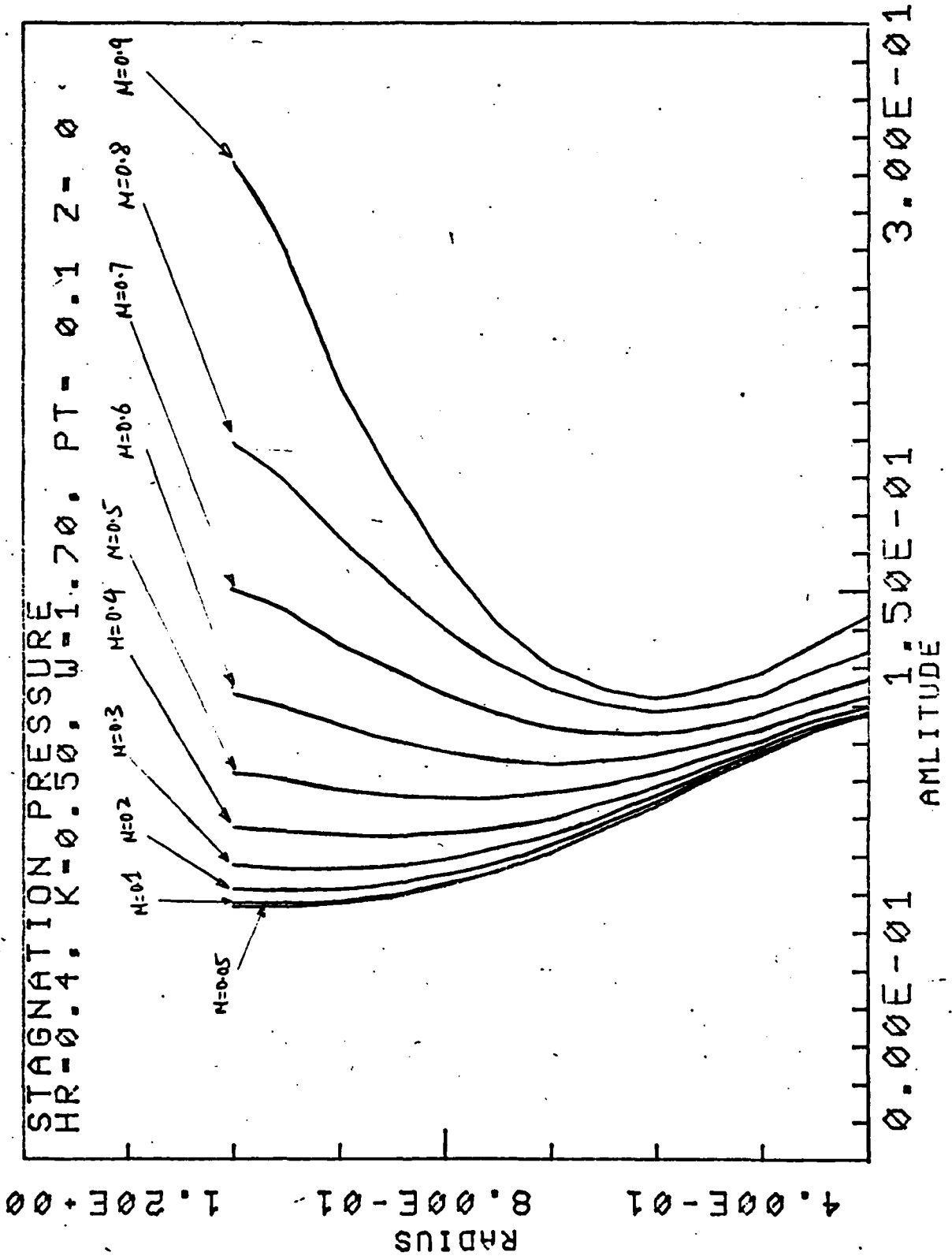
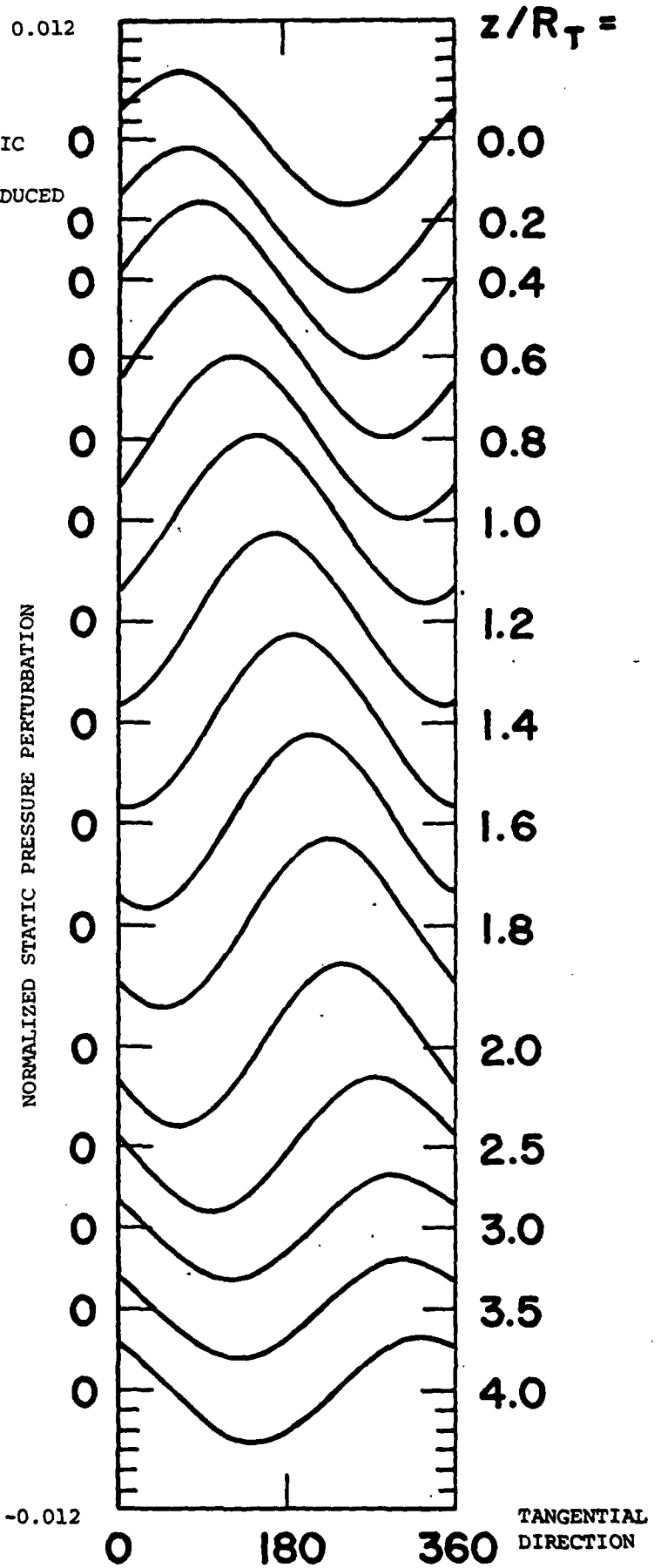


FIGURE 3.20:

DOWNSTREAM EVOLUTION OF STATIC
PRESSURE PERTURBATION FOR
STATOR WITH DISTORTION INTRODUCED
AT THE EXIT OF BLADE ROW

M = 0.1
R = 0.7
HR = 0.4
K = 0.5
W = 0.0
PT = 0.1



REFERENCES

- 3.1 Klein, H., "An Aerodynamic Screen for Jet Engines," Institute of the Aeronautical Sciences, Preprint No. 676, presented at the 25th Annual Meeting, January 28-31, 1957.
- 3.2 Glenny, D. E., "Ingestion of Debris into Intakes by Vortex Action," Ministry of Technology, Aeronautical Research Council CP No. 1114, London, 1970.
- 3.3 Bissinger, N. C., and Braun, G. W., "On the Inlet Vortex System," NASA CR-140182, September 1974.
- 3.4 Motycka, D. L., Walter, W. A., and Muller, G. L., "An Analytical and Experimental Study of Inlet Ground Vortices," AIAA Paper No. 73-1313, November 1973.
- 3.5 Motycka, D. L., and Walter, W. A., "An Experimental Investigation of Ground Vortex Formation during Reverse Engine Operation," AIAA Paper No. 75-1322, 1975.
- 3.6 Rodert, L. A., and Garrett, F. B., "Ingestion of Foreign Objects into Turbine Engines by Vortices," NACA TN3330, February 1955.
- 3.7 Motycka, D. L., "Ground Vortex - Limit to Engine/Reverser Operation," J. Eng. Power, Vol. 98, No. 2, pp 258-264, April 1956.
- 3.8 Colehour, J. L., and Farquhar, B. W., "Inlet Vortex," Journal of Aircraft, Vol. 8, No. 1, January 1971, pp 39-43.
- 3.9 Newmann, W. H., and Atassi, H., "A Two-Dimensional Potential Flow Model for Ground-Induced Effects on Jet and Fan Inlets," AIAA Paper No. 80-0388, January 1980.
- 3.10 Viguier, H. C., "A Secondary Flow Approach to the Inlet Vortex Flow Field," MIT Gas Turbine Laboratory, Report No. 155, 1980.
- 3.11 Hawthorne, W. R., "The Applicability of Secondary Flow Analysis to the Solution of Internal Flow Problems," in Fluid Mechanics of Internal Flows, Edited by Sovran, G., Elsevier Publishing Company, 1967.
- 3.12 Hess, J. L., and Smith, A. M. O., "Calculation of Potential Flow about Arbitrary Bodies," Progress in Aeronautical Sciences, Vol. 8, Pergamon Press, New York, pp 1-138, 1966.
- 3.13 Hess, J. L., "The Problem of Three-Dimensional Lifting Potential Flow and its Solution by Means of Surface Singularity Distribution," Computer Methods in Applied Mechanics and Engineering, Vol. 4, pp 238-319, 1974.
- 3.14 Rubbert, P. E., "Subsonic and Supersonic Panel Methods," in AIAA Lecture Series, "Applied Computational Aerodynamics", 1977.
- 3.15 Johnson, F. T., "A General Panel Method for the Analysis and Design Arbitrary Configurations in Incompressible Flows," NASA CR-3079, 1980.

- 3.16 Hess, J. L., Mack, D., and Stockman, N. O., "An Efficient User-Oriented Method for Calculating Compressible Flow in and about Three-Dimensional Inlets," McDonnell Douglas Report No. MDC J7733, also NASA CR-159578, April 1979.
- 3.17 DeSiervi, F., "A Flow Visualization Study of the Inlet Vortex," MIT Gas Turbine and Plasma Dynamics Laboratory Report No. 159, August 1981.
- 3.18 Tan, C. S., "Three-Dimensional Vorticity-Induced Flow Effects in Highly-Loaded Axial Compressors," Ph.D. Thesis, MIT, June 1978. Also GTL Report No. 131.
- 3.19 Tan, C. S., "Asymmetric Inlet Flows through Axial Compressors," GTL Report No. 151; see also 3.18.
- 3.20 Lifshits, A., "Combined Radial-Circumferential Inlet Distortion through Highly-Loaded Annular Blade Row," M.S. Thesis, Dept. of M.E., MIT, September 1978.
- 3.21 Munk, M., and Prim, R. C., "On the Multiplicity of Steady Gas Flows Having the Same Streamline Pattern," Proc. Nat. Acad. Sci., U.S., 33, 5, 1947.
- 3.22 Nemenyi, and Prim, R.C., "Some Geometric of Plane Gas Flow," J. of Math. & Phys., 27, 1948.
- 3.23 Kerrebrock, J. L., "Small Disturbances in Turbomachine Annuli with Swirl," GTL Report No. 125, MIT, 1975. Also AIAA J., 15, 6, June 1977.
- 3.24 Greitzer, E. M., and Strand, T., "Asymmetric Swirling Flow in Turbo-Machine Annuli," ASME Journal of Engineering for Power, 100, p. 617, 1978.
- 3.25 Hawthorne, W. R., McCune, J. E., Mitchell, N. A., and Tan, C. S., "Non-Axisymmetric Flow through an Annular Actuator Disc: Inlet Distortion Problem," ASME Journal of Engineering for Power, Vol. 100, p. 664, 1978.

TASK IV: 3-D COMPRESSOR BLADE-TO-BLADE FLOW: BLADE DESIGNA. Introduction

There has long been a need for a calculation procedure which can directly determine the blade shapes required for a particular turbomachine to achieve a certain specified task. This need appears to be particularly strong in addressing the importance of three-dimensional (3-D) effects in highly-loaded gas turbine stages.

Classical design technique involve engineering experience and intuition, combined with correlations of the latest available experimental data, and has been remarkably successful. Yet, notable failures do occur (often remaining a mystery as to why), and in any case extrapolation from broad-based experience toward designs into new regimes of performance is often tentative and expensive.

Basically, the turbomachine designer, especially the successful one, "will take any help [he] can get."

In this context, an extensive analysis of flow in bladed rotating machines was undertaken at the inception of this contract. In recent months, the effort has begun to bear fruit to an encouraging extent.

B. Problem Statement

Experience in this research, combined with many discussions with engineers in the industry, has helped us refine our understanding of the nature of the problem. For example, for a given compressor stage, the designer would often wish to be able to specify a given thickness profile for his blades (decided mainly by structural and in part "boundary layer", considerations). He then wishes to impose a "swirl schedule" -- a planned rate of introducing fluid rotation or swirl and/or chordwise pressure distribution -- through the blade row. The question then arises as to what

camber line should be chosen "to build the blade around"? How should the metal actually be cut?

C. Blade-to-Blade Flows

A direct calculational method to solve this problem has to be built around an analysis of the internal "blade-to-blade" flow in rotating machinery. In order to provide an advance, the method must evolve so as to be applicable to highly-loaded, 3-D flows, including transonic cases, in high - and low - hub/tip ratio geometries. It must, to this end, include realistic blade thickness, and should be applicable in any (axisymmetric) duct shape. And, very importantly, the blade-to-blade flow must be related correctly to the axisymmetric computer-code techniques in wide industry use.

Early efforts within this context focused on establishing appropriate "blade boundary conditions". These needed to be formulated non-linearly, so as not to restrict blade loadings.

Once this was done some "simple" forms for possible internal (intra-blade) flows which satisfied such conditions in periodic systems could be constructed. However, since these flows did not satisfy remaining boundary conditions (conditions on the casing; matching with upstream and downstream flows, etc.) their possible use had to be deferred pending the gathering of additional information.

Part of the necessary additional information arose from analysis of 3-D wake flows behind highly loaded axial compressors. This work has been reported earlier in journal publications and in M.I.T. research dissertations and reports, as well as in previous AFOSR progress reports.

D. 3-D-Blade-to-Blade Flow Analysis in Annuli

In the past year, progress has been made to utilize the above advances in the analysis of realistic three-dimensional blade-to-blade flows in a finite chord compressor stage. In particular, we have obtained an exact solution for the flow through a free vortex blade-row where a specified swirl schedule is given. A computer code has been built around this exact solution to calculate the geometry (camber line) of an infinitely thin blade that will produce a specified swirl schedule in an annular duct of constant hub-to-tip ratio. The actual calculational procedure is an iterative one.

During the development of the solution, the concept of an infinitely-bladed "actuator duct flow" was also evolved. This limiting flow is obtained (we imagine) by taking the blade number B to infinity while keeping the swirl schedule fixed. Care must be exercised because, in a pure mean "free-vortex flow", the streamlines would not shift at all in passing through the blades, implying that the bound vorticity representing the blades consists of purely radial vortex filaments. On the other hand, if this were so, then the blade surface would be purely radial throughout the axial extent of the intra-blade flow, but this cannot happen in the presence of free-vortex swirl.

This inconsistency has been eliminated through the introduction of the many bladed, "actuator duct flow" which allows the inclusion of bound tangential vorticity. In this flow the streamlines do shift in passing through the blade-row, allowing 3-D internal consistency of the flow pattern. The concept of many-bladed "actuator duct flow" verifies the notion that the "stacking lines" for the desired blade surface are of importance for the full determination of a proper limiting axisymmetric flow. (Along the "stacking line" the bound vortex filament is purely radial). The results from our "actuator-duct" computer code verifies that for a given swirl schedule, the required blade shape is strongly influenced by the choice of the position

of the stacking lines, thus indicating, in 3-D examples, that "stacking" is an important part of design.

In studying our results for a very high hub-to-tip ratio blade-row example, we find that the results from the computer code agree with two-dimensional results obtained through the Biot Savart Law. The solution can be used as a test case for (and interpretation of) existing axisymmetric codes presently in use.

As mentioned earlier, the description of azimuthally-structured (incompressible, finite-bladed) flow in a 3-D annular environment was formulated as an extension of our earlier wake theory studies. An important feature of this new result has been to enable demonstration of the power of the iterative method: even at very high loading and coarse spacing, satisfactory (i.e., practically useful) convergence was achieved when proper care regarding annular wall boundary conditions was exercised.

We are presently in the process of comparing these results with 2-D and mean-flow analyses of the corresponding blade rows. Some early results are illustrated in Figs. 4.1 - 4.4. These results indicate that blade discreteness and 3-D effects can be quite significant in design decisions. An important remaining task is to distill this information in a form actually useful to the practicing designer.

E. Extensions

The limitations implicit to these results are still likely to be too severe to allow direct engineering application even though important trends can be clearly recognized.

The major extensions now under way include i) adding realistic thickness; ii) adding compressibility effects and iii) treatment of blades flows through arbitrarily shaped annular ducts.

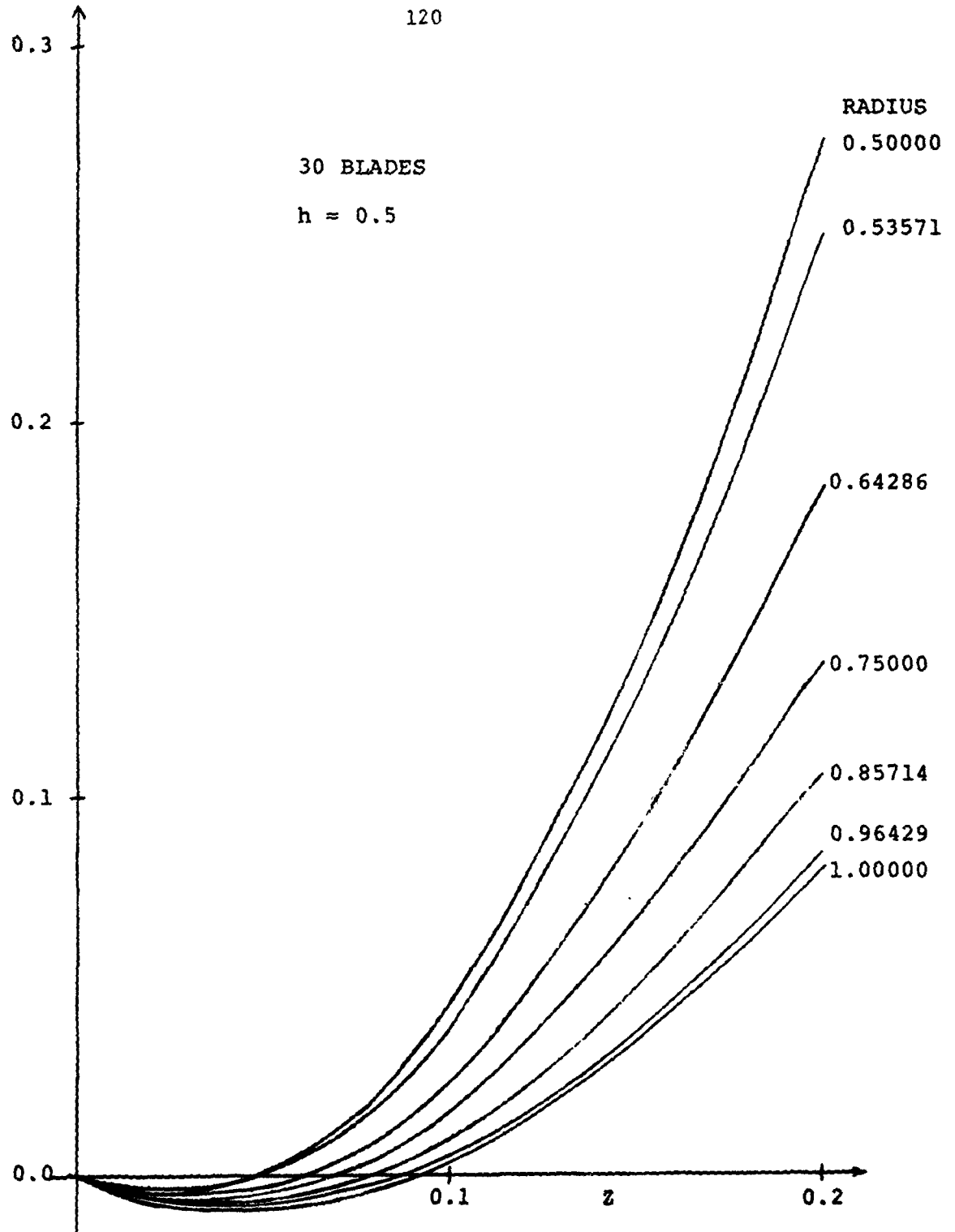


FIGURE 4.1 : 3D BLADE SHAPE; CAMBER LINE AT SEVERAL RADII WITH BLADE "STACKED" AT LEADING EDGE.

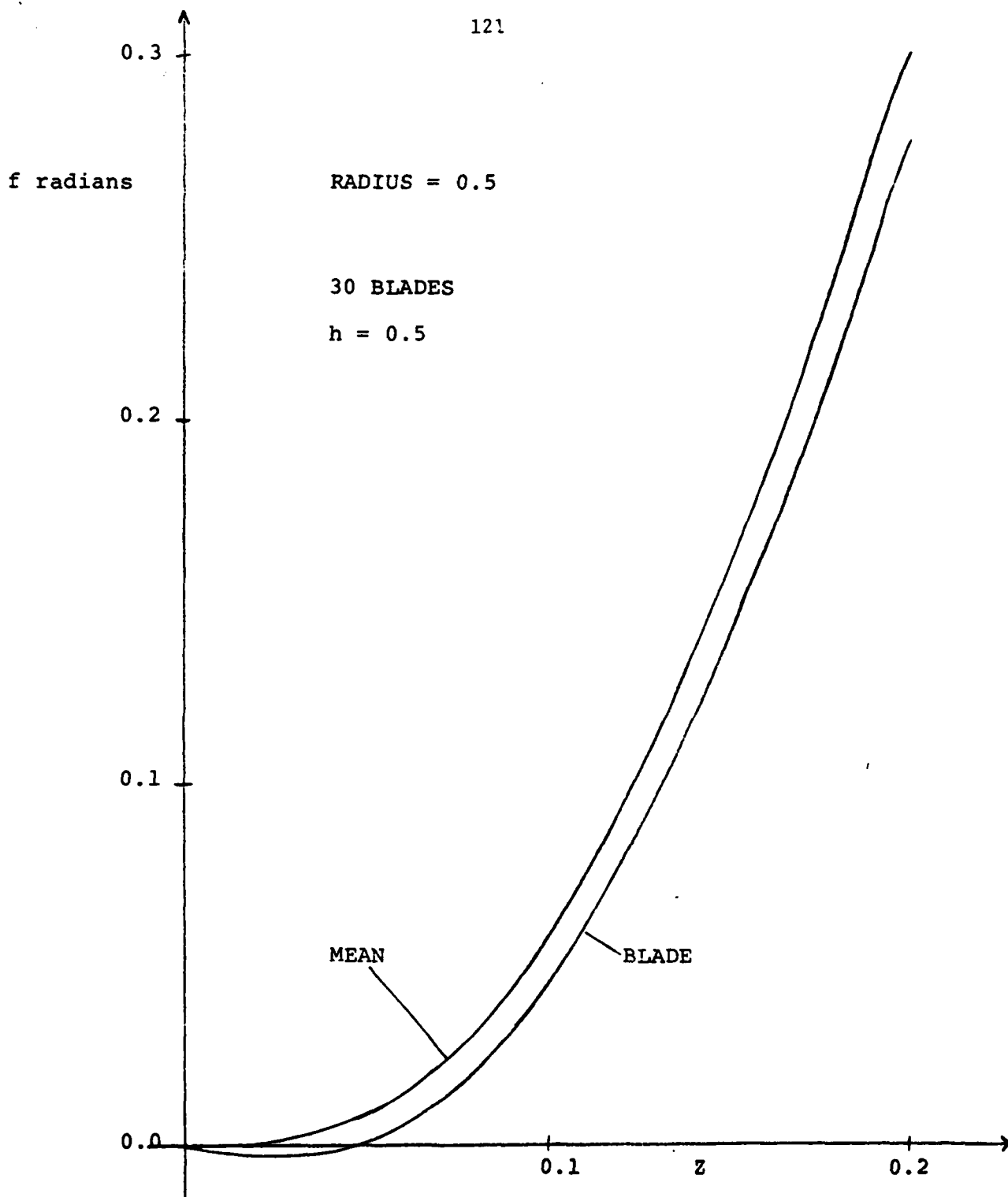


FIGURE 4.2: 3D BLADE CAMBER LINE NEAR HUB COMPARED WITH MEAN FLOW INTRABLADE STREAMLINE SAME RADIUS.

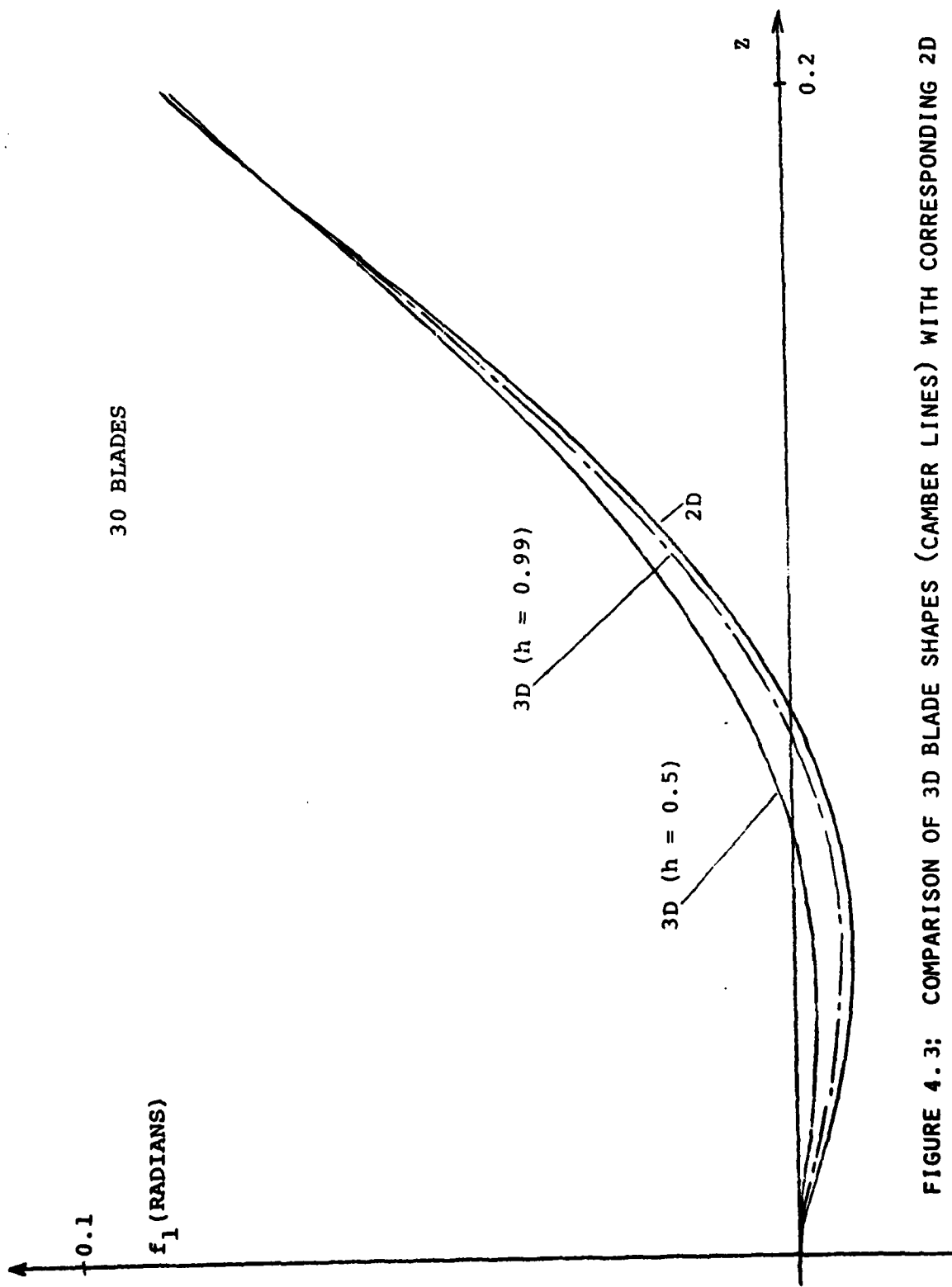


FIGURE 4.3: COMPARISON OF 3D BLADE SHAPES (CAMBER LINES) WITH CORRESPONDING 2D RESULTS AS FUNCTION OF HUB TIP RATIO.

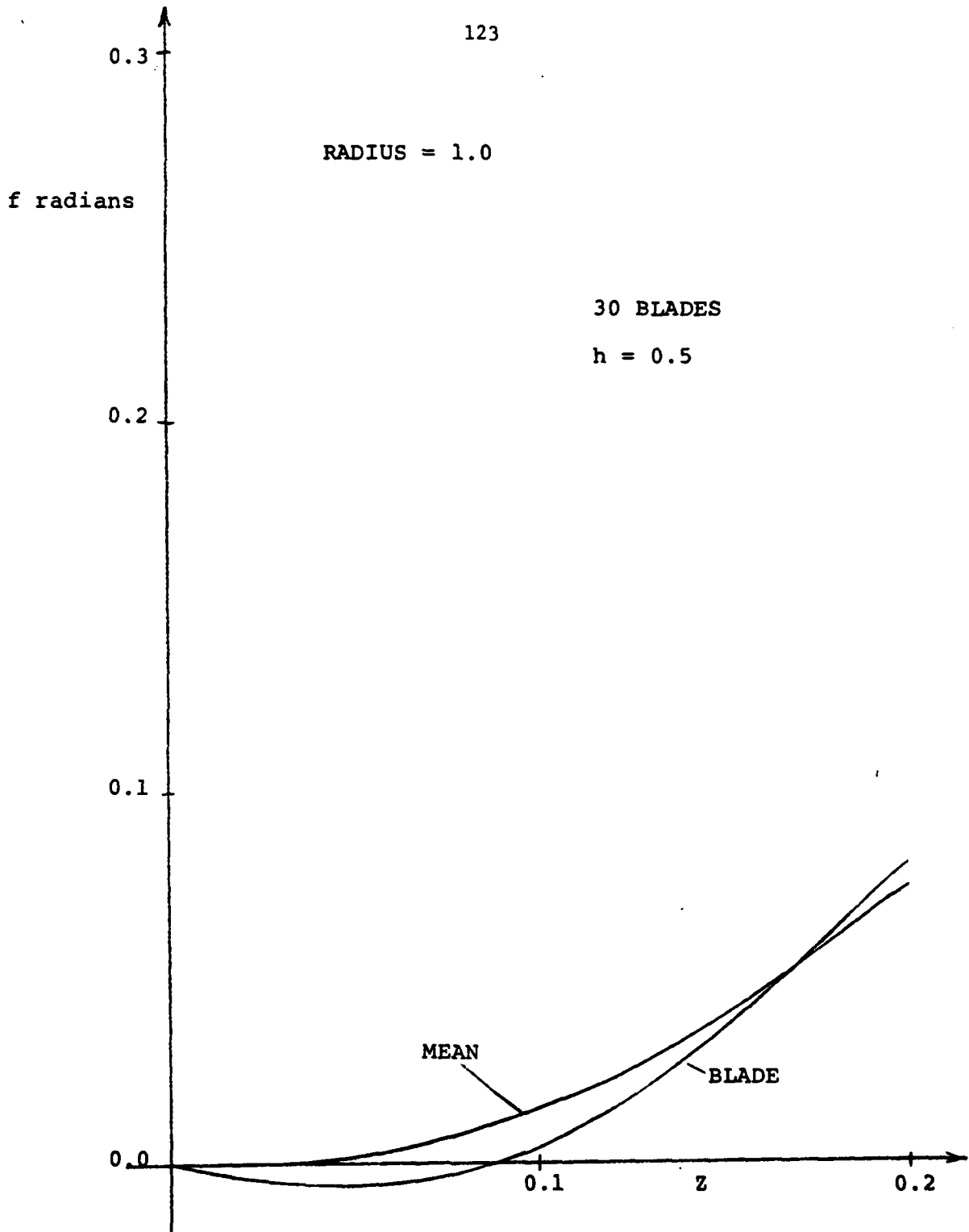


FIGURE 4.4: 3D BLADE CAMBER LINE NEAR SHROUD COMPARED WITH MEAN FLOW INTRABLADE STREAMLINE, SAME RADIUS

3. PUBLICATIONS

Publications in Technical Journals

(Based on work partially or wholly supported by this Contract.)

E. M. Greitzer, "The Stability of Pumping Systems - The 1980 American Society of Mechanical Engineers Freeman Scholar Lecture," presented at ASME Winter Annual Meeting, November 1980. ASME Journal of Fluids Engineering (invited review), Vol. 103, No. 2, pp. 193-243, June 1981.

W. T. Thompkins and S. S. Tong, "Inverse or Design Calculations for Non-Potential Flow in Turbomachinery Blade Passages," ASME paper 81-GT-78, presented at 1981 Gas Turbine Conference, Houston TX, March 9 - 12, 1981. Accepted for publication in Journal of Engineering for Power.

C. S. Tan, "Vorticity Modelling of Blade Wakes Behind Isolated Annular Blade-Rows: Induced Disturbances in Swirling Flows." ASME Journal of Engineering for Power, Vol. 103, No. 2, April 1981.

W. T. Thompkins and S. S. Tong, "A Design Calculation Procedure for Shock-Free or Strong Passage Shock Turbomachinery Cascades," prepared for 1982 Gas Turbine Conference, London, England.

C. S. Tan and W. R. Hawthorne, "Three-Dimensional Blade Design Using an Analytical Theory," to be submitted for publication in ASME Journal of Engineering for Power.

Reports

C. S. Tan, "Three-Dimensional Vorticity-Induced Flow Effects in Highly Loaded Axial Compressors," Part I, Ph.D. Thesis, MIT Department of Aeronautics and Astronautics, and GT&PDL Report #131, January 1980.

C. S. Tan, "Asymmetric Inlet Flows Through Axial Compressors," Part II, Ph.D. Thesis, MIT Department of Aeronautics and Astronautics, and GT&PDL Report #151, January 1980.

C. S. Tan, "Three-Dimensional Incompressible and Compressible Beltrami Flow Through a Highly-Loaded Isolated Rotor," MIT Department of Aeronautics and Astronautics, GT&PDL Report #147, October 1979.

Henri Charles Viguier, "A Secondary Flow Approach to the Inlet Vortex Flow Field," GT&PDL Report #155, November 1980.

Francesca De Siervi, "A Flow Visualization Study of the Inlet Vortex Phenomenon," GT&PDL Report #159, July 1981.

Mark E. Prell, "An Experimental Investigation of Stator Hub Treatment in an Axial Flow Compressor," GT&PDL Report #161, July 1981.

Theses

Saeed Farokhi, "Unsteady Three-Dimensional Flow in a Compressor with Inlet Flow Distortions," Ph.D. Thesis, MIT Department of Aeronautics and Astronautics, February 1980.

Mohammad Rahnema, "On Shear Flow Through Highly Loaded Three-Dimensional Cascades," M.S. Thesis, September 1980.

David P. Miller, "The Predictive Study of Flow Phenomena Behind an Axial Turbomachine Rotor," M.S. Thesis, MIT Department of Aeronautics and Astronautics, June 1980.

Henri Viguiier, "A Secondary Flow Approach to the Inlet Vortex Flow Field," M.S. Thesis, MIT Department of Mechanical Engineering, November 1980.

Francesca DeSiervi, "A Flow Visualization Study of the Inlet Vortex Phenomenon," M.S. Thesis, MIT Department of Mechanical Engineering, June 1981.

Mark E. Prell, "An Experimental Study of Stator Hub Treatment in an Axial Flow Compressor," M.S. Thesis, MIT Department of Aeronautics and Astronautics, June 1981.

Mohan Krishnan, "Actuator Duct Solutions for Flow Through an Isolated Blade-Row," M.S. Thesis, Department of Aeronautics and Astronautics, MIT, September 1981.

Alexander Lifshits, "Combined Radial-Circumferential Inlet Distortion Through Highly-Loaded Annular Blade Row," M.S. Thesis, Department of Mechanical Engineering, MIT, September 1981.

Keith E. Therrien, "An Experimental Investigation of a Transonic Compressor Using Blowdown and Streamline Curvature Analysis Techniques," B.S. & M.S. Thesis, Department of Mechanical Engineering, MIT, May 1981.

4. PROGRAM PERSONNEL

Principal Investigators:

Edward M. Greitzer
Associate Professor of Aeronautics and Astronautics

William T. Thompkins, Jr.
Associate Professor of Aeronautics and Astronautics

James E. McCune
Professor of Aeronautics and Astronautics

Co-Investigators:

Alan H. Epstein
Assistant Professor of Aeronautics and Astronautics
Associate Director of Gas Turbine & Plasma Dynamics Laboratory

Choon S. Tan
Research Associate

Collaborating Investigators:

Eugene E. Covert
Professor of Aeronautics and Astronautics
Director of Gas Turbine & Plasma Dynamics Laboratory

Frank H. Durgin
Research Associate

Sir William R. Hawthorne
Senior Lecturer

Graduate Students:

9/80 - Present	Peter Cheng
9/81 - Present	Thong Dang
9/79 - 6/81	Francesca DeSiervi*
6/79 - 2/80	Saeed Farokhi**
9/81 - Present	Philippe Kletzkine
9/79 - 6/81	Mohan Krishnan*
9/80 - Present	Wen Liu
2/80 - 8/81	Alexander Lifshits*
6/79 - 5/80	David Miller*
9/80 - Present	Wing-Fai Ng
9/79 - 1/81	Mark Prell*
9/79 - 8/80	Mohammad Rahnema*
9/79 - 6/81	Keith Theirrin*
9/79 - Present	Siu Shing Tong
6/80 - 11/80	Henri Viguier*

*Completed M.S. Thesis

**Completed Ph.D. Thesis

5. INTERACTIONS

Presentations and Lectures

E. M. Greitzer, Lectures on, "Unsteady Flows in Turbomachines," "Inlet Distortion," and "Surge and Rotating Stall," at ASME/ISU Turbomachinery Institute Course on Fluid Dynamics of Turbomachinery, Ames, Iowa, July 1980.

E. M. Greitzer, "Strut Induced Aerodynamic Forcing Functions in Axial Compressors," delivered at Joint NASA/AF/NAVY Symposium on Aeroelasticity in Turbomachines, NASA Lewis Research Center, Cleveland, Ohio, October 1980.

E. M. Greitzer, Lecturer in ASME Short Course, "Foundations of Axial Turbomachinery Aerodynamics," presented at ASME International Gas Turbine Conference, New Orleans, LA, March 1980, Houston TX, 1981.

E. M. Greitzer, Seminars on "Prediction of Compressor Performance in Rotating Stall," and "Asymmetric Swirling Flow in Turbomachine Annuli," Department of Mechanical Engineering, Virginia Polytechnic Institute, Blacksburg, VA, January 1980.

A. H. Epstein, "Computer Aided Data Collection and Reduction in A Blowdown Compressor Facility," presented at AGARD Fluid Dynamics Panel meeting on Integration of Computers and Wind Tunnel Testing, September 24-25, 1980, Chattanooga, TN.

E. M. Greitzer, "The Stability of Pumping Systems - the 1980 ASME Freeman Scholar Lecture," presented at United Technologies Research Center, October 1980, Pratt & Whitney Government Products Division, October 1980, Workshop on Unsteady Flows in Turbomachines, Cambridge University, April 1981.

E. M. Greitzer, "A Simple Model for Compressor Stall Cell Propagation," Seminar in Clarence Danforth Lecture Series in Airbreathing Propulsion, University of Cincinnati, January 1981.

The Gas Turbine and Plasma Dynamics Laboratory has an active seminar program with several speakers from industry and government per term. These seminars usually have the additional benefit of extended technical discussions between the speakers and the MIT personnel. During the time period discussed, these were:

Dr. L. H. Smith, Jr., Manager Compressor and Turbine Aerodynamics
General Electric Aircraft Engine Group (topic: "Flows in Multistage
Compressors.")

Dr. A. M. Pfeffer, Head Turbine Group, Pratt & Whitney Aircraft
(topic: "Turbine Cooling").

Mr. R. S. Mazzaway, Senior Research Engineer, Pratt & Whitney
Aircraft (topics: "Stagnation Stall", and "Surge Induced Structural
Loads in Gas Turbine Engines").

Dr. J. J. Adamczyk, NASA Lewis Research Center, (topic:
"Supersonic Stalled Flutter.")

Dr. W. Jansen, Northern Research and Engineering, (topic:
"Surge Margin Increase in Centrifugal Compressors due to Casing
Treatment.")

Dr. L. E. Snyder, Head, Structures Group, Detroit Diesel Allison,
Indianapolis, IN, (topic: "Turbomachinery Design to Avoid High Cycle
Fatigue.")

Dr. A. J. Wennerstrom, AFAPL (topic: "Design Technology for
Advanced Transonic Compressors.")

Mr. C. C. Koch, General Electric Company (topic: "Stalling Pressure
Rise Capability of Axial Flow Compressor Stages.")

Dr. J. M. Verdon, United Technologies Research Center
(topic: "Unsteady Compressible Flow Past a Loaded Cascade.")

Dr. A. A. Peracchio, Pratt & Whitney Aircraft (topic: "Development and Application of Noise Reduction Technology.")

Dr. A. J. Strasizar, NASA Lewis Research Center (topic: "Laser Anemometer Measurements in a Transonic Rotor.")

Dr. D. Ives, Pratt & Whitney Aircraft, (topic: "Aerodynamic Uses of Conformal Mapping in Industry.")

6. DISCOVERIES, INVENTIONS AND SCIENTIFIC APPLICATIONS

Discoveries: A previously unrecognized mechanism of inlet vortex formation has been discovered.

Inventions and Scientific Applications: Although no new "devices" have been developed, several of the methods discussed in the detailed task description are in fact either new or novel adaptations of existing techniques.

7. CONCLUDING REMARKS

In addition to the detailed technical discussions, we can also give a few general comments concerning the overall state of the AFOSR Multi-Investigator Program at MIT. The program appears to have achieved many of the goals which were initially set out. In particular the inverse design calculation procedure, the project on mechanisms of inlet vortex formation, and that on three-dimensional studies of highly loaded turbomachinery blading have led to new concepts and/or procedures. Further, the other projects, although relatively less far along, appear to show good potential as far as future efforts are concerned.

In addition, a very important aspect of this program has been the upgrading of the MIT capabilities for turbomachinery research. This is very apparent in the laboratory, but its effect is also seen in the overall research effort, where there now exists a "critical mass" of graduate students, faculty, and support staff who have a common interest in the type of problems addressed by this project and can interact fruitfully. Quite apart from the technical results, this active effort should result in an increased output of talented young engineers with a strong interest in high performance turbomachinery.